Development of Lavender oil Based Polymer Films for Emerging Technologies

Thesis submitted by

Christopher David EASTON BE (Hons) Qld

in April 2009

for the degree of Doctor of Philosophy

in the School of Engineering and Physical Sciences

James Cook University

Supervisors: Dr. Mohan Jacob and Dr. Graham Woods

DECLARATION

I declare that this thesis is my own work and has not been submitted in any form for another degree or diploma at any university or other institute of tertiary education. Information derived from the published and unpublished work of others has been acknowledged in the text, and a list of references is given.

Christopher Easton

April, 2009

STATEMENT OF ACCESS TO THIS THESIS

I, the under-signed, the author of this work, understand that James Cook University will make this work available for use within the University Library, and via the Australian Digital Thesis Network, for use elsewhere.

I understand that as an unpublished work, a thesis has significant protection under the Copyright Act. I do not wish to place any restriction on access to this thesis. However, any use of its content must be acknowledged and could potentially be restricted by future patents.

Christopher Easton

April, 2009

ACKNOWLEDGEMENTS

I would like to thank Mohan Jacob and Graham Woods for their supervision throughout this thesis.

I would also like to thank those people who provided advice and guidance through collaboration, specifically Prof. Jerzy Krupka, Prof. Robert Shanks, Prof. Christopher Berndt, A./ Prof. Bruce Bowden, Prof. Elena Ivanova, Prof. James Burnell, and Dr. Ron White.

Thank you to the electrical workshop crew (John Ellis, John Renehan, Lloyd Baker) for their assistance in the setup and maintenance of the experimental apparatus. The AFM and SEM facility offered by the JCU Advanced Analytical Centre is also acknowledged.

I would like to acknowledge the financial support provided by the Australian Postgraduate Award (APA), Rural Industries Research and Development Corporation (RIRDC) top-up scholarship, and the James Cook University Graduate Research Scheme (GRS). In addition, I would like to acknowledge G. R. Davis Pty. Ltd. for donating the LAEO monomer.

Cheers to Adam Ruxton for providing comedic relief throughout this thesis.

ABSTRACT

The fabrication of novel and optimised materials, in addition to the development of techniques and procedures for characterisation of thin film samples continues to gain interest in the material science/engineering research area. These new polymers have the potential to provide improvement for existing technology, as well as avenues for new applications in fields including organic (flexible) electronics, optical and biomedical. The focus of this work is to develop new polymers for use in the identified applications from environmentally friendly resources. In addition to the technological benefits of this work, implementation of Australian resources in these fields would provide great benefit to local industry. This philosophy led to the choice of *Lavandula angustifolia* essential oil (LAEO) produced in Australia for the fabrication of the new polymers. This thesis studies investigates the fabrication of essential oil based polymer thin films from LAEO and some of its major individual components.

The resultant LAEO based polymer films have been characterised using a number of techniques and instruments, including spectroscopic ellipsometry, Fourier transform infrared spectroscopy, nuclear magnetic resonance spectroscopy, dielectric resonator techniques, atomic force microscope, scanning electron microscope, and contact angle. Using these characterisation tools, the properties of the resultant polymers were defined.

The LAEO based polymers were shown to be primarily hydrocarbon based, with some oxygen containing functional groups including ketones and hydroxyl groups. The presence of aromatics was also confirmed which are most likely formed during the polymerisation process. It was found that an increase in RF power resulted in a greater loss in the monomer functional groups and was assigned to an increase in energy input into the plasma system and an increase in substrate temperature.

Optical characterisation of the LAEO based polymers fabricated at various RF power levels confirmed that they are optically transparent and isotropic. Refractive index ranged from 1.530 to 1.543 at 500 nm for films fabricated using RF powers from 10 to 75 W. The optical band gap was found to decrease with increasing RF power, with 2.75 at 10 W and 2.34 at 75 W, and thus is within the range of band gap values defined for semiconductors.

Surface images obtained at the micro- and nano-meter scales demonstrated that the LAEO based polymers were uniform, smooth and pinhole free. The average roughness was found to be less than a nanometer.

Stability of the polymer while in contact with various solvents was examined using contact angle measurements. It was discovered that the polymer is very stable while in contact with water, with contact angle ranging from mildly hydrophilic (81.93º) at 10 W to mildly hydrophobic (91.95º) at 75 W. The surface tension components of the polymer were derived from the contact angle data. The LAEO based polymer was found to be monopolar in nature. Interfacial tension values were obtained for the polymer-solvent systems and the solubility characteristics of the polymer derived. These results specified that the polymer should resist solubilisation from the solvents explored.

Adhesion quality testing was performed on samples fabricated at various RF power levels and on common substrate materials. The quality was found to improve with increasing RF power, and was associated with an increase in the interfacial bonding.

LAEO based polymers exposed to ambient conditions were monitored for 1400 hours to provide information concerning the ageing mechanisms using spectroscopic ellipsometry and FTIR spectroscopy. The bulk of the ageing was found to occur within the first 100 hours after deposition, with the ageing mechanism following the typical oxidation path via the inclusion of additional hydroxyl for the higher power samples. At 10 W however, the mechanism was different, where no apparent uptake of oxygen occurred, and instead there was a significant loss of thickness.

Thermal degradation results demonstrated that the stability of the LAEO based polymer increased with RF power. Heating to 405ºC resulted in minimal residue for all samples.

The major components of the LAEO monomer employed throughout this thesis were identified and polymers fabricated from these precursors. Overall it was found that the monomers with oxygen containing functional groups produced polymers with similar characteristics to that of the LAEO based polymer. The results indicated that polymers with similar characteristics to that of the LAEO based polymer could be fabricated from LAEO irrespective of the composition of the monomer.

Polymer thin films were fabricated from 1,8-cineole and the properties obtained using a number of techniques studied. This monomer can make up a significant portion of

LAEO, however there was no detectable amount in the LAEO employed during this thesis. This monomer is also known to be a major component of eucalyptus oil.

A new technique for measuring the permittivity of low permittivity thin films at microwave frequencies was developed. This technique provided an accurate and non-destructive characterisation tool for these types of materials which was not previously possible.

From the characterisation data obtained, the suitability of the polymer in particular applications was discussed. Potential applications identified include employing these polymers in semiconductor applications, in the biomedical field as bio-reactive (LAEO based polymer) and non-bio-reactive (1,8-cineole) coatings, and as a sacrificial material in air gap fabrication.

Overall, during this thesis polymer thin films were successfully fabricated from LAEO and the major components and the properties of these polymers were determined. Additionally, a new technique for measuring the dielectric parameters of low permittivity thin films was defined. Potential applications for these polymers have been identified based on the characterisation data, as well as avenues for future work.

CONTENTS

LIST OF PUBLICATIONS

The following is a list of publications by the author during the period of this thesis.

Pub. 1. (Chapter 2) M. V. Jacob, C. D. Easton, G. S. Woods, and C. C. Berndt, "Fabrication of a novel organic polymer thin film," *Thin Solid Films*, vol. 516, pp. 3884-3887, 2008.

Pub. 2. (Chapter 4) C. D. Easton, M. V. Jacob, and J. Krupka, "Non-destructive complex permittivity measurement of low permittivity thin film materials," *Measurement Science & Technology*, vol. 18, pp. 2869-2877, 2007.

Pub. 3. (Chapter 3) C. D. Easton, M. V. Jacob, R. A. Shanks, and B. F. Bowden, "Surface and chemical characterisation of polyLA thin films fabricated using plasma polymerisation," *Chemical Vapor Deposition*, In press.

Pub. 4. (Chapter 4) C. D. Easton and M. V. Jacob, "Optical Characterisation of RF Plasma Polymerised Lavandula Angustifolia Essential Oil Thin Films," *Thin Solid Films*, vol. 517, pp. 4402-4407, 2009.

Pub. 5. (Chapter 5) C. D. Easton and M. V. Jacob, "Ageing and thermal degradation of plasma polymerised thin films derived from Lavandula angustifolia essential oil," *Polymer Degradation and Stability*, vol. 94, pp. 597-603, 2009.

Pub. 6. (Chapter 6) C. D. Easton, M. V. Jacob, and R. A. Shanks, “Plasma polymerisation of the constituents of Lavandula angustifolia essential oil,” *Polymer Engineering and Science*, To be submitted.

Pub. 7. (Chapter 7) C. D. Easton, M. V. Jacob, and R. A. Shanks, "Fabrication and characterisation of polymer thin-films derived from cineole using radio frequency plasma polymerisation," *Polymer*, vol. 50, pp. 3465-3469, 2009.

Pub 8. (Chapter 5) C. D. Easton and M. V. Jacob, "Solubility and adhesion characteristics of plasma polymerised thin films derived from Lavandula angustifolia essential oil," *Journal of Applied Polymer Science*, In Press.

CHAPTER 1 INTRODUCTION

Polymers are implemented in many applications across diverse disciplines including the electronic, optical and biomedical fields. To produce a polymeric material for use in electronic applications, traditional 'wet' methods of synthesis include chemical and electrochemical polymerisation. Plasma polymerisation is a dry method of polymerisation. The phenomenon of plasma polymerisation has been known since 1874. However polymers produced by this technique were initially considered an undesirable by-product and as such it was not until the 1950's that significant attention was paid to this fabrication technique [1]. This method differentiates itself from traditional polymerisation techniques as plasma is implemented in the procedure. In addition, organic precursors that are unable to polymerise using conventional techniques have been found to undergo polymerisation using this technique. Interest in the use of plasma polymerisation originated due to its advantages, which include the ability to produce films that are of uniform thickness, pinhole-free, chemically inert and thermally stable [2-5]. In general, plasma polymerisation is considered a low cost and simplistic method to produce high quality polymer films. The low cost of this fabrication technique is attributed to the associated low consumption of precursor material and the absence of any need for other chemicals and/or solvents, therefore making it ecologically friendly [6].

A principal component of the polymerisation process is the monomer, which is the material from which the polymer is fabricated. A number of monomers have been implemented in the fabrication of plasma polymers, employing either continuous wave or pulsed plasma polymerisation. Examples include aniline, thiophene, vinyltriethoxysilane, perylene etc. [7-27]. The majority of the monomers employed in plasma polymerisation are hazardous to humans and the environment, requiring special handling and disposal procedures.

Previous work by other authors employing essential oils in the fabrication of polymer thin films is minimal. The electrical properties of films derived from lemongrass based [28] and the electrical and optical band gap properties of eucalyptus based [29] polymer

films produced via plasma polymerisation have been briefly described. In addition, the supervisor's initial work involved the use of tea tree oil (Jacob [30]) as a monomer. Free radical co- and terpolymerization employing linalool, a component of *Lavandula angustifolia* essential oil (LAEO), has been undertaken by Srivastava et. al. [31]. The feasibility of plasma polymerisation of LAEO was tested in 2005 [32]. This study was limited to a few samples and limited characterisation under restricted conditions.

1.1 RATIONAL

The basis of motivation for this project originates from two sources; the advancement of technology and the global interest in developing environmentally friendly products. There is a high demand for novel electronic materials due to the significant growth of novel communication and electronic devices in the last decade such as flexible displays, RFID tags, e-paper etc. Without materials that demonstrate the desirable characteristics required to advance current electronic technology and develop new electronic devices, avenues for progression become limited. Currently, this push stems from the reduction in size of integrated circuit (IC) technology, and the increase in operating frequencies of communication and electronic systems. These changes result in a reduction of distance between interconnecting lines. As this distance decreases, the interconnect lines begin to influence each other through means of resistance capacitance (RC) effects and eventually surpasses intrinsic gate delay to become the dominant source of signal delay within the IC [33]. The RC constant is a function of the resistivity of the metal used and the capacitance of the combined metal/insulator dielectric structure.

To reduce this signal delay, an insulating material with a lower dielectric constant can be used to reduce the capacitance, which can also reduce inductive cross talk and power consumption [33, 34]. The conventional insulating material used in IC fabrication is silicon dioxide, which has a dielectric constant of approximately 4. A number of dielectric materials exist with dielectric constants less than silicon dioxide; however it is not possible to implement just any material. Another important requirement for implementation in electronic devices is the ability to maintain thermal stability. The heat used to form the metal interconnecting lines can damage the polymer if it is not thermally stable up to the device fabrication temperature. In addition, the polymer

implemented should be able to dissipate heat efficiently [35], while improvement in the area of corrosion protection of interlayer dielectrics is considered necessary for future microelectronic devices [34]. Thus, there is much interest in obtaining insulating materials with low dielectric constants and that are thermally stable.

Much work has been done in the formation of organic thin-film-transistors (OTFT's) in order to replace existing inorganic semiconductors such as amorphous hydrated silicon (a-Si:H). A problem typically faced when attempting to implement organic semiconductors is due to relatively low carrier mobility. Interest exists in such materials as they can be implemented in new ways, such as fabricating flexible flat panel displays on plastic substrates. It is not possible to fabricate a-Si:H on such substrates. Reduction in manufacturing costs is also expected from implementing such materials. Thus fabrication of organic semiconducting polymers with high carrier mobility is desired. In general, these materials must be inexpensive, easy to manufacture, and possess stable characteristics with changing environmental conditions, unless otherwise required.

Material science plays an integral role in the development of biosensor design, regenerative medicine and tissue engineering. In the past, the use of synthetic polymers in these applications has involved taking the material from bulk samples. These materials were rarely modified prior to implementation, and thus lead to issues with biocompatibility, degradation and inadequate mechanical properties. Therefore there is strong interest in developing biomaterials with properties that are tailored for this particular application. Some uses included controlled drug delivery systems, polymer-coated stents and controlled release systems for proteins. The use of plasma polymers in this field continues to gain interest, with review articles available outlining the work done in this area [6, 36].

The second source of motivation originates from the global interest in developing environmentally friendly products. Resources employed for the fabrication of typical electronic materials can be harmful. If superior materials could be produced from an alternative source that was environmentally friendly with minimal mark-up of cost, then the integration of such materials would prove to be a viable option. In addition to these

advantages, if such a material could be produced from an Australian agricultural resource, then it would prove to be a great benefit to local industry. Thus based on these criteria, the material selected for producing organic thin films was an Australian essential oil, specifically LAEO.

1.2 RESEARCH OBJECTIVES

The aim of this research is to fabricate polymer thin films from LAEO and optimise the properties of the resultant polymer by varying the deposition conditions. There are a number of deposition conditions that can be tuned to optimise the properties of the resultant polymer, including reactor configuration, input RF power, monomer flow rate, substrate temperature, deposition time, and system pressure [3]. Procedures for the characterisation of the thin films will be defined and implemented. Upon completion of the characterisation stage, the applications that the films are best suited for can be determined. Identifying the materials currently in use in the selected applications and comparing their characteristics with the LO polymer films will provide a benchmark for the potential success of implementing the new polymer thin films.

Based on this criteria, the research questions have been defined as follows:

- Is it possible to fabricate lavender oil (*Lavandula angustifolia*) polymer thin films with optimised characteristics and what are the properties of these films?
- What are the established procedures for characterisation of thin films and are any new techniques and/or procedures necessary in order to achieve a more comprehensive set of results for the new thin films being studied?
- What applications are these films best suited for and it is possible to implement these films in the identified applications?

Overall, the work completed in this thesis is expected to have a significant impact on the research and applied fields. Establishing a framework for identifying essential oils as potential candidates and identifying possible applications will lead to the expansion

of use of such resources in the fabrication of electronic materials. Such expansion will provide great benefit to local producers of the monomer. The procedures necessary for the characterisation of the polymer will be established, where new techniques will be derived when necessary. By developing polymers derived from LAEO, it will demonstrate that these raw materials can be successfully employed to obtain polymer thin films with optimised properties.

1.3 THESIS ORGANISATION

This thesis is presented as a series of chapters, each representing a manuscript at various stages of publication. It has been arranged to provide cohesion when reading each chapter in sequential order. However, each publication is expected to stand on its own and therefore summaries and references to previous results have been included in the manuscripts to provide better flow.

The work reported in this thesis was done by the author Christopher Easton and has included discussions with supervisors and experts as evident in the publications. Project supervisors Dr. Mohan Jacob (all Chapters) and Dr. Graham Woods (Chapter 2) are included to acknowledge their contribution through training, funding and feedback. Prof. Christopher Berndt (Chapter 2) provided experience and advice in the area of plasma modifications of surfaces. Prof. Jerzy Krupka (Chapter 4) provided expertise in dielectric resonator techniques and assistance in the error analysis. Prof. Robert Shanks (Chapters 3, 6, and 7) and A/Prof. Bruce Bowden (Chapter 3) provided knowledge on the chemical analysis of the polymers, specifically confirmation of FTIR and NMR data interpretation, and access to necessary equipment. All experiments were performed solely by the author, with the exception of the NMR experiment presented in Chapter 3. After it was confirmed experimentally that the resolution obtained from the NRM equipment located at JCU was not sufficient for these polymers, facilities at the Australian Institute of Marine Science (AIMS) were accessed through collaborative facility.

The thesis is organised in the following format. Chapter 2 introduces the thin film fabrication procedure and provides details on the experimental apparatus employed throughout this thesis. Initial characterisation results obtained for the polymer fabricated under a single set of deposition conditions using spectroscopic ellipsometry and a scanning electron microscope are presented.

The chemical and surface properties of the polymer fabricated at various RF powers are examined in Chapter 3. Fourier transform infrared and nuclear magnetic resonance spectroscopy are used to study the chemical structure of the polymers. The surface topology of the polymers are examined using an atomic force microscope, while the hydrophilicy of the polymer is determined using water contact angle measurements.

Chapter 4 provides an overview of the electromagnetic characterisation of the polymer thin films. The optical properties of the LAEO based polymer fabricated at various RF powers, including refractive index, extinction coefficient, transparency, and optical band gap, are explored (Section 3.1). A new method for obtaining the complex permittivity of low permittivity thin films is presented and the dielectric properties of the polymer fabricated under a single set of deposition conditions reported (Section 3.2).

Polymer stability under varying conditions is investigated in Chapter 5. The solubility of the polymer fabricated at various RF power levels while in contact with six solvents is explored, while the adhesion properties to common substrates are examined (Section 5.1). Using spectroscopic ellipsometry and Fourier transform infrared spectroscopy, the properties of the films are examined while exposed to ambient conditions for an extended period of time, and when exposed to elevated temperatures (Section 5.2).

Chapter 6 studies the polymerisation of major individual components of LAEO and compares the properties with those of the LAEO based polymer. The major components employed are identified using gas chromatography – mass spectrometry. Employing plasma polymerisation to fabricate polymer thin films from the identified components using a single set of deposition conditions, the properties are derived. Characterisation is performed using spectroscopic ellipsometry, Fourier transform infrared spectroscopy, atomic force microscope, and water contact angle measurements.

1,8-cineole can be a major component of LAEO, however in the monomer employed in this thesis there is detectable amount. This component exhibits some favourable

medicinal properties. The fabrication and characterisation of polymer thin films from 1,8-cineole are described in Chapter 7.

Concluding remarks are summarised in Chapter 8, including an overview of potential applications and avenues for future work.

REFERENCES

[1] H. Yasuda, "Glow-Discharge Polymerization," *Macromolecular Reviews Part D-Journal of Polymer Science*, vol. 16, pp. 199-293, 1981.

[2] C. Nastase, D. Mihaiescu, F. Nastase, A. Moldovan, and L. Stamatin, "Effect of p-toluene sulphonic acid doping on the properties of plasma polymerized aniline thin films," *Synthetic Metals*, vol. 147, pp. 133-138, 2004.

[3] F. F. Shi, "Recent advances in polymer thin films prepared by plasma polymerization Synthesis, structural characterization, properties and applications," *Surface & Coatings Technology*, vol. 82, pp. 1-15, 1996.

[4] U. S. Sajeev, C. J. Mathai, S. Saravanan, R. R. Ashokan, S. Venkatachalam, and M. R. Anantharaman, "On the optical and electrical properties of rf and a.c. plasma polymerized aniline thin films," *Bulletin of Materials Science*, vol. 29, pp. 159-163, 2006.

[5] H. Biederman and D. Slavinska, "Plasma polymer films and their future prospects," *Surface & Coatings Technology*, vol. 125, pp. 371-376, 2000.

[6] R. Forch, A. N. Chifen, A. Bousquet, H. L. Khor, M. Jungblut, L. Q. Chu, Z. Zhang, I. Osey-Mensah, E. K. Sinner, and W. Knoll, "Recent and expected roles of plasma-polymerized films for biomedical applications," *Chemical Vapor Deposition*, vol. 13, pp. 280-294, 2007.

[7] C. A. Pfluger, R. L. Carrier, B. Sun, K. S. Ziemer, and D. D. Burkey, "Cross-Linking and Degradation Properties of Plasma Enhanced Chemical Vapor Deposited Poly(2-hydroxyethyl methacrylate)," *Macromolecular Rapid Communications*, vol. 30, pp. 126-132, 2009.

[8] E. Radeva, K. Kolentsov, L. Yourukova, D. Zhechev, and E. Dimova, "Optical and photoluminescent properties of plasma polymer films used in

electroluminescent display structures," *Journal of Physics and Chemistry of Solids*, vol. 70, pp. 169-172, 2009.

[9] M. M. Hossain, J. Mussig, A. S. Herrmann, and D. Hegemann, "Ammonia/Acetylene Plasma Deposition: An Alternative Approach to the Dyeing of Poly(ethylene terephthalate) Fabrics at Low Temperatures," *Journal of Applied Polymer Science*, vol. 111, pp. 2545-2552, 2009.

[10] I. Blaszczyk-Lezak, F. J. Aparicio, A. Borras, A. Barranco, A. Alvarez-Herrero, M. Fernandez-Rodriguez, and A. R. Gonzalez-Elipe, "Optically Active Luminescent Perylene Thin Films Deposited by Plasma Polymerization," *Journal of Physical Chemistry C*, vol. 113, pp. 431-438, 2009.

[11] A. M. Lyakhovich, V. I. Kodolov, and M. A. Shirobokov, "The mechanism of formation of polymer films from heptane in a low-temperature, low-pressure plasma," *High Energy Chemistry*, vol. 42, pp. 492-497, 2008.

[12] X. Y. Zhao, M. Z. Wang, Z. Wang, and B. Z. Zhang, "Structural and dielectric properties of conjugated polynitrile thin films deposited by plasma polymerization," *Thin Solid Films*, vol. 516, pp. 8272-8277, 2008.

[13] V. Cech, J. Zemek, and V. Perina, "Chemistry of Plasma-Polymerized Vinyltriethoxysilane Controlled by Deposition Conditions," *Plasma Processes and Polymers*, vol. 5, pp. 745-752, 2008.

[14] B. Thierry, M. Jasieniak, L. de Smet, K. Vasilev, and H. J. Griesser, "Reactive epoxy-functionalized thin films by a pulsed plasma polymerization process," *Langmuir*, vol. 24, pp. 10187-10195, 2008.

[15] K. Vasilev, L. Britcher, A. Casanal, and H. J. Griesser, "Solvent-induced porosity in ultrathin amine plasma polymer coatings," *Journal of Physical Chemistry B*, vol. 112, pp. 10915-10921, 2008.

[16] S. J. Cho, I. S. Bae, Y. S. Park, B. Hong, W. Park, S. C. Park, and J. H. Boo, "The characteristics of organic-inorganic hybrid low-k thin films by PECVD," *Surface & Coatings Technology*, vol. 202, pp. 5654-5658, 2008.

[17] Y. S. Lin and C. L. Chen, "Plasma polymerization of organovanadium oxides onto flexible PET/ITO substrates for flexible electrochromic devices," *Plasma Processes and Polymers*, vol. 5, pp. 471-481, 2008.

[18] C. Yu, S. C. Wang, M. Sosnowski, and Z. Iqbal, "Plasma-enhanced chemical vapor deposition of polyperinaphthalene thin films," *Synthetic Metals*, vol. 158, pp. 425-429, 2008.

[19] D. Bhattacharyya, W. J. Yoon, P. R. Berger, and R. B. Timmons, "Plasma-polymerized multistacked organic bipolar films: A new approach to flexible high-k dielectrics," *Advanced Materials*, vol. 20, pp. 2383-+, 2008.

[20] Y. Yuan, C. S. Liu, and M. Yin, "Plasma polymerized n-butyl methacrylate coating with potential for re-endothelialization of intravascular stent devices," *Journal of Materials Science-Materials in Medicine*, vol. 19, pp. 2187-2196, 2008.

[21] G. J. Cruz, J. Morales, and R. Olayo, "Films obtained by plasma polymerization of pyrrole," *Thin Solid Films*, vol. 342, pp. 119-126, 1999.

[22] R. K. John and D. S. Kumar, "Structural, electrical, and optical studies of plasma-polymerized and iodine-doped poly pyrrole," *Journal of Applied Polymer Science*, vol. 83, pp. 1856-1859, 2002.

[23] G. J. Cruz, J. Morales, M. M. CastilloOrtega, and R. Olayo, "Synthesis of polyaniline films by plasma polymerization," *Synthetic Metals*, vol. 88, pp. 213-218, 1997.

[24] N. V. Bhat and D. S. Wavhal, "Preparation and characterization of plasma-polymerized thiophene films," *Journal of Applied Polymer Science*, vol. 70, pp. 203-209, 1998.

[25] J. G. Wang, K. G. Neoh, and E. T. Kang, "Comparative study of chemically synthesized and plasma polymerized pyrrole and thiophene thin films," *Thin Solid Films*, vol. 446, pp. 205-217, 2004.

[26] K. Hosono, I. Matsubara, N. Murayama, W. Shin, and N. Izu, "Effects of discharge power on the structure and electrical properties of plasma polymerized polypyrrole films," *Materials Letters*, vol. 58, pp. 1371-1374, 2004.

[27] R. Dagostino, F. Cramarossa, and F. Illuzzi, "Mechanisms of Deposition and Etching of Thin-Films of Plasma-Polymerized Fluorinated Monomers in Radiofrequency Discharges Fed with C2f6-H2 and C2f6-O2 Mixtures," *Journal of Applied Physics*, vol. 61, pp. 2754-2762, 1987.

[28] D. S. Kumar and M. G. K. Pillai, "Conduction mechanism in plasma polymerized lemongrass oil films," *Thin Solid Films*, vol. 353, pp. 249-253, 1999.

[29] D. S. Kumar, K. Nakamura, S. Nishiyama, H. Noguchi, S. Ishii, K. Kashiwagi, and Y. Yoshida, "Electrical and optical properties of plasma polymerized eucalyptus oil films," *Journal of Applied Polymer Science*, vol. 90, pp. 1102-1107, 2003.

[30] M. V. Jacob, personal communication.

[31] A. Shukla and A. K. Srivastava, "Terpolymerization of linalool, styrene, and methyl methacrylate: Synthesis, characterization, and a kinetic study," *Polymer-Plastics Technology and Engineering*, vol. 41, pp. 777-793, 2002.

[32] C. Easton, "Fabrication of Novel Electronic Materials from Australian Natural Resources," in *Electrical and Electronic Engineering*, vol. Bachelor of Engineering. Townsville: James Cook University, 2005.

[33] G. Maier, "Low dielectric constant polymers for microelectronics," *Progress in Polymer Science*, vol. 26, pp. 3-65, 2001.

[34] I. S. Bae, C. K. Jung, S. H. Jeong, S. J. Cho, Y. J. Yu, J. G. Kim, and J. H. Boo, "Comparison of their electrical, optical, and electrochemical properties of as-grown plasma polymerized organic thin films by PECVD," *Thin Solid Films*, vol. 515, pp. 407-410, 2006.

[35] U. Gubler, M. Raunhardt, and A. Stump, "Measurement technique for thermal conductivity of thin polymer films," *Thin Solid Films*, vol. 515, pp. 1737-1740, 2006.

[36] K. S. Siow, L. Britcher, S. Kumar, and H. J. Griesser, "Plasma methods for the generation of chemically reactive surfaces for biomolecule immobilization and cell colonization - A review," *Plasma Processes and Polymers*, vol. 3, pp. 392-418, 2006.

[37] R. Shellie, L. Mondello, P. Marriott, and G. Dugo, "Characterisation of lavender essential oils by using gas chromatography-mass spectrometry with correlation of linear retention indices and comparison with comprehensive two-dimensional

gas chromatography," *Journal of Chromatography A*, vol. 970, pp. 225-234, 2002.

[38] T. J. Morgan, W. E. Morden, E. Al-Muhareb, A. A. Herod, and R. Kandiyoti, "Essential oils investigated by size exclusion chromatography and gas chromatography-mass spectrometry," *Energy & Fuels*, vol. 20, pp. 734-737, 2006.

[39] R. Shellie, P. Marriott, and C. Cornwell, "Characterization and comparison of tea tree and lavender oils by using comprehensive gas chromatography," *Hrc-Journal of High Resolution Chromatography*, vol. 23, pp. 554-560, 2000.

CHAPTER 2 THIN FILM FABRICATION

A thin film fabrication facility was established within the Electronic Materials Research Lab (James Cook University) to fabricate plasma polymer thin films from LAEO. This chapter presents an introductory paper describing the experimental apparatus employed and the initial characterisation results. The paper forms the basis for later chapters on fabrication and characterisation of the LAEO based polymer. In later chapters, the deposition process is further optimised to customise the properties of the resultant polymers.

2.1 FABRICATION OF A NOVEL ORGANIC POLYMER THIN FILM

Construction of the thin film fabrication facility and initial characterisation results for the polymer derived from LAEO are presented in this paper. The experimental apparatus included a custom made glass polymerisation cylindrical tube, RF generator, matching network, copper electrodes, double stage rotary vacuum pump and gauge. The properties of the LAEO based polymer film fabricated at an RF power of 25 W were examined using a scanning electron microscope (SEM). Samples were characterised using spectroscopic ellipsometry. The deposition rate was also examined. “Fabrication of a novel organic polymer thin film” (Pub. 1.) is published in Thin Solid Films (Elsevier). This paper involved collaboration with Prof. Christopher Berndt.

FABRICATION OF A NOVEL ORGANIC POLYMER THIN FILM

M. V. Jacob, C. D. Easton, G. S. Woods and C. C. Berndt

Electronic Material Research Lab., School of Engineering, James Cook University,

Townsville QLD 4811 AUSTRALIA.

Email: Mohan.Jacob@jcu.edu.au

Abstract

Fabrication of organic polymer thin films and organic semiconductors are critical for the development of sophisticated organic thin film based devices. Radio Frequency plasma polymerisation is a well developed and widely used fabrication technique for polymer thin films. This paper describes the fabrication of an organic polymer thin film from a monomer based on Lavandula angustifolia. Several polymer thin films were manufactured with thicknesses ranging from 200 nm to 2400 nm. The energy gap of the polymer thin film was measured to be 2.93 eV. The refractive index and extinction coefficient was determined to be 1.565 (at 500 nm) and 0.01 (at 500 nm) respectively. The organic polymer thin film demonstrates the possibility of an environmentally friendly, cost effective organic semiconductor.

Keywords: thin film polymer, plasma polymerisation, organic semiconductor.

1. Introduction

Advancement in thin film technology has been a prime area of research during the last few decades. Even though the first organic semiconductor (Violanthrone) was discovered in 1954 [1], it was not until the Nobel prize in Chemistry was awarded in 2000 for the discovery of conducting plastics that significant research was performed in this field. Recently increased interest in organic thin film materials has arisen due to their extensive applications in the fields of mechanics, flexible electronics and optics [2, 3]. Polymer organic thin films are employed typically in microelectronics and have been used in a wide variety of applications such as perm selective membranes and protective coatings; as well as electrical, optical and biomedical films [4-9]. Employment of polymer thin films as interlayer dielectrics is another application due to their low dielectric constant.

Usually physical vapour deposition and chemical vapour deposition (CVD) are used to prepare thin films. Plasma polymerization, which is a luminous CVD process, is often used to make polymer thin films [10]. The plasma polymerization may also be termed as a "chemical glow discharge" since the polymers are deposited as a thin film onto surfaces in the immediate environment of a glow discharge of the constituent organic gases. Plasma polymerization is an important technique for fabricating thin polymer films since it may be employed for almost any organic vapour [4]. Plasma polymerisation results in high quality thin films that have demonstrated desirable properties including generally being homogenous, pin hole free, chemically inert, insoluble, mechanically tough and thermally stable [11]. The quality of the film can be controlled by adjusting instrument parameters such as monomer flow rate, current density, Radio Frequency (RF) power and vacuum pressure. However, the implementation of devices based on organic thin films has been hampered by poor thermal and chemical stabilities, as well as poor mechanical properties [7]. There remain many challenges in developing polymer thin films of high quality for implementation in electronic and optical applications.

Although plasma polymerization occurs predominantly in the glow region, the volume of glow is not always the same as the volume of the reactor. Both volume of glow discharge and the intensity of the glow depend on the discharge mode, the discharge power and the pressure of the system. The power input employed in plasma

polymerization initiates and sustains the plasma, and also leads to fragmentation of the monomer. An increase in the applied voltage between two parallel plate electrodes will eventually lead to an abrupt increase in current due to breakdown of the gases between the electrodes [8]. Therefore, the plasma is a direct consequence of the gas ionisation between the electrodes in the reactor. Under plasma conditions, the monomer molecules undergo fragmentation and deposit as polymer molecules, and a non-polymer forming by-product such as hydrogen gas is evolved. Within the present work we harness this principle in a controlled fashion to deposit a polymer precursor that results in predicable physical properties.

Plasma polymers do not exhibit regularly repeating units; the chains are branched and are randomly terminated with a high degree of crosslinking. They adhere well to solid surfaces. Pyrolysis results of plasma-polymerized organosilicones [12] suggest a cationic oligomerization from the electron bombardment of the monomer followed by UV initiated crosslinking in the solid phase to produce the final product. Chemical reactions that occur under plasma conditions are generally very complex and nonspecific in nature. Glow discharge polymerization of organic compounds proceed by the free radical mechanism [5, 13-15] and the extent of ionization is small. The combination and recombination of these radicals form high molecular weight compounds that are polymeric in character. The free radicals that are trapped in these films continue to react and change the polymer network over time. Since radicals are formed by fragmentation of monomer, some elements and groups may be absent in the resulting polymer. Crosslinking reactions occur on the surface or in the bulk of the newly forming plasma polymer between oligomers. The film may also change due to reaction with oxygen and water vapor in the atmosphere.

The polymer deposition rate depends linearly on the current density [16]. The minimum power necessary for the plasma polymerization of a given monomer differs significantly between materials because the discharge power needed to initiate a glow discharge varies for each monomer. The crosslinking in a plasma polymer increases with the intensity and energy of bombarding ions. If the interelectrode distance is too large, then, at a given applied potential, the local electric field in the plasma will be too low to

deliver sufficient energy to the electrons. The atoms in a vacuum travel in straight lines; thus, if there is residual gas in the chamber then the atoms will collide with the gas and lose energy as heat. At higher pressures, the collisions will cause atoms to condense in air before reaching the substrate surface; thereby giving rise to powder deposits.

The preparation and properties of plasma polymerized thin films based on aniline, pyrrole, thiophene etc. have been studied previously [17-21]. The literature reports on the growth of such thin films and the reaction conditions. However, reports on employing RF techniques for the preparation of thin films based on essential oils are rare [22]. In this work we have used an organic oil, specifically *Lavandula angustifolia* as the monomer and a polymer thin film has been fabricated from this natural material. Furthermore, we have characterized the so-formed thin films with regard to optical and electrical properties.

2. Experiments

A schematic of the experimental arrangement used to fabricate the polymer thin films is shown in Fig. 1 where a custom-made RF plasma polymerization cell is the central component. An ultrasonically clean glass substrate is placed between the electrodes, Fig. 1. A rotary vacuum pump has been used to obtain a pressure of 300 mT. The tube is initially flushed with argon gas and the gas was not used during deposition. An RF generator operating at 13.56 MHz delivers RF energy of 25 W into the chamber using capacitive coupling, which has been attained by means of external copper electrodes separated by a distance of 11 cm. The thin film is deposited at room temperature, a pressure of 300 mTorr and 25W RF power. Five millilitre of the monomer is used every time and the vapours of the monomer are released gradually into the chamber. The rate of the monomer flow is controlled by using a vacuum stop cock so that the glow discharge is maintained. Optimisation of the deposition conditions was performed by altering; i) the distance between the monomer outlet and the electrodes, ii) the distance between the electrodes, iii) the pressure and iv) RF power. These parameters were varied to obtain transparent, smooth and uniform thin film thickness across the substrate of dimensions 25 mm × 75 mm.

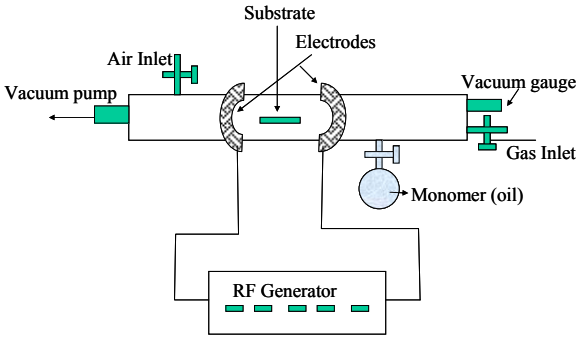

Figure 1: RF plasma polymerization experimental arrangement.

3. Results and Discussion

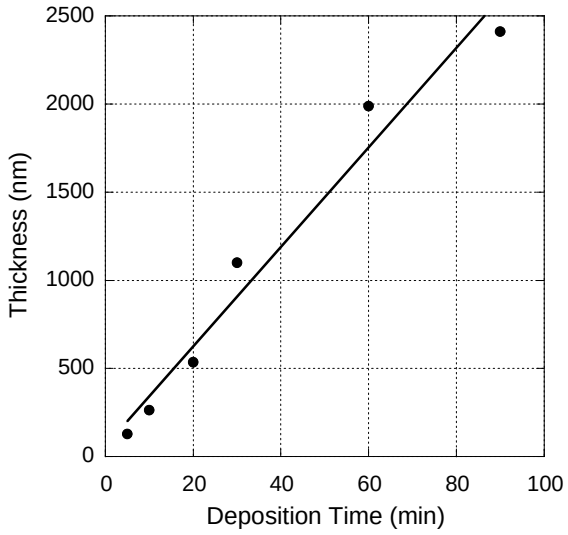

Figure 2: Thickness of *Lavandula angustifolia.* thin film as a function of deposition time

We have polymerised the *Lavandula angustifolia* monomer under RF glow discharge and the resulting polymers were deposited on to a glass substrate. A spectroscopic technique was implemented to measure the thin film thickness. The thickness of the film was studied as a function of deposition time, as shown in Fig. 2. This study demonstrated that a film thickness of 200 nm could be achieved in 5 minutes. The rate of deposition could be increased by adjusting the deposition conditions that enables the rapid growth of thin films in a short period of time. Under the selected deposition conditions the film thickness could be controlled by changing the deposition time. The

maximum deposition time we have used is 90 minutes and the film thickness was 2400 nm. Scanning Electron Microscopy (SEM *JEOL JSM-5410LV*) was employed to investigate the surface morphology. The surface as shown in Fig. 3 is smooth and pinhole free; thereby explicitly implying that polymers fabricated using this technique are suitable for electrical and optical applications.

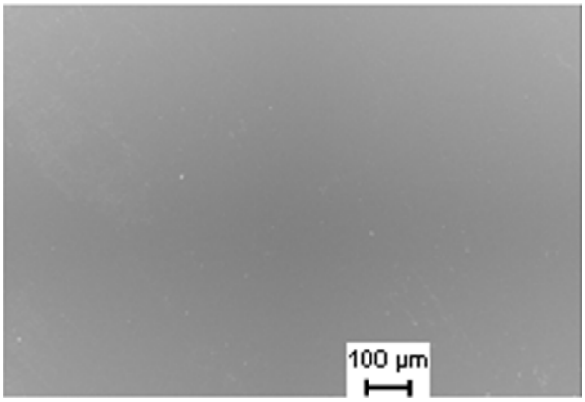

Figure 3: SEM picture of film fabricated at 25 W, scale = 100 µm. The coating is quite featureless with a smooth surface and few defects.

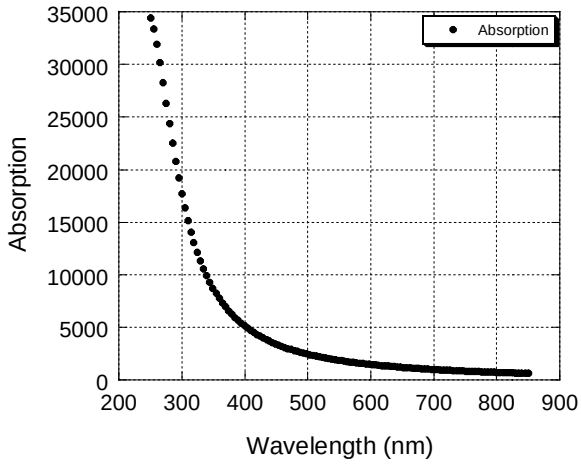

Figure 4: Absorption as a function of Wavelength measured using the ellipsometric technique.

Spectroscopic ellipsometry uses polarized light to characterize thin films and is very effective in finding the energy gap, thickness, refractive index and extinction coefficient

of the sample. When subjected to polarized light, an absorbing material will absorb and reflected parts of the light energy. Employing the use of the TFProbe SE Variable Angle Spectroscopic Ellipsometer (*Angstrom Sun Technologies Inc.*) the optical properties of the sample were investigated. The sample under test was deposited at a RF power of 25 W for 30 mins on a glass substrate. The thickness of the film was 1370 nm. The optical absorption of the sample is shown in Fig. 4.

The refractive index and extinction coefficient of the material was studied in the wavelength range of 250 nm to 850 nm (Fig. 5). The refractive index and extinction coefficient values range from 1.635 to 1.540 and 0.070 to 0.005 respectively. The refractive index is slightly above that of glass; however dopants could be used to decrease the refractive index so that the thin film could be used for antireflection applications. The permittivity of the sample was also studied to determine the suitability of using the sample at RF and microwave frequencies. The complex permittivity values are shown in Fig. 6. The real part of permittivity (k) is between 2.37 and 2.67 in the wavelength region 400 nm to 1100 nm and, hence, it is a potential low-k material. The permittivity values are also verified at microwave frequencies (results not shown here).

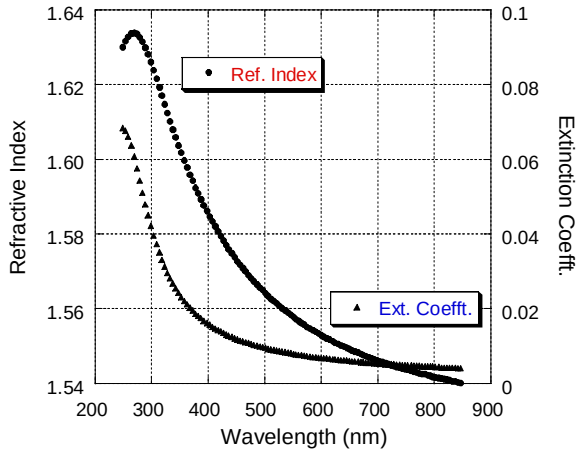

Figure 5: Refractive index and extinction coefficient as a function of wavelength measured using the ellipsometric technique.

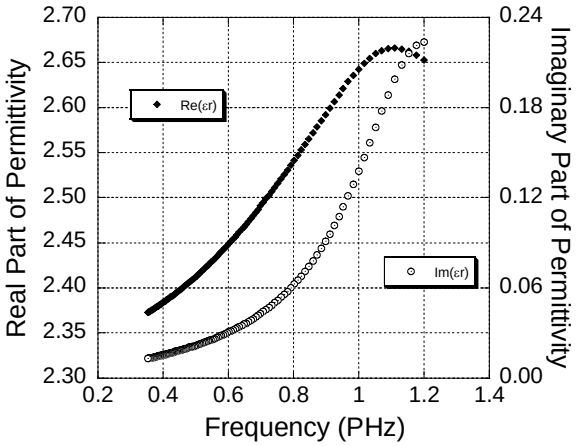

Figure 6: Real and Imaginary Part of Permittivity as a function of Frequency measured using the ellipsometric technique.

The energy gap of the polymer thin film is 2.93 eV and lies within the band gap of semiconductors. Therefore, organic polymer thin films derived from *Lavandula angustifolia* are potential candidates for implementation as organic semiconducting devices or circuits. The properties of the plasma polymerised thin films can be altered by changing the deposition conditions such as RF power, pressure and presence of inert gas. These conditions will be varied to engineer the optical and dielectric properties of the material. In addition, doping materials can be employed to alter the electrical conductivity. Different applications need specific requirements of the properties, which can be obtained by altering the deposition conditions so that particular functionalities can be addressed.

4. Conclusions

A low permittivity polymer thin film is fabricated from a monomer based on *Lavandula angustifolia* using RF plasma polymerization technique. The energy gap of the thin film is estimated using ellipsometry as 2.93 eV. The measured refractive index and real part of permittivity is 1.56 and 2.42 at 500 nm. The film thickness can be varied from 200 nm to 2400 nm by varying the deposition time. The fabricated transparent thin film could be a potential entrant in many electrical and optical applications. More studies will be carried out to engineer the optical properties and to reduce the energy gap of the material so that the polymer could be used in many organic semiconductor and organic

polymer applications such as flexible displays, photoelectric applications and RF identification tags.

Acknowledgements

This project is funded by RIRDC and James Cook University CDG grant and the support is greatly acknowledged. Authors are also grateful to support obtained under ARC Discovery Project DP0449996. CDE is grateful to the APA and RIRDC Scholarship.

References

[1] H. Inokuchi, Org. Electron. 7 (2006) 62.

[2] A. B. Gil'man, A. I. Drachev, High Energy Chem. 40 (2006) 70.

[3] Z. V. Vardeny, A. J. Heeger, A. Dodabalapur, Synth. Met. 148 (2005) 1.

[4] A. Hiratsuka, I. Karube, Electroanalysis 12 (2000) 695.

[5] S. Gaur, G. Vergason, in: Proceedings of the Society of Vacuum Coaters 43rd Annual Technical Conference, Denver, U.S.A, April 15–20, 2000, p.353.

[6] J. H. Burroughes, D. D. C. Bradley, A. R. Brown, R. N. Marks, K. Mackay, R. H. Friend, P. L. Burns, A. B. Holmes, Nature 347 (1990) 539.

[7] F. F. Shi, Surf. Coat. Technol. 82 (1996) 1.

[8] Y. Osada, H. Biederman, Plasma Polymerization Processes, Elsevier Science Pub., New York ,1992

[9] K. J. Kitching, V. Pan, B. D. Ratner, in: H. Biederman (Ed.), Plasma Polymer Films, Imperial College Press, London 2004, p. 325.

[10] H. Yasuda, Q. S. Yu, Plasma Chem. Plasma Process. 24 (2004) 325.

[11] U. S. Sajeev, C. J. Mathai, S. Saravanan, R. R. Ashokan, S. Venkatachalam, M. R. Anantharaman, Bull. Mater. Sci. 29 (2006) 159.

[12] M. Gazicki, A. M. Wrobel, and M. Kryszewski, Applied Polymer Symposia, (1984) 1.

[13] H. Yasuda, T. Hsu, J. Polym. Sci., Part A: Polym. Chem. 15 (1977) 81.

[14] L. V. Shepsis, P. D. Pedrow, R. Mahalingam, M. A. Osman, Thin Solid Films 385 (2001) 11.

[15] J. M. Tibbitt, R. Jensen, A. T. Bell, M. Shen, Macromolecules 10 (1977) 647.

[16] T. Willliams, M. W. Hayes, Nature 209 (1966) 769.

[17] G. J. Cruz, J. Morales, R. Olayo, Thin Solid Films 342 (1999) 119.

[18] G. J. Cruz, J. Morales, M. M. CastilloOrtega, R. Olayo, Synth. Met. 88 (1997) 213.

[19] N. V. Bhat, D. S. Wavhal, J. Appl. Polym. Sci. 70 (1998) 203.

[20] J. G. Wang, K. G. Neoh, E. T. Kang, Thin Solid Films 446 (2004) 205.

[21] S. Saravanan, C. J. Mathai, S. Venkatachalam, M. R. Anantharaman, New J. Phys. 6 (2004).

[22] D. S. Kumar, K. Nakamura, S. Nishiyama, H. Noguchi, S. Ishii, K. Kashiwagi, Y. Yoshida, J. Appl. Polym. Sci. 90 (2003) 1102.

CHAPTER 3 CHEMICAL AND SURFACE CHARACTERISATION

Information concerning the molecular and structural composition of a plasma polymer is an essential component to the overall characterisation of the material. Identification of the primary constituents of the monomer and resulting polymer gives an indication of the degree of fragmentation induced during the polymerisation process, in addition to the formation of new chemical structures. Defining the molecular bonds and components such as free radicals present in a polymer allows for the identification of possible stability issues depending on the environment conditions that the polymer is subjected to during implementation and storage. In this chapter, the chemical and surface properties are presented as a paper.

3.1 SURFACE AND CHEMICAL CHARACTERISATION OF POLYLA THIN FILMS FABRICATED USING PLASMA POLYMERISATION

The affect of RF power on the chemical structure and surface properties of the LAEO based polymer was examined in this paper. Chemical characterisation was performed using Fourier transform infrared (FTIR) spectroscopy. Nuclear magnetic resonance (NMR) spectroscopy was employed for the low power samples to complement the FTIR data. An atomic force microscope (AFM) was used to provide information concerning the surface profile of the polymers fabricated at various RF powers. Water contact angle (WCA) data was also obtained to provide information concerning the polarity and stability of the polymer. "Surface and chemical characterisation of polyLA thin films fabricated using plasma polymerisation." (Pub. 3.) is published in Chemical Vapor Deposition (Wiley InterScience). This paper involved collaboration with Prof. Robert Shanks and A/Prof. Bruce Bowden.

SURFACE AND CHEMICAL CHARACTERISATION OF POLYLA THIN FILMS FABRICATED USING PLASMA POLYMERISATION

Christopher D Easton[1], Mohan V Jacob[1]*, Robert A Shanks[2] and Bruce F Bowden[3]

[1]Electronic Materials Research Lab, School of Engineering, James Cook University, Townsville, 4811, Australia

[2]Applied Sciences, RMIT University, GPO Box 2476V, Melbourne, 3001, Australia

[3]School of Pharmacy and Molecular Sciences, James Cook University, Townsville, 4811, Australia

*Corresponding author. Tel.: +61 7 47814379; fax: +61 7 47815177; Email: Mohan.Jacob@jcu.edu.au

Abstract

Polymer thin films derived from the essential oil of *Lavandula angustifolia* (LA) were fabricated using plasma polymerisation and their surface and chemical characteristics investigated. The surface morphology of the polyLA films was examined using an atomic force microscope (AFM). The polymer was found to be uniform and pinhole free, where the average roughness of the films was found to be less than a nanometre and independent of the RF power employed during fabrication. Fourier transform infra-red (FTIR) spectroscopy analysis of the polyLA film was performed. Comparison of the FTIR spectra for polyLA film with that of the starting monomer demonstrated that many of the original functional groups were retained during the polymerisation process. Bands assigned to C=C stretching were lost due to their participation in the polymerisation reactions. A decrease in intensity of most of the remaining bands in the FTIR spectra for the polyLA films was found with increased RF power employed during fabrication. This was attributed to reactions such as dehydration of hydroxyl, cyclisation and aromatisation associated with alkenes. In addition, it was found that the duration of exposure to UV irradiation and ion bombardment had an insignificant affect on the chemical structure of the polyLA film. NMR spectra of the polymer fabricated at

low RF power revealed the presence of aromatics in the chemical structure. Water contact angle measurements demonstrated that the polyLA films ranged from mildly hydrophilic to mildly hydrophobic and were stable while in contact with water.

Keywords: Plasma polymer, FTIR, AFM, Chemical structure, thin films

1. Introduction

Production of polymer thin films from organic materials has recently gained significant attention, in particular for implementation in organic electronics.[1] Plasma polymerisation provides a method for fabricating organic thin films for use in such applications using materials that do not normally polymerise using conventional techniques.[2] Information concerning the molecular and structural composition of a polymer thin film is an essential component to the overall characterisation of the material. Identification of the constitution of the monomer and resulting polymer gives an indication of the degree of fragmentation induced during the polymerisation process.

The chemical components of *Lavandula angustifolia* essential oil (LAEO) are well known and have been identified using gas chromatography.[3-5] LAEO contains a number of components including hydrocarbons, in addition to metabolites that contain ester, ketone and ether groups. The content of these compounds contained in LAEO can vary over a considerable range, however the major components are typically 1,8-cineole (approx. 0.1 – 20 %), linalool (approx. 23 – 57 %) and linalyl acetate (approx. 4 – 35 %).[3]

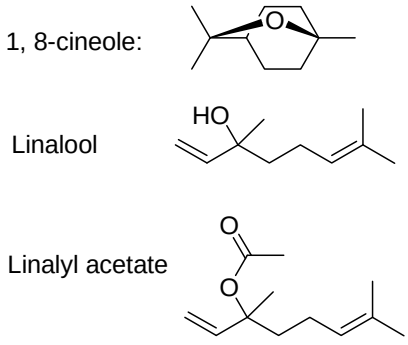

Scheme 1: Major components of LAEO

Recently, fabrication of an organic polymer based on LAEO was reported.[6] These polymer films were fabricated from a natural, non-synthetic source that is environmentally friendly. As outlined in the previous study, the optical properties of these films were promising, with a refractive index and extinction coefficient at 500 nm of 1.565 and 0.01 respectively. It was reported that these polymers possess an optical

band gap value within the range of semiconductors. In addition to the potential electrical and optical applications, this polymer has the potential to be implemented in the biomedical field either as a fouling or non-fouling material depending on its properties.

The aim of this paper is to relate plasma input power with surface morphology, chemical characteristics, and physical properties of thin films derived from LAEO through plasma polymerisation. Herein the LAEO based polymer films will be referred to as PolyLA. An objective will be to obtain images of the surface profile using an atomic force microscope (AFM) and surface roughness that will be quantified using the image analysis software supplied. The effect of RF power and deposition time on the resulting chemical structure of the polymers will be investigated using Fourier transform infra-red (FTIR) spectroscopy. Nuclear magnetic resonance (NMR) spectroscopy will be undertaken to expand further on the polyLA chemical structure, while the physical properties of the surface will be examined via water contact angle measurements.

2. Results and Discussion

2.1 AFM study of polyLA films

AFM images were obtained in semi-contact mode of the polyLA films to provide information of the surface of the polymer and the effect of the deposition parameter RF power. Images of the films fabricated at 25, 40 and 75 W of scan size 1 x 1 μm are presented in Figure 1, Figure 2, and Figure 3 respectively. Scan size of 10 x 10 μm are not shown, however, their information was employed for determination of the average roughness for each film surface (Table 1).

The morphology of the films on a nanometer scale appears to change as a result of a change in the input RF power. For the 25 W treated film, the peaks and corresponding troughs are relatively broad. As RF power is increased however, the peaks become narrower and their number increased. This change in the surface structure however does not have any significant affect on the average roughness. These results demonstrate that the polyLA films are very smooth, uniform, and pinhole free.

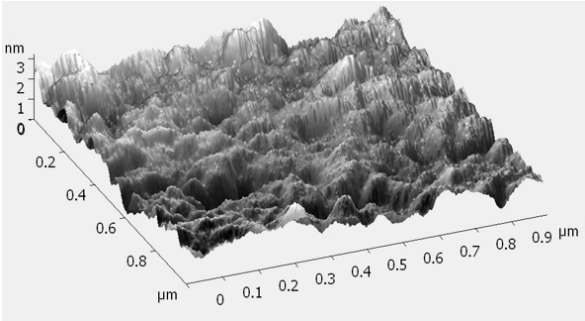

Figure 1: 3D AFM image of polyLA film fabricated at 25 W measuring 1 µm x 1 µm.

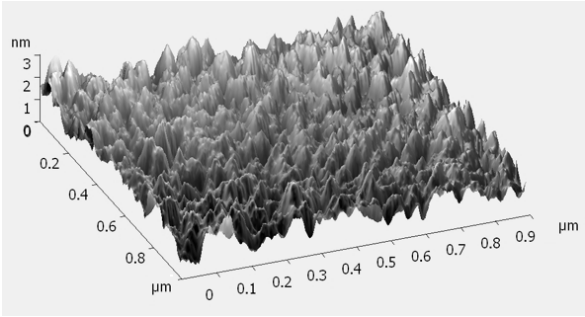

Figure 2: 3D AFM image of polyLA film fabricated at 40 W measuring 1 µm x 1 µm.

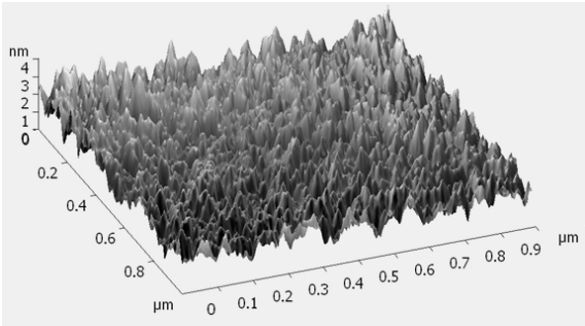

Figure 3: 3D AFM image of polyLA film fabricated at 75 W measuring 1 µm x 1 µm.

Table 1: Average roughness determined for sample fabricated at three different RF power levels; scan area 10 µm.

RF power	Roughness (nm)
25 W	0.418
40 W	0.318
75 W	0.368

2.2 FTIR analysis of polyLA films

2.2.1 Effect of RF power

FTIR spectra of *L. angustifolia* monomer in addition to polyLA films fabricated at various RF powers are presented in Figure 4 with the corresponding FTIR assignments listed in Table 2 based on the peak assignments presented in reference [7]. Considering first the spectrum for the monomer, a broad peak at 3463 cm^{-1} corresponding to an O-H stretch indicates the presence of alcohol. Strong bands related to C=O (1739 cm^{-1}) and C-O (1249 cm^{-1} and 1172 cm^{-1}) indicated stretching of ester groups was present. 1110 cm^{-1} is assigned to a C-O stretch of an ether group. Bands at 3088 cm^{-1} and 1644 cm^{-1} associated with C=C stretching, while 1019, 997, 921, 834, 690 cm^{-1} can be assigned to C-H deformation. Stretching of methyl (2970 cm^{-1} and 2869 cm^{-1}) and methylene (2927 cm^{-1}) groups is indicated by strong bands in the spectrum, in addition to bending (1451 cm^{-1} and 1371 cm^{-1}). The bands present in the FTIR spectrum of the *L. angustifolia* monomer are therefore what were predicted based on the components expected to be present from results obtained using gas chromatography by other authors.[3-5]

Comparing the results for the polyLA films with that of the monomer, it is apparent that upon polymerisation the number of bands in the spectra has reduced. For the film fabricated at the lowest RF power setting (Figure 4(b)), the bands relating to C-H stretching of methyl and methylene appear unaffected by the polymerisation process. C-H bending of methyl groups is still present, however the band for the symmetric bend has reduced in magnitude. The broad peak assigned to O-H stretching is still present, however diminished. The strong band at 1739 cm^{-1} assigned to the ester C=O stretch observed in the monomer is no longer visible, instead a C=O stretch at 1710 cm^{-1} associated with a ketone is now present. It is possible that ester band is still present but obscured by the ketone. The C=O stretch for the ketone was not visible in the monomer, but it is possible that it was obscured by the strong ester band. Bands assigned to C=C are no longer present, in addition to those assigned to C-H deformation. Scission of the carbon double bonds is expected to occur first upon polymerisation as it has the smallest value of dissociation energy of the bonds present in monomer.[8] The retention of C-O bonds in the chemical structure of the polyLA films is an important factor when considering the degradation of the polymer. Polymers containing oxygen are typically

less stable than hydrocarbon polymers, where the dissociation energy of C-O bonds is relatively low, while the lone electron pairs of these bonds can lead to acid/base reactions resulting in new reaction paths.[9]

As the RF power is increased, most bands in the spectra for the polyLA films experience a reduction in magnitude, as indicated in Table 2. Only those assigned to stretching of C-H associated with methyl and methylene appear unaffected by an increase in RF power, in the range studied. Compared to the spectrum for the monomer, it can be concluded that an increase in RF power results in a greater loss of functional groups. This change in FTIR spectra with increase in RF power is attributed to two factors:

a) increased energy input into the plasma system,

b) increased substrate temperature due to RF heating.

The energy input, in this case RF power, is believed to have the greatest influence on the properties of a plasma polymer of all deposition parameters as the magnitude of energy input determines the degree of fragmentation of the monomer.[10] Therefore increasing the RF power will result in an increase of fragmentation of the monomer and a decrease in the intensity of the bands in the measured FTIR spectrum.

During fabrication, the substrate is placed within the glow discharge. Due to its placement within the reactor, the substrate is subjected to a large amount of energy that results in an increase in substrate temperature dependent on the RF power applied. Lopez et al.[11] demonstrated that an increase in substrate temperature will result in a reduction in the retention of the original precursor moieties. This finding was ascribed to an increase in condensation or adsorption of non-excited gaseous species in the deposition region and thus an increase in the concentration of non-fragmented molecules. It has been shown that an increase in substrate temperature can result in a decrease in deposition rate,[12-14] and is the determining factor for producing films at increased deposition times for increased RF powers.

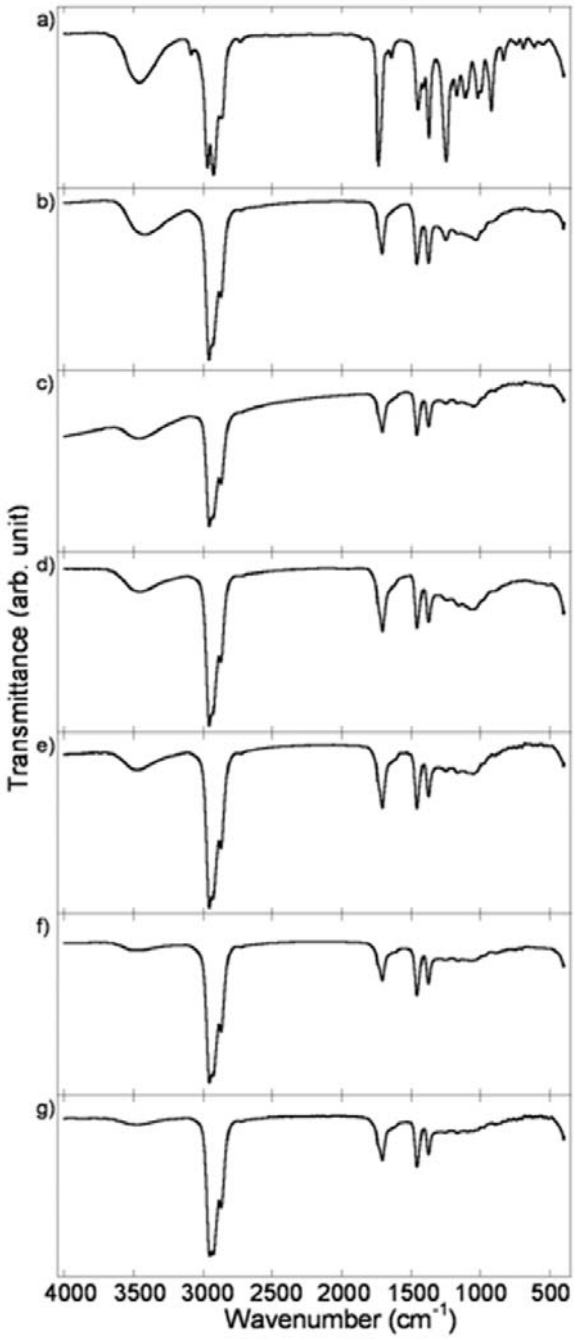

Figure 4: FTIR spectra for a) L. angustifolia monomer, and polyLA films fabricated an at RF power of b) 10 W, c) 20 W, d) 25 W, e) 30 W, f) 50 W, g) 75 W.

Table 2: FTIR assignments for *L. angustifolia* monomer and PolyLA. Vibrational modes: v_a ≡ asymmetrical stretching, v_s ≡ symmetrical stretching, v ≡ stretching, δ_a ≡ asymmetrical bending, δ_s ≡ symmetrical bending.

Wavenumber (cm^{-1})	Relative intensity	Assignment
L. angustifolia monomer:		
3463	Medium (broad)	v(O-H)
3088	Weak	v(C=C)
2970	Very strong	v_a(C-H)
2927	Very strong	v_a(C-H)
2869	Medium	v_s(C-H)
1739	Very strong	v(C=O)
1644	Weak	v(C=C)
1451	Medium	δ_a(C-H)
1371	Strong	δ_s(C-H)
1249	Very strong	v(C-O)
1172	Medium	v(C-O)
1110	Medium	v(C-O)
1019, 997, 921, 834, 690	Medium to small	C-H deformation
Polymer Films:		
~ 3460	Medium to weak[a]	v(OH)
~ 2959	Very strong	v_a(C-H)
2930	Very strong	v_a(C-H)
2873	Medium	v_s(C-H)
1710	Medium[a]	v(C=O)
1460	Medium[a]	δ_a(C-H)
1376	Medium to small[a]	δ_s(C-H)
1248	Small to non-existent[a]	v(C-O)
1162	Very small to non-existent[a]	v(C-O)
1052	Very small to non-existent[a]	v(C-O)

[a] Relative intensity diminishes with increase of RF power

2.2.2 Effect of deposition time

PolyLA films on KBr for the FTIR analysis were fabricated at different deposition times with respect to the RF power employed in order to obtain films of comparable thickness. Casserly et al.[15] in their study of the effect of substrate temperature on the polymerisation of poly(methyl methacrylate) indicated that increased UV irradiation and ion bombardment associated with longer deposition times resulted in loss of functional groups. In order to determine whether deposition time has an affect on

chemical composition of the polyLA films and to confirm the validity of the FTIR analysis presented in section 3.2.1, the effect of deposition time on the chemical structure of polyLA was undertaken. For this study, RF power of 75 W was chosen as the affect of UV irradiation and ion bombardment on the polyLA film should be greatest at the highest RF power level. The FTIR spectra for polyLA films fabricated at 75 W with a deposition time of 10 and 30 min is presented in Figure 5. The FTIR spectra of the polyLA film do not appear to be affected by the length of deposition and thus the duration of exposure of UV irradiation and ion bombardment. The peak and trough seen in the figure at approximately 2350 cm^{-1} is associated with the removal of CO_2 from the spectrum and thus can be ignored.

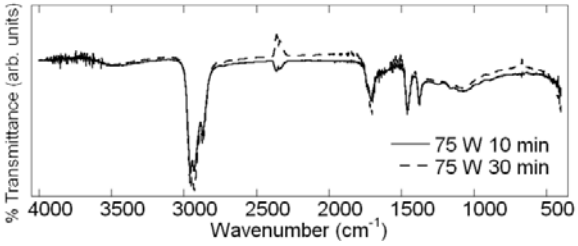

Figure 5: FTIR spectra for polyLA films fabricated at 75W with a deposition time of 10 and 30 min.

2.3 NMR Spectroscopy

NMR analysis was performed on the polyLA sample fabricated at an RF power of 10 W. It was discovered that the polyLA film fabricated at high RF power levels was insoluble in chloroform, indicative of a crosslinked polymer. In addition, the amount of sample required to obtain a clear spectrum meant that numerous samples produced under identical conditions were needed. Therefore, due to these issues only the 10 W sample was analysed.

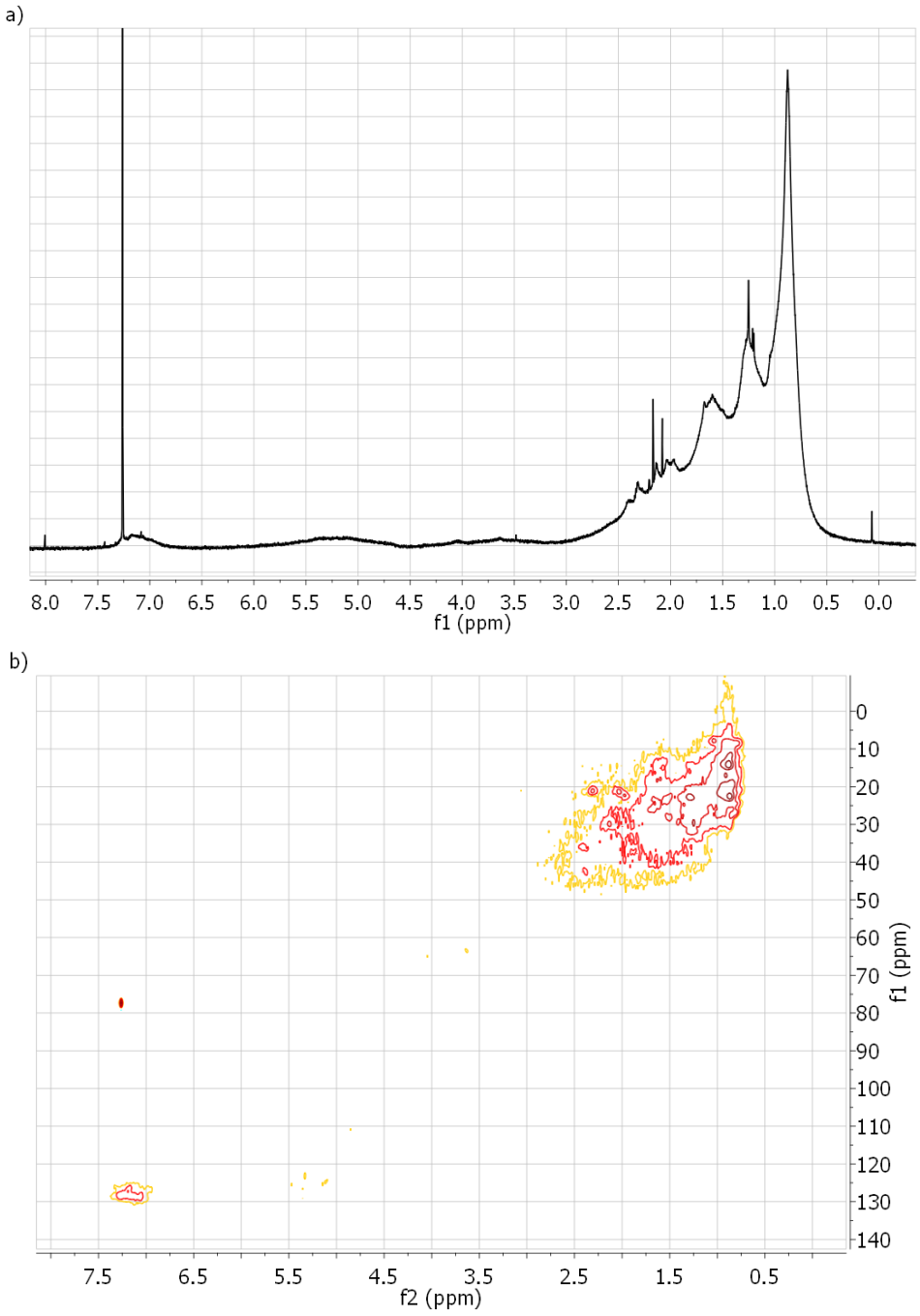

Figure 6: a) 1H-NMR and b) HSQC plots of polyLA sample fabricated at 10 W

The 1H-NMR and heteronuclear single quantum coherence (HSQC) plots of the polyLA sample are presented in Figure 6 a) and b) respectively, where spectra assignments were performed using [16]. The strong peak at 7.26 ppm corresponds to the solvent (residual $CHCl_3$ in the 99.6% chloroform-d) and therefore can be ignored. The large group of

peaks located between approximately 0.5 to 2.5 ppm in the proton spectrum and between 0 to 48 ppm in the ^{13}C spectrum corresponds primarily to acyclic hydrocarbons. For example the strong peak at 0.88 ppm in the 1H-NMR spectrum corresponds to CH_3-C-C. The broad peak centred at approximately 3.6 ppm confirms the presence of oxygen in the film and is allocated to CH_x-OR, where x is 2 or 3. The broad peak centred at approximately 7.2 ppm is assigned to hydrogens on aromatic rings. The presence of aromatics in the polymer is unexpected. FTIR spectra in section 2.2 provided no indication of aromatics in the polymer structure at this power level, and thus the C=C and C=CH stretching signals are assumed to be too weak to be identified with FTIR spectroscopy. In addition, no aromatics were identified in the NMR spectra for the LAEO (data not shown). Therefore these aromatics are formed during the polymerisation process, most likely via dehydration of the linalool hydroxy group, cyclization of the resultant polyene structures and dehydrogenation reactions of six-membered ring structures thus formed or from cineol. The singlets at approximately delta 2.0 and 2.1 are indicative of residual acetate and methyl ketone functionality and hence confirm the 1710 cm^{-1} carbonyl peak observed in the IR spectra.

2.4 Water Contact Angle

The one-touch drop dispenser employed in the KSV 101 system provides neither an advancing nor receding contact angle, but rather the equilibrium contact angle. Equilibrium contact angle values as a function of time have been reported by other authors, including Alexander and Duc.[17] Contact angle values for PTFE (City Plastics Pty Ltd) were measured as a means of verifying the experimental procedure. The data was well represented by a linear fit with equation $y = -0.01x + 119.95$ and $R^2 = 0.97$, where x represents time. At time $x = 0$, the measured water contact angle on PTFE is 119.95º and is comparable to that obtained by Alexander and Duc ($y = -0.05x + 119$), thus confirming the experimental procedure.

Water contact angle data for polyLA films fabricated at various power levels is presented in Figure 7; the error bars in the plot represent the 95% confidence levels at each time interval. An increase in the fabrication RF power results in an increase in the water contact angle. This result compliments the FTIR data where the increase in RF

power results in a decrease in the amount of oxygen present in the sample and as such indicates production of a material that is less polar. The water contact angle of the polyLA film can be tuned to a certain degree with RF power to produce a sample that ranges from weakly hydrophilic to a sample with a weakly hydrophobic surface. It has been demonstrated previously[18] that plasma polymerised films with contact angles between 60 to 90° provide favourable dose response of ^{125}I-protein A uptake to human immunoglobulin G (hIgG). As the contact angles obtained in this work fall within this range, there is the potential to implement the polyLA films as bio reactive surfaces.

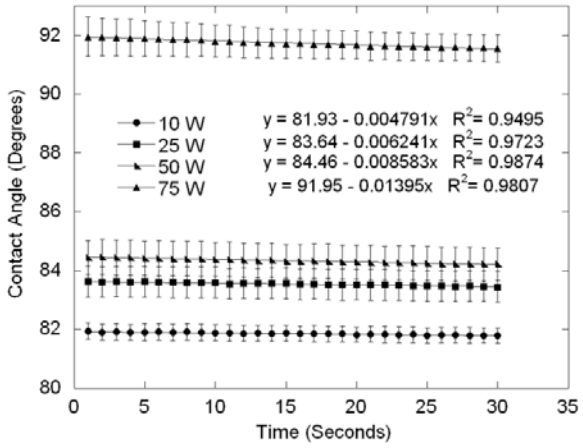

Figure 7: Water contact angle vs. time for polyLA film fabricated at various power levels.

Alexander and Duc[17] measured the rate of decrease in contact angle of water on PTFE as -0.05º s^{-1}, while on poly(acrylic acid) (PAA) the rate was -0.2º s^{-1}. The greater rate of decrease in PAA was attributed to reorientation of functionalities at the water-near surface interface in response to the aqueous environment. Evaporation was considered not to be the cause of the decrease in contact angle with time, while the decrease observed for PTFE was not addressed. In addition, the water contact angle vs. time plots for plasma polymerised acrylic acid-co-1,7-octadiene (PPAAc-co-Oct) samples exhibited two distinct regimes; an initial non-linear decrease followed by a linear rate equal to that measured for PAA. The initial rapid rate of change in contact angle was attributed to the absorption of water by the sample. In this study, the rate of change in water contact angle was -0.01º s^{-1} for PTFE and up to -0.01º s^{-1} for the polyLA samples,

while no initial rapid rate of change in contact angle was measured for the polymer. These results indicate that it is highly unlikely that interactions such as swelling or reorientation of polar groups are occurring at the liquid-solid interface, and thus the polyLA samples are very stable when in contact with water.

3. Conclusion

AFM investigation of the polyLA films demonstrated that the surface roughness is independent of the RF power used during fabrication, with a roughness value in the order of nanometres. The polymer was shown to be very smooth, uniform and pinhole free. FTIR analysis of the *L. angustifolia* monomer demonstrated a number of vibrational modes related to hydrocarbons in addition to ester, ether and alcohol groups. Some of the functional groups observed in the monomer have been retained during the polymerisation process, however C=C was not observed to be present in the FTIR spectra for the polyLA films. An increase in RF power during fabrication results in a reduction of magnitude of the remaining groups except for the bands assigned to stretching of C-H associated with methyl and methylene, which appear unaffected. The diminishing intensity of the FTIR spectra with respect to RF power was attributed to increased fragmentation of the monomer thus reducing the retention of the original constitutes. The deposition time and thus the duration of exposure to UV irradiation and ion bombardment was found to have an insignificant affect on the measured FTIR spectra. NMR spectra was collected for the polyLA sample fabricated at 10 W. The primary hydrocarbon nature of the polymer was confirmed, while the presence of aromatics not seen in the FTIR spectra was identified. Water contact angle was collected for samples fabricated at various power levels. Increasing the RF power resulted in changing the sample from weakly hydrophilic to weakly hydrophobic, while the polyLA samples proved to be stable while in contact with water.

4. Experimental

L. angustifolia monomer obtained from G. R. Davis Pty. Ltd. was used for fabrication of the plasma polymer films using the experimental arrangement outlined in[6] at various RF power levels and deposition times. The polymer films were fabricated at a starting pressure of approximately 250 mT. RF energy (13.56 MHz) was delivered to the

deposition chamber via external copper electrodes separated by a distance of 11 cm. Approximately 5 mL of the monomer is placed into the holder and replaced after each subsequent deposition. Prior to placement of substrate within the polymerisation cell, the monomer inlet is opened briefly to allow the oil to degas. During deposition, the monomer inlet is again opened and the vapour is released into the chamber, where the flow rate is controlled via a vacuum stopcock. The deposition time was adjusted between 15 to 40 min to ensure samples of 1 μm were obtained for the study of the affect of RF power on the resulting chemical structure. Two different types of substrate were employed in this study; glass slides for AFM, and KBr discs were deposited onto directly for the FTIR analysis. The glass slides were cleaned first with a solution of Extran and distilled water, then ultrasonically cleaned for 15 min, rinsed with Propan-2-ol and air-dried. The wet cleaning procedure was not employed for the KBr discs. Prior to fabrication, all substrates were pre-treated with Ar plasma in order to produce an oxygen-free surface.[19]

Analysis of the surface morphology was undertaken at the Advanced Analytical Centre (AAC), James Cook University using the NT-MDT NTEGRA Prima AFM.

FTIR was employed to determine the chemical structure of the polymer thin films (RMIT – Perkin-Elmer Spectrum 2000 FTIR Spectrometer; JCU – Nicolet Maxim). Spectra were obtained in transmission mode in the region of 4000 – 400 cm^{-1}, where 32 scans were acquired for each sample at a resolution of 1 cm^{-1} for the Perkin-Elmer system and approximately 2 cm^{-1} for the Nicolet system. CO_2 and H_2O were accounted for in the spectra by the background substraction procedure, where the background was recorded under the same atmospheric conditions.

The Bruker 600 MHz Avance NMR spectrometer, fitted with a cryoprobe, and located at the Australian Institute of Marine Science (AIMS) Townsville was used to obtain the NMR spectra of the polyLA sample fabricated at 10 W. Samples were fabricated at identical conditions on glass which were removed by scraping off the polymer using a blade and subsequent dissolution in 99.6% chloroform-d from Sigma-Aldrich.

Contact angle measurements were performed using the KSV 101 system supplied by KSV Instruments Ltd. The setup includes a CCD camera, sample stage, syringe and one-touch drop dispenser. The height of each drop is confirmed using the CCD camera prior to each measurement to ensure consistency in drop volume. Drop volume of approximately 8 μL was employed, where 6 to 8 drops were used for each measurement. Double distilled water produced using the Labglass Delta system (Labglass Pty Ltd) was employed for the measurements. Using the one-touch drop dispenser, the drop is placed on the surface, triggering the software (KSV CAM software) to begin recording. An image is recorded every second for 30 in order to monitor the contact angle as a function of time. The image processing software was used to determine the contact angle by fitting the measured drop profile with the Young-Laplace equation.

Acknowledgements

The authors are grateful to the financial support provided under the RIRDC and ARC LIEF and DP schemes. CDE is grateful to the APA and RIRDC scholarships. We are thankful to Dr. B. Rengarajan (RMIT) for help in obtaining the FTIR spectra.

References

[1] Z. V. Vardeny, A. J. Heeger, A. Dodabalapur, *Synth. Met.* **2005**, *1*, 1.

[2] A. Hiratsuka, I. Karube, *Electroanalysis* **2000**, *9*, 695.

[3] R. Shellie, L. Mondello, P. Marriott, G. Dugo, *J. Chrom.* **2002**, *1-2*, 225.

[4] T. J. Morgan, W. E. Morden, E. Al-Muhareb, A. A. Herod, R. Kandiyoti, *Energy & Fuels* **2006**, *2*, 734.

[5] R. Shellie, P. Marriott, C. Cornwell, *J. High Resolut. Chrom.* **2000**, *9*, 554.

[6] M. V. Jacob, C. D. Easton, G. S. Woods, C. C. Berndt, *Thin Solid Films* **2008**, *12*, 3884.

[7] J. Coates, in: *Encyclopedia of Analytical Chemistry* (Eds: R. A. Meyers), John Wiley & Sons Ltd, Chichester **2000**, p. 10815.

[8] A. Hollander, J. Thome, in: *Plasma Polymer Films* (Eds: H. Biederman), Imperial College Press, London **2004**, p. 248.

[9] A. Hollander, J. Thome, in: *Plasma Polymer Films* (Eds: H. Biederman), Imperial Collage Press, London **2004**, p. 252.

[10] H. Yasuda, *Luminous Chemical Vapor Deposition and Interface Engineering*, Marcel Dekker, New York **2005**.

[11] G. P. Lopez, B. D. Ratner, *Langmuir* **1991**, *4*, 766.

[12] A. v. Keudell, W. Moller, *J. Appl. Phys.* **1994**, *12*, 7718.

[13] H. Kersten, H. Deutsch, H. Steffen, G. M. W. Kroesen, R. Hippler, *Vacuum* **2001**, *3*, 385.

[14] D. Hegemann, M. M. Hossain, E. Korner, D. J. Balazs, *Plasma Processes. Polym.* **2007**, *3*, 229.

[15] T. B. Casserly, K. K. Gleason, *Chem. Vap. Deposition* **2006**, *1*, 59.

[16] R. M. Silverstein, F. X. Webster, D. J. Kiemle, *Spectrometric Identification of Organic Compounds*, John Wiley & Sonds, Inc., NJ **2005**.

[17] M. R. Alexander, T. M. Duc, *Polymer* **1999**, *20*, 5479.

[18] S. Kurosawa, N. Kamo, N. Minoura, M. Muratsugu, *Mater. Sci. Eng. C* **1997**, *4*, 291.

[19] M. C. Kim, S. H. Cho, J. G. Han, B. Y. Hong, Y. J. Kim, S. H. Yang, J. H. Boo, *Surf. Coat. Technol.* **2003**, 595.

CHAPTER 4 ELECTROMAGNETIC CHARACTERISATION

This chapter presents two papers that outline the electromagnetic characterisation of the LAEO based polymer films. The first paper provides a comprehensive review of the optical properties of the thin films, expanding on the work presented in Chapter 2 (see Section 4.1). The second paper presents a new technique for obtaining the dielectric properties of low permittivity thin films at microwave frequencies and the results obtained for the LAEO based polymer (see Section 4.2).

4.1 Optical Characterisation of Radio Frequency Plasma Polymerised Lavandula Angustifolia Essential Oil Thin Films

This paper describes the optical properties of the LAEO based polymers fabricated at various input RF power levels and thicknesses. These results expand on the properties obtained in Chapter 2 in order to provide a comprehensive optical characterisation of the polymer. The characterisation was performed employing spectroscopic ellipsometry and UV-Vis spectrometry. Properties that were examined included the refractive index, extinction coefficient, thickness, surface roughness, optical anisotropy, and optical band gap. A detailed review of the spectroscopic ellipsometry methodology is also provided, in addition to the optical models employed. "Optical characterisation of radio frequency plasma polymerised *Lavandula angustifolia* essential oil thin films" (Pub. 4.) is published in Thin Solid Films (Elsevier).

OPTICAL CHARACTERISATION OF RADIO FREQUENCY PLASMA POLYMERISED *LAVANDULA ANGUSTIFOLIA* ESSENTIAL OIL THIN FILMS

C. D. Easton and M. V. Jacob*

Electronic Materials Research Lab, School of Engineering, James Cook University, Townsville QLD 4811, Australia

*Corresponding author. Tel.: +61 7 47814379; fax: +61 7 47815177; Email: Mohan.Jacob@jcu.edu.au

Abstract

Optically transparent RF plasma polymerised thin films were fabricated from *Lavandula angustifolia* essential oil under varying RF power levels and their optical properties investigated. The refractive index, extinction coefficient, absorption and optical band gap of the thin films in addition to their thickness and roughness were investigated using the spectroscopic ellipsometry and UV-Vis spectroscopy in the wavelength range 200 – 1000 nm (6.199–1.239 eV). For films fabricated under the RF power from 10W to 75W, the refractive index values vary from 1.530 to 1.543 at 500nm. Even though the refractive index is unaffected by the RF power, the optical band gap tends to decrease with increasing RF power, with 2.75 at 10 W and 2.34 at 75 W.

Keywords: Polymer; Thin film; Plasma polymerisation; Optical properties.

1. Introduction

In recent years the interest in polymer thin films derived from organic materials has increased significantly, in particular for use in organic electronics [1]. Thin organic polymer layers have the potential to be implemented in many electrical, optical and biomedical applications. Examples of such applications include perm selective membranes, protective barriers, anti-reflective coatings, light emitting diodes, biochemical and gas sensors just to name a few [2-7].

Traditional methods of polymer synthesis include chemical and electrochemical polymerisation; however plasma polymerisation has become a respective method for producing organic films. The phenomena of plasma polymerisation has been known since 1874, however polymers produced by this technique were initially considered an undesirable by-product and as such significant attention was not paid until the 1950's [8]. The appeal of this technique lies in the fact that it allows for the polymerisation of organic materials that do not normally polymerise using conventional procedures [2]. Polymers produced using plasma polymerisation are typically of a high quality with desirable properties including being homogenous, pin hole free, insoluble and chemically and physically stable [9, 10].

Optical characterisation can provide an insight into the possible applications of the material and can be used to establish other important design and optimisation parameters. The refractive index, extinction coefficient and transparency of a material can give an indication of its usefulness as a protective coating or in optoelectronic applications. The optical band gap, E_O, of a material is a significant parameter for describing the electronic structure of amorphous materials [11]. Measurement of E_O provides an indirect method of estimating the energy gap (E_g) of the material. However E_O will underestimate the value of the energy gap by the width of the range of localised states in the valence or conduction band [12]. The width of these localised states and thus the difference between E_O and E_g is determined by the degree of disorder of the polymer, where the degree of disorder in plasma polymers is typically high. The ability to tailor the value of E_O of a material is an important attribute as it can provide flexibility when considering the application of a polymer thin film. An example of this

is allowing for the choice of wavelength of light and thus colour emitted from a diode [13].

Recently, the fabrication of an organic polymer from *Lavandula angustifolia* essential oil was reported [14], with a detailed examination of the surface and chemical characteristics of the material described previously [15]. The chemical composition of this monomer has been described previously using gas chromatography techniques [16, 17]. The *Lavandula angustifolia* essential oil contains a large number of hydrocarbon based components, and metabolites containing carbonyl and hydroxyl groups. This essential oil is a non-synthetic, environmentally friendly resource and hence an advantage of using it as a monomer is that the fabrication procedure and resulting polymer will also be environmentally friendly. It was demonstrated that the polymer is uniform and pinhole free, exhibiting a smooth surface that is structurally stable while in contact with water. The optical characteristics suggest that the thin film has the potential to be implemented in optoelectronic and semiconductor applications.

This work focuses on determining the optical constants of the organic polymer thin film. Herein the *Lavandula angustifolia* based polymer films will be referred to as PolyLA. Plasma polymerisation has been employed in order to obtain polymer thin film samples at a number of RF power levels. The effect of changing the RF power level on the optical constants on the polymer has been studied using Ultraviolet-visible (UV–Vis) spectroscopy and variable angle spectroscopic ellipsometry over the wavelength range of 200 –1000 nm (6.199–1.239 eV). UV–Vis Spectroscopy was employed to estimate sample thickness and to measure the absorbance in the UV and Visible region. Spectroscopic ellipsometry is a characterisation technique that been implemented in the past to determine the optical properties of polymer thin films [18-21]. The refractive index n, extinction coefficient k, absorption coefficient and thickness were derived from the experimental data via regression analysis. The relation between refractive index and thickness for the polymer samples has been investigated, in addition to the presence of optical anisotropy. Values of optical band gap have been derived from ellipsometry data.

2. Experimental procedures

L. angustifolia monomer supplied by G. R. Davis Pty. Ltd. (80 Bayldon Road, Queanbeyan NSW 2620, Australia) was used for fabricating the plasma polymer films on to glass substrate using the procedure outlined in [14] at various RF power levels (10 W, 20 W, 25 W, 30 W, 50 W and 75 W). The monomer was used without further purification. The experimental setup includes a custom made cylindrical RF plasma polymerisation cell of dimensions 0.75 m in length and an inner diameter of 0.055 m. Polymer films were fabricated at a pressure of approximately 33 Pa. RF energy (13.56 MHz) was delivered to the deposition chamber via external copper electrodes separated by a distance of 11 cm. Approximately 5 mL of the monomer is placed into the holder and replaced after each subsequent deposition. Prior to placement of substrate within the polymerisation cell, the monomer inlet is opened briefly to allow the oil to degas. During deposition, the monomer inlet is again opened and the vapour is released into the chamber, where the flow rate is controlled via a vacuum stopcock. Substrates were cleaned first with a solution of Extran MA 03 (Merck) and distilled water, then placed in a sonicator filled with distilled water and ultrasonically cleaned for 15 minutes, rinsed with Propan–2–ol and air-dried. Prior to fabrication, substrates were pre–treated with Ar plasma in order to produce an oxygen–free surface [9]. Absorbance and the approximate thickness of the films were obtained using an Avantes 2048 spectrometer.

The ellipsometric parameters Ψ and Δ are related to the Fresnel coefficients (*Rp* and *Rs*) and the complex reflection coefficient (ρ) by the following equation [22]:

$$\rho = \frac{R_p}{R_s} = \tan(\Psi) e^{i\Delta} \quad (1),$$

where *Rp* and *Rs* represents the Fresnel coefficient for the p– and s– directions, respectively. Parameters Ψ and Δ were obtained over the wavelength range of 200–1000 nm (6.199–1.239 eV) using a variable angle spectroscopic ellipsometer (model M-2000, J. A. Woollam Co., Inc.). Data was obtained at three different angles of incidence, φ=55º, 60º, and 65º. It is important to collect data near the Brewster angle of the material in order to minimise noise and systematic errors in the measured data [23]. Therefore the ellipsometric parameters were measured at a number of angles of

incidence to determine the most appropriate values. Ψ and Δ are used to derive the optical constants based on a model of the sample built in the J. A. Woollam Inc. analysis software (WVASE32) via regression analysis. Transmission data was also collected for each sample using the ellipsometer and used in the regression analysis in order to provide a comprehensive model of the sample under test.

Once the regression analysis is complete and a fit between the experimental data and model has been obtained, a quantitative measure of the quality of the fit is derived. The mean-squared error (MSE) is defined as [24, 25]:

$$MSE = \frac{1}{2N - M} \sum_{i=1}^{N} \left[\left(\frac{\Psi_i^{\mathrm{mod}} - \Psi_i^{\mathrm{exp}}}{\sigma_{\Psi i}^{\mathrm{exp}}} \right)^2 + \left(\frac{\Delta_i^{\mathrm{mod}} - \Delta_i^{\mathrm{exp}}}{\sigma_{\Delta i}^{\mathrm{exp}}} \right)^2 \right] \quad (2),$$

where N is the number of Ψ and Δ pairs, M is the number of fit parameters used in the model, and σ is the standard deviation of the experimental data points. Ideally a MSE value of zero is desired after performing the regression analysis, however this value is dependent on the amount of information available, the quality of the data, and how accurately the model reflects the sample. Therefore it is possible to obtain a MSE smaller than 1 in some instances, however it is also possible that a considerably higher MSE will be the smallest possible value due to the available data.

In order to create a model to relate the measured ellipsometric parameters to the optical properties of the material under test, oscillators are implemented. These oscillators represent the dielectric function of the material as a linear summation of real and complex terms as a function of wavelength, inverse wavelength or photon energy [26]. For conjugated polymers, harmonic oscillators such as Lorentzians or Gaussians are typically employed [18]. Originally two Gaussian oscillators were implemented, however it was discovered using 1 Gaussian and 1 Tauc–Lorentz oscillator produced a better fit to the data, with a lower MSE and lower average correlation between fitting terms. The Tauc–Lorentz oscillator term, derived by Jellison and Modine [27], is based on the Tauc joint density of states [28] and the Lorentz calculation [29] for the imaginary part of the dielectric function (ε_2):

$$\varepsilon_2(E) = \left[\frac{AE_0C(E-E_g)^2}{(E^2-E_0^2)^2 + C^2E^2} \times \frac{1}{E} \right], E > E_g \quad (3),$$
$$= 0, E \le E_g$$

A is a constant, E_g is the optical band gap, E_0 is the peak transition energy and C is the broadening term. The real part of the dielectric function (ε_1) can be found using Kramers-Kronig integration:

$$\varepsilon_1(E) = \varepsilon_1(\infty) + \frac{2}{\pi} P \int_{E_g}^{\infty} \frac{\xi \varepsilon_2(\xi)}{\xi^2 - E^2} d\xi \quad (4),$$

where P represents the Cauchy principal part of the integral and ε1(∞) is an additional fitting parameter. This equation can be solved in closed form and can be found in an erratum by Jellison and Modine [30].

As for the Gaussian oscillator, the formulas for the real and imaginary part of the dielectric function are as follows [26, 31]:

$$\varepsilon_2(E) = Ae^{-\left(\frac{E-E_n}{\sigma}\right)^2} - Ae^{-\left(\frac{E+E_n}{\sigma}\right)} \quad (5),$$

$$\varepsilon_1(E) = \frac{2}{\pi} P \int_{E_g}^{\infty} \frac{\xi \varepsilon_2(\xi)}{\xi^2 - E^2} d\xi \quad (6),$$

where A represents the amplitude, En the peak position, and σ the full width at half maximum.

3. Results and discussion

3.1 Modelling of Ellipsometric data

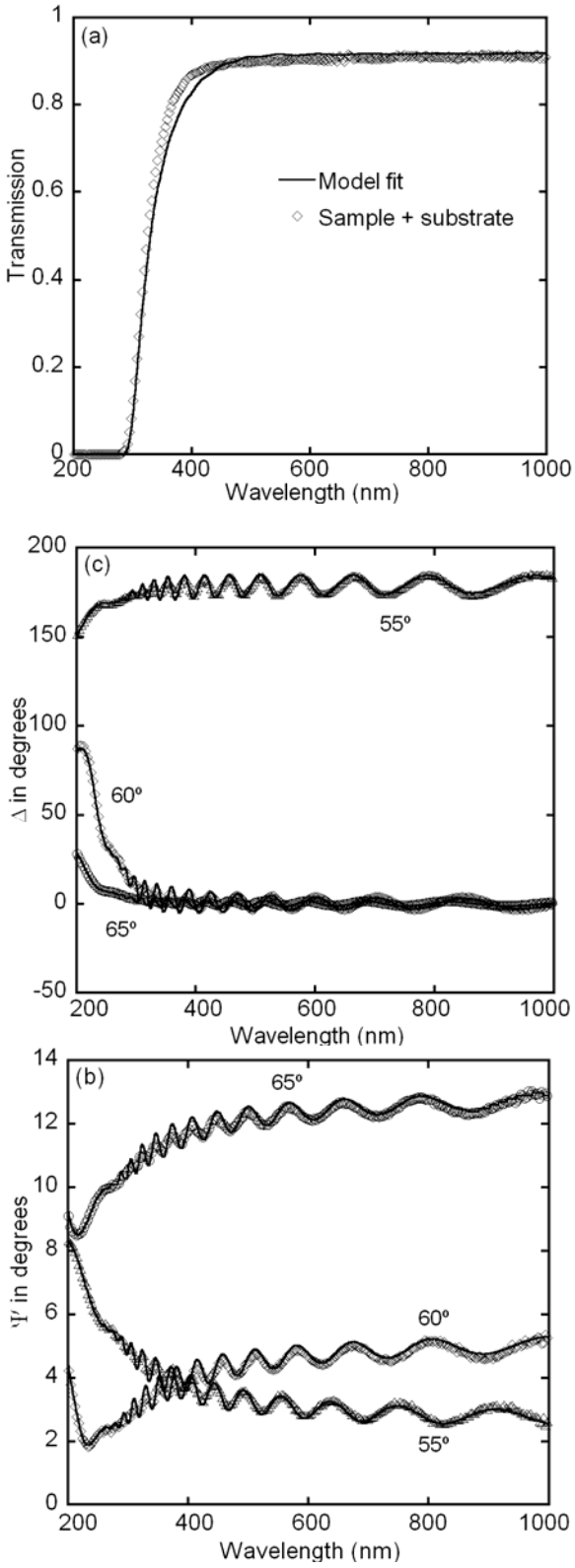

Figure 1: (a) Transmission spectra, (b) Ψ and (c) Δ spectra at different φ for 25 W polyLA film on glass substrate (MSE=2.953). Symbols are the experimental points and the full lines are the model fits.

For each sample a model was created within the analysis software using the ellipsometric parameters (Ψ, Δ) and transmission data collected using the ellipsometer. These models consisted of a layer for the substrate, a general oscillator layer to represent the polymer, and a roughness layer. Data was collected for the glass substrate prior to fabrication in order to produce an accurate representation for the model. The roughness layer is an effective medium approximation comprising of a mixed composition with 50% polymer and 50% voids. An example of the experimental Ψ, Δ and transmission data along with the generated data from the model for a sample fabricated at an RF power of 25 W is shown in Fig. 1. For the samples fabricated in this study, the generated data from the model was found to produce a good fit for the experimental data, with an MSE of 2.953 in this particular case.

3.2 RF power dependence of optical constants

PolyLA polymer films fabricated at 10, 20, 25, 30, 50 and 75 W were measured using the spectroscopic ellipsometer and the UV-Vis spectrometer. All other deposition parameters, including deposition time (7 mins), were kept constant during fabrication. UV-Vis spectroscopy was used to provide a rough estimate of the thickness of each sample as an error of 10% is expected from this technique. These thickness values were used as a starting point for determining a more accurate value using ellipsometry. Table 1 contains the thickness and roughness values measured obtained from spectroscopic ellipsometry.

Table 1: Thickness and Roughness for samples fabricated at various RF power levels measured using spectroscopic ellipsometry.

RF power (W)	Thickness (nm)	Roughness (nm)
10	903	0.41
20	593	0.49
25	618	0.52
30	580	0.47
50	393	0.23
75	237	2.06

UV-Vis absorption spectrums of all 6 sample types are presented in Fig. 2. It is believed that the main absorption peak may be the result of pi-pi* transitions. This data

demonstrates that the absorption profile is repeatable over the RF power range employed during fabrication. Unlike similar studies [9], shifting of the peak position and/or broadening of the peak is not seen for an increase in RF power.

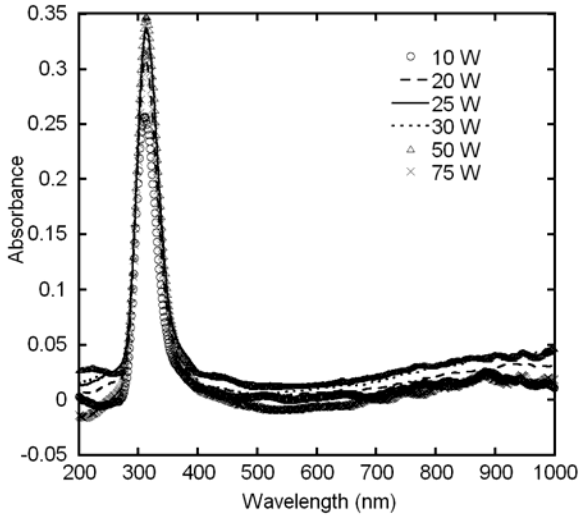

Figure 2: UV-Vis absorption spectrum vs. RF power in polyLA.

Outside the main absorption peak, the absorbance is below 0.05 in all cases and thus is insignificant. As the peak is outside of the visible region of the spectrum, the absorbance spectrum confirms that these polymer films are optically transparent. On the high wavelength side of the peak, the absorbance tends to increase with increasing wavelength. In this wavelength region, a decrease in the transmission spectra occurs for the same samples (Fig. 3.), however is not present in the transmission spectra for substrate + sample using a glass slide from a different batch (Fig. 1.). Therefore the increase in absorbance and also the decrease in transmission in the higher wavelength region are attributed to the substrate and not the polymer. Using the UV-Vis spectrometer, a reference spectrum of the substrate is taken prior to deposition and subtracted from the spectrum of the sample + substrate to produce the absorbance spectrum for the polymer sample. It appears that the UV-Vis spectrometer is unable to completely remove absorbance of this magnitude caused by the substrate from the resulting spectrum.

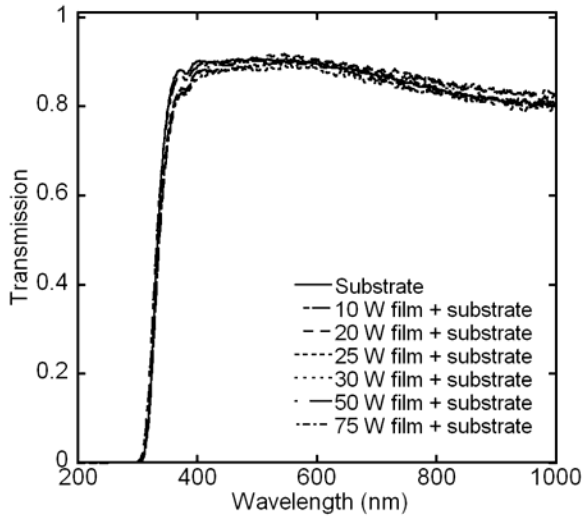

Figure 3: Transmission spectra of polyLA films fabricated at various RF power levels + glass substrate.

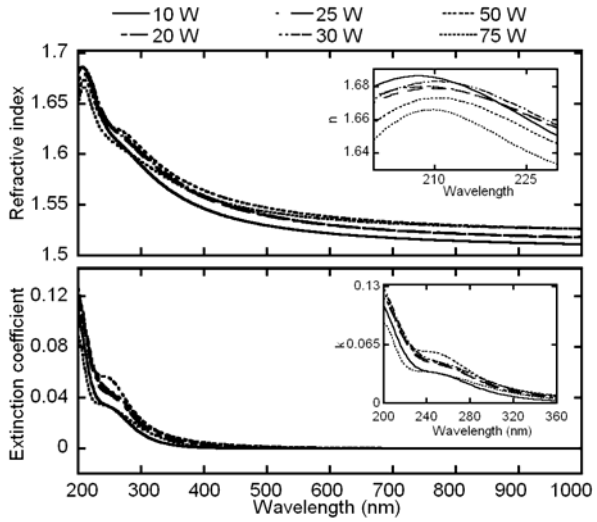

Figure 4: Refractive index (n) and extinction coefficient (k) vs. RF power in polyLA films.

Transmission spectra, in addition to the refractive index and extinction coefficient profiles of polyLA films fabricated at 6 different RF power levels are presented in Figs. 3. and 4. respectively. The transmission spectrum presented here demonstrates that the RF power has no significant affect on the transparency of the resulting polymer. As noted previously, the small decrease in the transmission spectrum for longer

wavelengths is attributed to the substrate and not the sample. This absorption however has been accounted for by the substrate layer in the optical model when deriving the refractive index and extinction coefficient profiles. If it was not the case, the affect caused by the substrate would be reflected in the refractive index and extinction coefficient profiles.

Considering the refractive index and extinction coefficient profiles as a function of RF power, it is observed that all sample exhibit the same general shape, with a sharp peak in the refractive index at short wavelengths corresponding to an abrupt increase in the extinction coefficient (Fig. 4.). At the peak of refractive index, an increase in RF power corresponds to a lower peak value. However, at wavelengths longer than approximately 400 nm, an increase in RF power results in a lower value of n. At 500 nm, the refractive index ranges from 1.530 to 1.543 for the RF power range of 10 W to 75 W, or 0.013.Thus this result reveals that the refractive index can be adjusted by changing the RF power during deposition, nevertheless the degree of tuneability is rather insignificant. As for the extinction coefficient, for wavelengths longer than 500 nm the magnitude is zero in all cases. The peak in k seen at lower wavelengths consists of two slopes. Extinction coefficient profiles between samples are approximately the same, with a small decrease across the wavelength region seen for the 10 and 75 W samples relative to the other samples.

3.3 Thickness dependence of optical constants

Ellipsometry data was taken for polyLA films fabricated at 25 W with different film thicknesses and the corresponding refractive index and extinction coefficient profiles derived (Fig. 5.). The shape of the refractive index profiles for all samples is identical, except for the 81 nm thick sample. The fit of the model to the experimental data for this sample was poor in comparison to the other samples and is considered the source of the deviation. A shift to higher values of n with an increase of thickness over the measured wavelength range for is observed for thicknesses up to 1071 nm. For the thickest sample (1592 nm), the shift in n only occurs at short wavelengths, where at wavelengths greater than approximately 400 nm, the refractive index is essentially identical to that of the 1071 nm thick sample. The shift in n vs. thickness shown in Fig. 5. is comparable to that

found by Gaynor et al. [20] for polyparaxylylene films grown by chemical vapour deposition which were deemed to not have significant thickness dependence on the refractive index. Therefore these shifts are insignificant and thus the refractive index is not dependent on thickness. In terms of the extinction coefficient, the profiles are essentially identical for the majority of the measured spectra. However there is a noticeable difference at the short wavelength end where the value peaks, where the magnitude of the peak increases with increased thickness.

It should be noted that the glass slides employed for the thickness dependence study were from a different batch than those used in the RF power dependence study. A small (1%) shift in the refractive index and extinction coefficient profiles can be seen between the two studies when comparing the results of polymers fabricated under identical conditions (i.e. the 25 W samples). This shift is attributed to the differences between the substrate batches and is insignificant in this case.

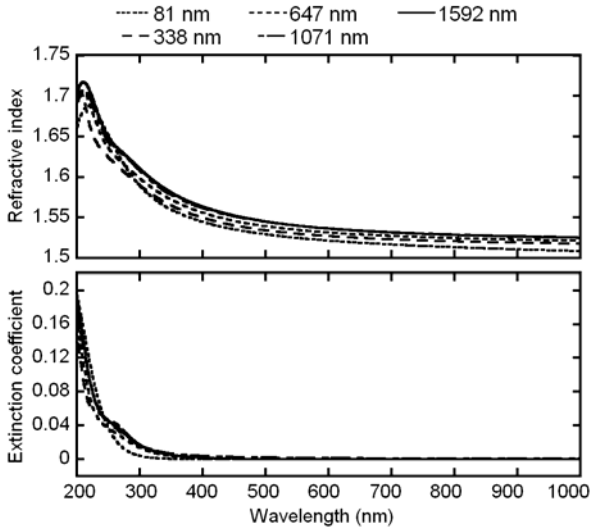

Figure 5: Refractive index (n) and extinction coefficient (k) vs. thickness for polyLA thin film fabricated at 25 W power.

3.4 Optical anisotropy

Experimental data collected using ellipsometry was used to establish whether the polyLA films exhibited optical anisotropy. Considering the polymer as a three

dimensional object, uniaxial anisotropy occurs when the polymer chains lie in the plane of the film, while for biaxial anisotropy to arise, there must also be order of the chains in the plane. As plasma polymers consist of highly crosslinked polymer chains with a high degree of branching and disorder, optical anisotropy is not expected in this case. Ellipsometric data was measured at three different azimuth in-plane angles for a 25 W sample as shown in Fig. 6. The three sets of data are almost identical, therefore there is no significant in–plane anisotropy for the polyLA films. In order to test for out-of-plane anisotropy, uniaxial anisotropy was added to the model using the analysis software. It was found that the model was not sensitive to uniaxial anisotropy as the change in the fit and MSE were insignificant. Hence the polyLA films are optically isotropic.

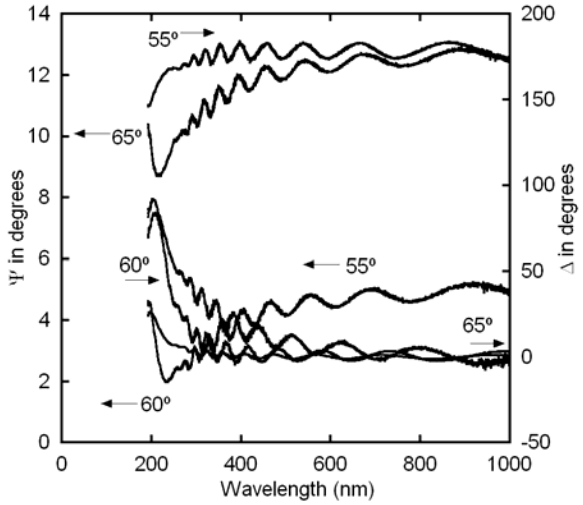

Figure 6: Ψ and Δ spectra for 25 W polyLA film on glass substrate at three different azimuth in-plane angles of 0º, 45º and 90º.

3.5 Optical band gap

Absorption coefficient data obtained from spectroscopic ellipsometer measurements was used to determine the E_O values for the fabricated polymer films. E_O is typically found using the Tauc relation [32]:

(7),

where hv is the energy of light, and p is a constant connected to the density–of–states distribution in the transport gap in the band tails and thus determines the type of transition. The factor B provides information on the length of localised state tails, where a smaller B represents longer tails [33]. The index p can take values of 2, 3, ½ and 3/2 depending on the nature of the electronic structure. In order to determine E_O for the material under test, the most appropriate value for p must first be sort. For semiconducting plasma polymer thin films, a parabolic function for the density of states distribution is typically assumed (p=2), although p=3 has been shown to provide a better fit in some cases [33, 34].

An example of a fit of p=2 and p=3 on a polyLA sample fabricated at 25 W based on absorption coefficient data obtained from ellipsometry is presented in Fig. 7. In this case, p=3 provides the best fit (data for p=½ and 3/2 not shown). E_O values for films fabricated at the 6 different RF power levels were calculated using p=3 (Table 2). The optical band gap was obtained using software implemented in Scilab. The linear section of the curve is extrapolated to the abscissa and the intersection represents the value of E_O. PolyLA films demonstrate an E_O of between 2.75 to 2.34 over the RF power range of 10 to 75 W. Hence the optical band gap of this polymer film can be selected by controlling the RF power employed during fabrication.

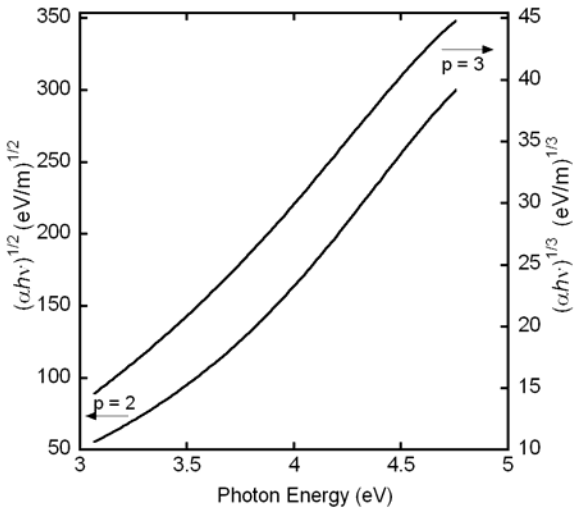

Figure 7: Absorption edge of 25 W polyLA film obtained from ellipsometric data, derived from Equation 7 for n = 2 and n = 3.

Table 2: Optical band gap E_O vs. RF power in polyLA

RF power (W)	E_O (eV)
10	2.75
20	2.71
25	2.55
30	2.49
50	2.55
75	2.34

Comparing the optical band gap value obtained previously for the 25 W sample (2.93 eV) [14], with that obtained in this study (2.55), it can be seen a small discrepancy exists. The previous reported value was obtained via a third party using a different spectrometric ellipsometer. It was derived from the ellipsometric parameters by including it as a fit parameter in the model rather than extracting the value from the absorption coefficient data. We have found for these particular polymer films that allowing E_O to be a fit parameter during the regression analysis can result in E_O taking a value over a considerable range and thus produce unrealistic results. This indicates that the data is not sensitive to E_O in the model and thus is believed to be the reason for the difference between the values. Therefore in this study E_O was determined using the absorption coefficient data and the Tauc relation rather than allowing E_O to be a fit parameter in the model.

4. Conclusion

The optical properties of polymer thin films fabricated from L. angustifolia using RF plasma polymerisation were investigated using UV-Vis spectroscopy and spectroscopic ellipsometry. Ellipsometry data was used to substantiate the isotropic nature of the thin film. Thickness and roughness values for samples fabricated between 10 W to 75 W were determined. Transmission spectra of the samples confirmed that they are optically transparent and that this parameter is independent of RF power. The refractive index and extinction coefficient of the polyLA films exhibited very little dependence on RF power and film thickness. Refractive index at 500 nm ranged from 1.530 to 1.543 for the specified RF power range, while the maximum value of extinction coefficient at this wavelength was 0.001. For these polymers, p=3 was found to provide the best fit for the density of states distribution when employing the Tauc relation to determine the optical

band gap. Overall E_O tends to decrease with increasing RF power, with 2.75 at 10 W and 2.34 at 75 W. The independence of the refractive index on the RF power level projects the PolyLA thin films as a potential optically stable material for optical applications.

Acknowledgments

The authors are grateful to the financial support provided under the RIRDC and ARC LIEF and DP schemes. CDE is grateful to the APA and RIRDC scholarships.

References

[1] Z. V. Vardeny, A. J. Heeger, A. Dodabalapur, Synth. Met. 148 (2005) 1.

[2] A. Hiratsuka, I. Karube, Electroanalysis 12 (2000) 695.

[3] S. Gaur, G. Vergason, in: (Eds.), 43rd Annual Technical Conference Proceedings of Society of Vacuum Coaters, Denver, April 15–20, 2000, (2000) 353.

[4] J. H. Burroughes, D. D. C. Bradley, A. R. Brown, R. N. Marks, K. Mackay, R. H. Friend, P. L. Burns, A. B. Holmes, Nature 347 (1990) 539.

[5] F. F. Shi, Surf. Coat. Technol. 82 (1996) 1.

[6] Y. Osada, H. Biederman, *Plasma Polymerization Processes*, Elsevier Science Publishers, NY, 1992.

[7] K. J. Kitching, V. Pan, B. D. Ratner, in: H. Biederman (Ed.), Plasma Polymer Films, Imperial College Press, London, 2004.

[8] H. Yasuda, Macromolecular Reviews Part D-J. Polym. Sci. 16 (1981) 199.

[9] M. C. Kim, S. H. Cho, J. G. Han, B. Y. Hong, Y. J. Kim, S. H. Yang, J. H. Boo, Surf. Coat. Technol. 169 (2003) 595.

[10] U. S. Sajeev, C. J. Mathai, S. Saravanan, R. R. Ashokan, S. Venkatachalam, M. R. Anantharaman, Bull. Mater. Sci. 29 (2006) 159.

[11] J. Tyczkowski, R. Ledzion, J. Appl. Phys. 86 (1999) 4412.

[12] E. A. Davis, N. F. Mott, Philos. Mag. 22 (1970) 903.

[13] J. Tyczkowski, in: H. Biederman (Ed.), Plasma Polymer Films, Imperial College Press, London, 2004, p. 202.

[14] M. V. Jacob, C. D. Easton, G. S. Woods, C. C. Berndt, Thin Solid Films 516 (2008) 3884.

[15] C. D. Easton, M. V. Jacob, R. A. Shanks, B. F. Bowden, Chem. Vapor Depos. (Accepted for publication).

[16] R. Shellie, L. Mondello, P. Marriott, G. Dugo, J. Chromatogr., A 970 (2002) 225.

[17] R. Shellie, P. Marriott, C. Cornwell, Hrc-J. High Resolut. Chromatogr. 23 (2000) 554.

[18] M. Campoy-Quiles, P. G. Etchegoin, D. D. C. Bradley, Synth. Met. 155 (2005) 279.

[19] A. Sharma, Deepak, S. Kumar, M. Katiyar, A. K. Saxena, A. Ranjan, R. K. Tiwari, Synth. Met. 139 (2003) 835.

[20] J. F. Gaynor, S. B. Desu, J. Mater. Res. 11 (1996) 236.

[21] Y. X. Li, L. Yan, R. P. Shrestha, D. Yang, Z. Ounaies, E. A. Irene, Thin Solid Films 513 (2006) 283.

[22] G. E. Jellison, Thin Solid Films 450 (2004) 42.

[23] H. A. Al-Attar, A. D. Telfah, Opt. Commun. 229 (2004) 263.

[24] L. G. Castro, D. W. Thompson, T. Tiwald, E. M. Berberov, J. A. Woollam, Surf. Sci. 601 (2007) 1795.

[25] J. G. E. Jellison, Thin Solid Films 313-314 (1998) 33.

[26] J. A. Woollam Co., Inc., Guide to Using WVASE32, WVASE32 Addendum E: General Oscillator Layer, 2001.

[27] G. E. Jellison, F. A. Modine, Appl. Phys. Lett. 69 (1996) 371.

[28] J. Tauc, R. Grigorovici, A. Vancu, Phys. Status Solidi 15 (1966) 627.

[29] F. Wooten, *Optical Properties of Solids*, Academic, New York, 1972.

[30] G. E. Jellison, F. A. Modine, Appl. Phys. Lett. 69 (1996) 2137.

[31] D. D. Meneses, M. Malki, P. Echegut, J. Non-Cryst. Solids 352 (2006) 769.

[32] J. Tauc, Mater. Res. Bull. 5 (1970) 721.

[33] J. Tyczkowski, in: H. Biederman (Ed.), Plasma Polymer Films, Imperial College Press, London, 2004, p. 149.

[34] J. Tyczkowski, M. Kryszewski, J. Phys. D-Appl. Phys. 17 (1984) 2053.

4.2 NON-DESTRUCTIVE COMPLEX PERMITTIVITY MEASUREMENT OF LOW PERMITTIVITY THIN FILM MATERIALS

Complex permittivity measurements are necessary for the overall electromagnetic characterisation of the polymer. This paper introduces a new technique for measuring the complex permittivity of low permittivity thin film materials. Formulation of this characterisation technique was required as the measurement resolution of existing dielectric resonator techniques was not adequate for the type of polymer under test. Existing procedures are reviewed, and the sample and equipment requirements between the different measurement strategies are contrasted. A new measurement procedure is outlined and the results are confirmed using established procedures. The error associated with this measurement procedure is also examined. Dielectric constant and loss tangent values of the LAEO based polymer at 10 and 20 GHz are presented. "Non-destructive complex permittivity measurement of low permittivity thin film materials" (Pub. 2.) is published in Measurement Science and Technology (IOP Publishing). This paper involved collaboration with Prof. Jerzy Krupka.

NON-DESTRUCTIVE COMPLEX PERMITTIVITY MEASUREMENT OF LOW PERMITTIVITY THIN FILM MATERIALS

C D Easton[1], M V Jacob[1] and J Krupka[2]

[1]Electronic Materials Research Lab, Electrical and Computer Engineering, School of Engineering, James Cook University, Townsville Australia

[2]Department of Electronics and Information Technology Warsaw University of Technology, Poland

Abstract

Complex permittivity measurement of low permittivity thin films is necessary to understand the fundamental properties and to implement these materials in devices. A new technique has been developed employing split post dielectric resonators at operating frequencies of 10 GHz and 20 GHz to measure relative permittivity and loss tangent of low permittivity materials. The results have been confirmed by comparing the measurements with that of thick films fabricated on quartz substrate. This paper substantiates the validity of performing non-destructive measurements of the complex permittivity of thin polymer films which was not previously possible with the split post dielectric resonator technique. A detailed error analysis of the measurement procedure is also reported in this paper.

Keywords: dielectric measurements, thin polymer films

1. Introduction

Accurate electromagnetic characterisation of a sample is vital for understanding the properties of new materials and hence allows for the material to be categorised and assigned to specific applications, or new applications derived. Many methods exist for determining the dielectric constant and loss tangent of a sample, though these are difficult to implement when the sample is a thin film with thickness ranging 100 to 1000 nm. Typically the methods used for the microwave characterisation of dielectric materials are classified into two groups based on the measurement structure implemented, namely transmission-line and resonant methods. These include one port coaxial and waveguide cells, open-ended probes, free-space transmission/reflection or reflection methods, microwave microscope methods, microwave cavity methods, stripline and microstrip methods [1-8]. Each technique has its own limitations including the frequency at which the measurements can be performed and the type of material that can be measured. Frequency-domain methods are however preferred when measurement resolution is of concern, which is of importance for low-loss materials [3]. Coaxial and waveguide methods are commonly used for determining the electromagnetic properties of materials, however rely on additional measurement fixtures and specific geometric dimensions of the sample to obtain accurate results. These methods are not ideal for the dielectric characterisation of low-k (permittivity) thin film materials.

The scanning microwave microscope is a near-field characterisation technique which can be used to determine the dielectric constant of a sample at microwave frequencies with high spatial resolution. A typically microwave microscope consists of a microwave resonator with a sharp tip (probe) which is protruding from a thin metal shielding wall, while electronics such as a voltage controlled oscillator and a frequency counter are implemented in order to obtain the measurement. When in operation, a sample brought into close proximity to the tip will cause a reduction in the energy stored in the electromagnetic field depended on the sample permittivity [9]. This results in a change in the resonant frequency and quality factor of the resonator [8]. Use of a microwave microscope for characterising low dielectric constant samples has been limited as this technique is typically implemented for materials with high-k.

Recently, Talanov et al. [9-11] have developed a new probe in order to provide a non-contact, non-invasive measurement system for low-k materials. The equipment requirements for this system, such as the tip-sample distance control mechanism to provide distances of 50 – 100 nm between tip and the sample, can prove costly. No attempt has been made by the authors to explain the effect on the measurements if the surface roughness of the samples is larger than the 'expected' few nanometres. In addition, the calibration and measurement procedures require multiple measurements of standard and test samples to obtain the final measurement for a single sample, thus indicating a lengthy procedure. The accuracy of this system has been estimated to be ± 2%, providing the film thickness can be determined with accuracy down to a fraction of a percent, which is comparable to split-post dielectric resonator techniques.

From the available methods, microwave resonant cavity techniques are considered to provide the greatest measurement sensitivity [3]. Split Post Dielectric Resonator technique is a modified dielectric resonator method that has been successfully implemented in measuring the electromagnetic properties of thick planar materials such as Printed Circuit Board materials, dielectric and ferroelectric substrates at the frequency range of 1-10 GHz [12-14]. However, this method cannot provide sufficient resolution to estimate permittivity if the film thickness or permittivity is very small. Microwave cavity methods include $TE_{01\delta}$ mode and TM_{0n0} mode cavities (Hakki-Coleman resonator, Split-post dielectric resonator), Fabry-Perot resonators, and Whispering gallery mode resonators [5]. These methods can be difficult to implement for thin films due to the shape requirements for the sample. Improvements in the modelling of electromagnetic fields has led to the formation of resonant cavities for the measurement of samples with a specific shape, such as the split post dielectric resonator [5]. This technique is also used for the measurement of ferroelectric thin films. Theoretically it is possible to characterise low-k thin films using split post dielectric resonator technique but the measurement resolution will not be sufficient for films with a thickness of less than 1 μm. The feasibility of acquiring higher thickness is proposed in reference [15]. This paper thoroughly examines the suitability of using split post dielectric resonator as a tool for microwave characterisation of low-k polymer thin films by using different layers of the thin film and verifies the method by fabricating thick films using the same experimental procedure.

2. Experiment

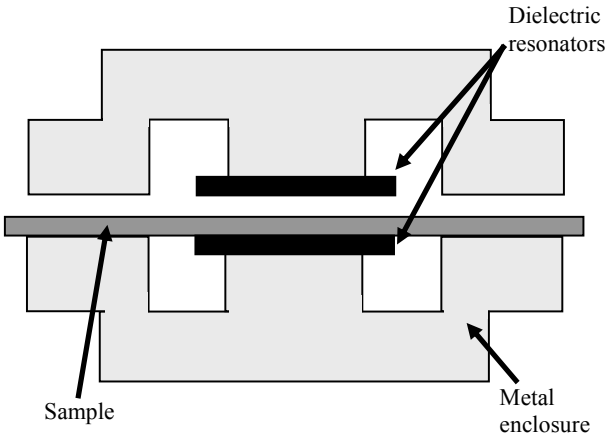

Figure 1: Schematic of Split Post Dielectric Resonator

The $TE_{01\delta}$ mode split post dielectric resonator technique has been successfully implemented in the past for obtaining the accurate electromagnetic properties of planar materials [5, 12, 14, 16]. A schematic of a split post dielectric resonator is shown in figure 1. The characterisation of a thin film using a split post dielectric resonator involves measuring the resonant frequency and Q-factor of the substrate without the film (pre-deposition), then repeating the same measurement but with the substrate and film (post-deposition) in place. The dielectric constant and loss tangent of the film can then be determined numerically from the shifts in the resonant frequency and Q-factor caused by the film. As previously reported [15], the shift in the resonant frequency and Q-factor caused by the sample must be measurable. For a material with a relative permittivity of approximately 2.6, an adequate frequency shift of 1 MHz with 2% uncertainty can be obtained for samples of thickness of 5μm or greater for a 10 GHz split post dielectric resonator, and 2.3 MHz for 20 GHz split post dielectric resonator (figure 2). The thickness of a typical polymer thin film can range from 10 to 1500 nm (0.01 to1.5 μm), and thus is not adequate to obtain the required frequency shift. However, a number of thin films can be stacked to obtain a sufficient thickness. The air gaps caused by stacking the samples has no affect on the sensitivity of the measurements performed since the electric field is continuous across the dielectric-air interface, thus relying on the surface of the sample to be uniform [5, 12]. The accuracy and repeatability of this technique is verified by placing the sample into the resonator at

the same position for each consecutive measurement. This ensures that the same sample area is measured by the resonator in the case of multiple measurements for the same group of samples.

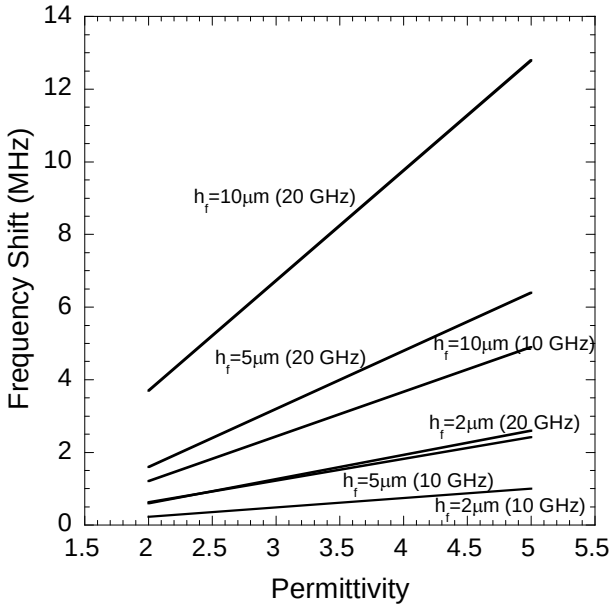

Figure 2: Resonant frequency shifts as a function of relative permittivity for various film thicknesses for a 10 GHz and 20 GHz split-post dielectric resonator.

Low permittivity polymer thin films were deposited on thin Teflon foils of uniform thickness of 19 μm using the RF plasma polymerisation technique. The thickness of the thin films was measured employing an optical spectrometric technique. Test samples were fabricated by masking the Teflon sheet before deposition such that only half of the substrate was deposited on, as shown in figure 3. This allows the reference to be measured from the same Teflon sheet as the sample was deposited, which results in a reduced possibility of variation between the reference substrate and the substrate with the deposited film. The thickness of the polymer thin film is increased by stacking different layers of the films, one to six stacked sheets. The number of stacked sheets can be varied to accommodate the thickness of a particular set of samples, and is only restricted by the height of the sample space within the resonant cavity. All measurements were performed at the same temperature, 23°C. The humidity in the room however is not controlled and thus could add additional error. Therefore measurement

of the resonant frequency and Q-factor of the substrate and substrate together with sample are taken one after the other in order to reduce the time between measurements and thus minimise variation caused by external influences. In addition, the resonant frequency and Q-factor of the empty resonator is taken at the beginning and end of a set of measurements for a sample group in order to monitor the error caused by changes in humidity. Removal order of Teflon sheets from a stack is as follows unless stated otherwise: sheet #1, #2, #3, #4, #5, and #6. Thick polymer films were also deposited on quartz substrate under similar deposition conditions with increased deposition time in order to evaluate the measurement technique. Every effort was taken to ensure the position of the sample within the dielectric resonator is the same for each recurring measurement to avoid unnecessary error**.** HP 8722C network analyser was used to measure the resonant frequencies and unloaded Q-factors of the 10 GHz and 20 GHz split post dielectric resonator containing the test samples. The quartz coverslips implemented were made from GE type 124 quartz with a dielectric constant of 3.75 at 20^{o}C, 1 MHz [17].

Figure 3: Cross section view of a number of substrates with film deposited on half of the surface area stacked together for measurement of the sample and of the reference.

3. Results and Discussion

The resonant frequency (f_0) and unloaded Q-factor (Q_0) have been measured for a split post dielectric resonator loaded with low permittivity (low-k) polymer thin film deposited on Teflon foil and thick film deposited on Quartz substrate. The real part of the complex permittivity is computed from measured resonant frequencies of the resonator using the following equation:

(1),

where: h_f is thickness of the sample under test, f_S is the resonant frequency of split post dielectric resonator with substrate only, f_f is the resonant frequency of the resonator with film and substrate. K_ε is a parameter which varies with ε_f and h_f, and has been evaluated for a number of ε_f and h_f using the Rayleigh-Ritz technique. An iterative procedure is then used to evaluate subsequent values of K_ε and ε_f from equation (1).

The real part of permittivity and loss tangent of the thin films were calculated using numerical techniques from the measured Q_0 and f_0 values and the results are reported in table 1. The values stated in table 1 for the polymer on Teflon with varying layers are the mean values of the data taken for four sets of Teflon samples (Groups 1, 2, 3 and 4), each averaged over a number of measurements. Multiple sets of samples with the same number of films but with different thicknesses were employed in order to confirm the repeatability of the technique. The mean values for both permittivity and loss tangent data of the Teflon samples are within the tolerance of the expected values obtained from the Quartz sample measurements for the 6, 5, 4 and 3 layer stacks for both 10 and 20 GHz. Thicknesses for each of the Teflon samples are shown in table 2. The affect of changing the film removal order was also studied (tables A5 and A10), however it was shown that such a change in the experimental setup had no affect on the resulting measurement. It was also revealed that measurements taken on different days and at different times resulted results within the experimental error, thus confirming the repeatability of the process. The small difference observed between measurements taken early in the day to those taken at later times of the same day (tables A2 and A3) is attributed to humidity changes in the room. The measurements obtained for Groups 1, 2, 3, and 4 are contained within the appendix in tables A1 – A9. For the thick polymer films (5020 nm for 10 GHz and 4420 nm for 20 GHz) deposited on quartz substrate, the permittivity was found to be 2.60 and 2.63 and loss tangent 0.020 and 0.016 at 10 GHz and 20 GHz respectively. The optical measurements (ellipsometry) forecast relative permittivity of approximately 2.37 for the fabricated polymer thin film but there are no alternative methods to compare the results at the same frequency.

Table 1: Split post dielectric resonator 10 GHz and 20 GHz measurements at 23 ˚C for Quartz and Teflon substrates.

Material	Thickness (μm)	Frequency 10 GHz Permittivity (ε_f)	Loss Tangent ($\tan\delta_f$)	Frequency 20 GHz Permittivity (ε_f)	Loss Tangent ($\tan\delta_f$)
Quartz	190	3.69	8.28E-05	3.82	2.10E-04
Teflon (6 sheets)	114	2.04	3.01E-04	2.05	3.01E-04
Polymer on Quartz	5.020 4.420	2.60 ± 0.18	0.020 ± 0.005	2.63 ± 0.18	0.016 ± 0.005
Polymer on Teflon (2 layers)	--	2.40 ± 0.22	0.023 ± 0.008	2.67 ± 0.21	0.019 ± 0.007
Polymer on Teflon (3 layers)	--	2.43 ± 0.21	0.022 ± 0.006	2.55 ± 0.20	0.021 ± 0.005
Polymer on Teflon (4 layers)	--	2.58 ± 0.21	0.022 ± 0.005	2.61 ± 0.19	0.020 ± 0.004
Polymer on Teflon (5 layers)	--	2.57 ± 0.20	0.021 ± 0.004	2.63 ± 0.19	0.020 ± 0.003
Polymer on Teflon (6 layers)	--	2.57 ± 0.20	0.021 ± 0.003	2.61 ± 0.18	0.021 ± 0.003

Table 2: Thickness of samples deposited on Teflon sheets

	Group 1	Group 2	Group 3	Group 4
Sheet number	Thickness (nm)	Thickness (nm)	Thickness (nm)	Thickness (nm)
#1	1320	1000	1210	1980
#2	980	1070	1220	1590
#3	960	950	1540	1590
#4	1090	820	1030	1260
#5	1100	730	1020	1580
#6	900	850	1300	1290
Total	6350	5420	7320	9290

An investigation of the feasibility of characterisation of the polymer thin film deposited on Teflon foils was also carried out. The resolution of the measurement was not adequate with the use of one layer (film thickness ~ 1000nm), though for two layers (film thickness ~ 2000nm) sufficient shift in the frequency is noticed and hence the measurement of the relative permittivity and loss tangent is obtained at 10GHz. At 20

GHz however, a much larger shift in the resonant frequency is required. A precise measurement was obtained once the thickness was greater than 4 μm and the frequency shift was greater than 2 MHz. A shift smaller than 2 MHz, corresponding to a thickness of less than approximately 3.7 μm, resulted in a large deviation in the relative permittivity and loss tangent measurements with respect to the expected results. Unlike the 10 GHz resonator, it was not possible to obtain an accurate result for the relative permittivity and loss tangent using a small thickness for the 20 GHz resonator.

For six layers of the thin film and film on quartz the permittivity and loss tangent are 2.57 and 2.60, and 0.021 and 0.020 respectively at 10 GHz. At 20 GHz the corresponding values are 2.61 and 2.63, and 0.021 and 0.016. The 20 GHz resonator is expected to have a greater accuracy than the 10 GHz but is sensitive to external factors such as humidity and thermal drift of the network analyser. Therefore, in order to compensate for such external influences a larger frequency shift is recommended. A relatively small variation in both the permittivity and loss tangent is seen between the two methods, thus confirming the accuracy of this proposed measurement technique. Hence it is possible to obtain a sufficient thickness and thus a sufficient frequency shift by stacking an appropriate number of samples in order to achieve accurate results of relative permittivity and loss tangent. Such a technique allows for the non-destructive measurement of polymer films using a split post dielectric resonator where the thickness of a single sample is not sufficient to obtain an adequate frequency shift. Thin Teflon sheets are significantly cheaper than other substrates such as Quartz, thus this technique also offers a cost effective alternative when performing characterisation and optimisation of novel polymer materials.

4. Error Analysis

Numerical electromagnetic analysis of a split post dielectric resonator structure for thin films deposited on a specific low permittivity substrates shows that variations of coefficients K (Eq. 1) are smaller than 1% and relative uncertainties of resonant frequency measurements are smaller than 0.001%. Thus errors of real permittivity measurements employing the split post dielectric resonator can be estimated assuming one of the conditions:

1. The substrate with the film is measured at exactly at the same position in the resonator as the substrate without film.

Or

2. Substrate is either very thin or its permittivity is very close to unity.

In such cases the error analysis can be simplified by assuming that only the resonant frequency shift $S_f = f_s - f_f$ is determined but that the film thickness is not precisely measured. Using Eq. (1), the maximum uncertainty of real permittivity can be derived for the perfectly uniform substrate as:

$$\frac{\Delta\varepsilon_f}{\varepsilon_f} = \frac{\Delta h_f}{h_f}\frac{\varepsilon_f - 1}{\varepsilon_f} + \frac{\Delta S_f}{S_f}\frac{\varepsilon_f - 1}{\varepsilon_f} \quad (2),$$

where: $\frac{\Delta h_f}{h_f}$ is the uncertainty associated with film thickness and $\frac{\Delta S_f}{S_f}$ is the uncertainty associated with measuring the resonance frequency shift.

The error in permittivity measurement for different number of layers due to both uncertainty in film thickness measurement and resonant frequency shift has been determined and the results are shown in figure 4. This study clearly shows that the error in measurement is predominantly due to the error in thickness measurement. A spectroscopic technique was used for the thickness measurement and the results are compared with ellipsometry. An error of approximately 10% is expected in the thickness measurement when using the spectroscopic technique. The effect of a change in thickness on the permittivity for the 10 GHz and 20 GHz resonators is analyzed and exhibited in figure 5. This data is based on the resonant frequency and Q-factor obtained for six layers. The origin represents the original data for a thickness of 5337 nm (6 layers) while subsequent data points are obtained by varying the thickness while keeping the resonant frequency and Q-factor constant. For an error of 0.5 μm in the thickness, the subsequent error in the dielectric constant can be as large as 0.143 (10 GHz) and 0.168 (20 GHz). It was found based on the magnitude of the results for dielectric constant the influence on the real part of permittivity is higher. Therefore

higher accuracies could be attained by precisely measuring the thickness and measuring the permittivity at higher frequencies.

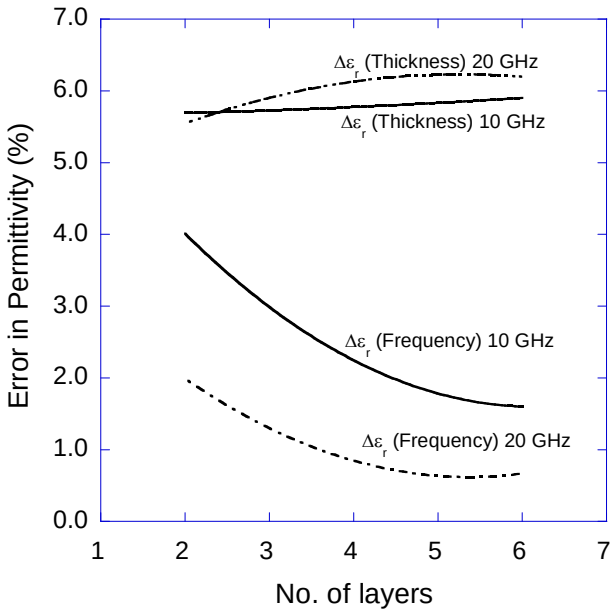

Figure 4: The estimated error in permittivity due to the uncertainty in thickness and resonant frequency measurement.

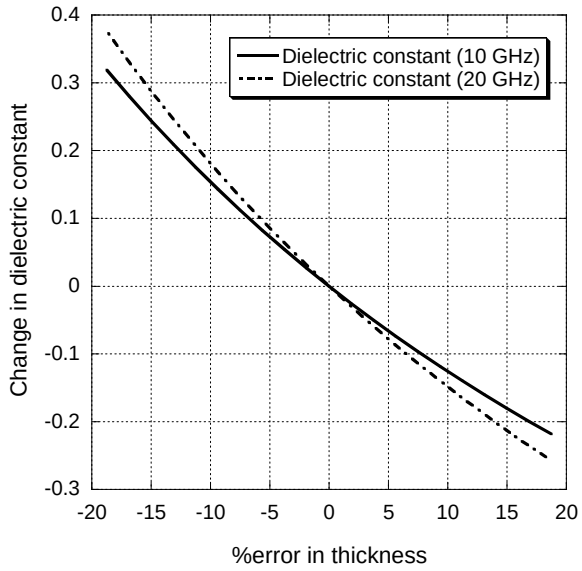

Figure 5: Effect of a change in thickness on the dielectric constant values for the 10 GHz and 20 GHz resonators.

If the conditions relating to the substrate are not satisfied, then additional error relating to the repeatability of the split post dielectric resonator measurements should be taken into account:

$$\frac{\Delta\varepsilon_f}{\varepsilon_f} = \frac{\Delta h_f}{h_f}\frac{\varepsilon_f - 1}{\varepsilon_f} + \frac{\Delta S_f}{S_f}\frac{\varepsilon_f - 1}{\varepsilon_f} + \frac{\Delta h_s}{h_f}\frac{\varepsilon_s - 1}{\varepsilon_f} \quad (3),$$

where: $\frac{\Delta h_s}{h_f}$ represents the uncertainty associated with different "effective thicknesses" of the substrate before film deposition and after film deposition. This can be related to a horizontal shift of a non-uniform substrate under test using the split post resonator. To obtain exactly the same "effective thickness" of substrate in those two measurements, the substrate with and without the film must be situated at exactly the same positions in the split post dielectric resonator. Even though the error due to this term is small, it could be hard to exactly measure the reference and the sample at the same position and hence the maximum uncertainty caused by the third term can be estimated as 0.5 %. Figure 6 exhibits the maximum possible error in the measurements reported in this paper.

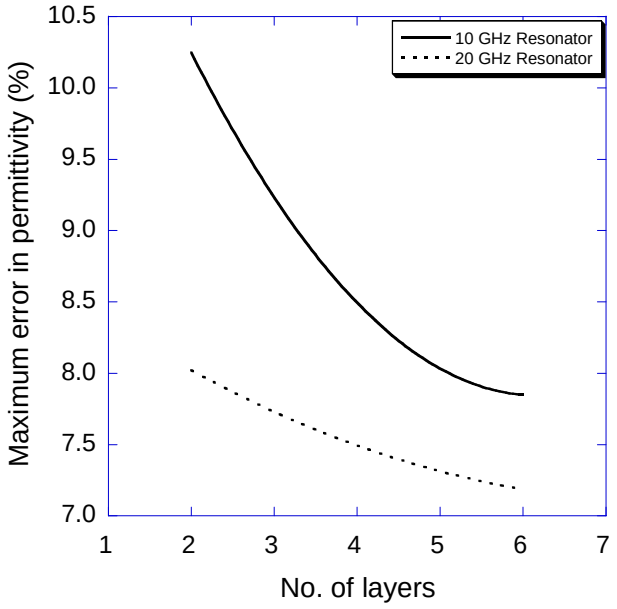

Figure 6: The maximum error estimated for the permittivity measurement.

When calculating the real part of complex permittivity of the sample deposited on quartz, Eq. (2) can be used to determine the uncertainty of the measurement. However, for the thin films, the conditions relating to the substrate cannot be met and thus additional errors need to be taken into account. As one might expect, measurements of low permittivity films in this case are not possible within acceptable tolerance limits.

One additional requirement for precise measurements is temperature stability of the resonant structure. Usually there is a long time delay between the measurements taken with the uncoated substrate (reference) and substrate coated with thin film sample. In order to mitigate measurement errors associated with the frequency drift due to possible temperature variations of the split post dielectric resonator, additional measurements of the empty resonator before measurements of the resonator with the substrate and with the film and substrate are performed. If there was any difference between the resonant frequencies of the empty resonator it was necessary to correct resonant frequency f_S according to (4):

$$f_{S2} = f_{S1} + (f_{02} - f_{01}) \quad (4),$$

where f_{S2} is the corrected resonant frequency, f_{S1} is the resonant frequency prior to correction, and f_{01} and f_{02} are the resonant frequencies of the empty resonator before and after measurement of the sample.

The uncertainty of dielectric loss tangent measurements for thin film samples as a function of dielectric loss tangent for various sample thicknesses using the 20 GHz split post dielectric resonator is shown in figure 7. Loss tangent errors are defined assuming that the Q-factor of the sample is measured with uncertainty of 1%. Such a graph is valid for both Teflon and Quartz substrates. For the 10 GHz resonator the graph would be similar, where for low loss thin films errors would increase approximately by a factor (ΔfQ) of $\frac{f_{S20GHz}}{f_{S10GHz}} \times \left(\frac{Q_{S20GHz}}{Q_{S10GHz}} \right)$, where f_S is the resonant frequency of appropriate resonator with substrate and Q_S is the Q-factor of appropriate resonator with substrate. The factor, ΔfQ, results in approximately 1.16 times increase in the total uncertainty in the dielectric loss tangent measurements for the sample on Quartz using the 10 GHz resonator compared with the 20 GHz resonator, 1.27 for samples in groups 1 and 2, and

1.2 for samples in groups 3 and 4. The difference in ΔfQ for groups 1 and 2 compared to groups 3 and 4 is attributed to the use of a different batch of Teflon sheets. For the measurement of the loss tangent for the quartz and Teflon substrates, the uncertainty is given as approximately 2×10^{-5} [13].

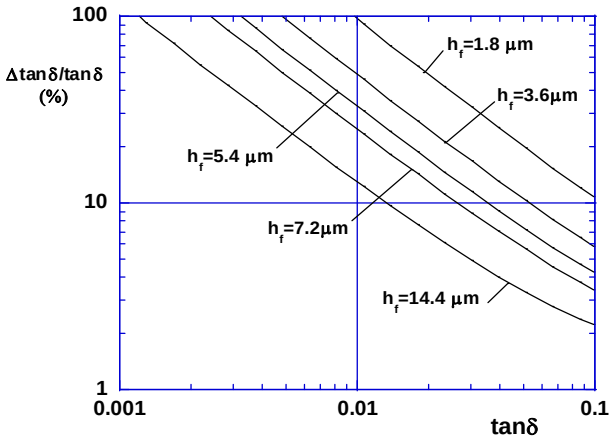

Figure 7: Uncertainty of dielectric loss tangent measurements for thin film samples using the 20 GHz SPDR.

5. Conclusion

It has been demonstrated that the electromagnetic properties of very thin, low permittivity and low loss films can be measured accurately at both 10 GHz and 20 GHz by employing a modified split post dielectric resonator technique. The modified technique involves depositing the polymer film onto a number of thin, low loss substrates and stacking on top of each other to obtain adequate thickness. The technique was confirmed by comparing the measured dielectric constant and loss tangent of a polymer film deposited on Quartz with that of a polymer film deposited on a number of layers of Teflon. A good agreement exists between the results obtained for the two different methods, thus confirming the validity of the new method.

Acknowledgments

This work was financially supported by the Rural Industries Research and Development Corporation (RIRDC). CDE is grateful to James Cook University for the Australian

Postgraduate Award (APA). We would also like to thank Dr. G. Woods for his valuable comments.

Appendix

Data pertaining to the measurement of the permittivity and loss tangent of the four groups of samples (Group 1, 2, 3 and 4) and their associated error are shown in tables A1 – A9. Graphical representation of this data is also supplied with figures A1 – A4 that compares the values obtained from the Teflon sheet samples to that obtained from the Quartz sample and the tolerance of the Quartz sample measurement. Figures A5 and A6 demonstrate the standard deviation of the permittivity and loss tangent data for both the 10 GHz and 20 GHz respectively. A general trend can be seen where the deviation decreases with an increase in the number of Teflon sheets, as is expected when the sample thickness is increased and thus a larger frequency shift is obtained from the resonator measurement.

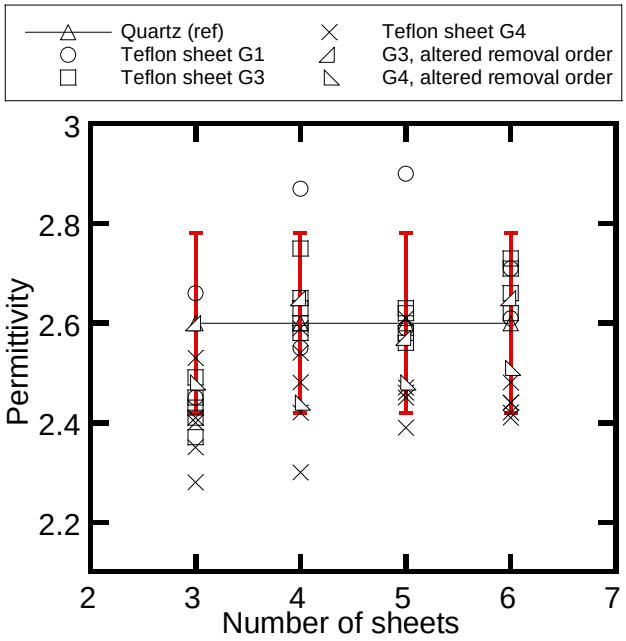

Figure A1: 10 GHz Permittivity data, all Teflon sheet samples

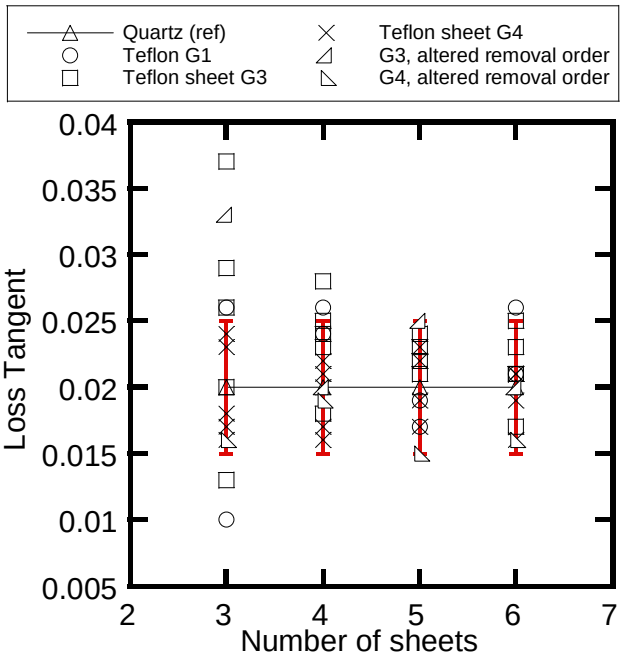

Figure A2: 10 GHz Loss tangent data, all Teflon sheet samples

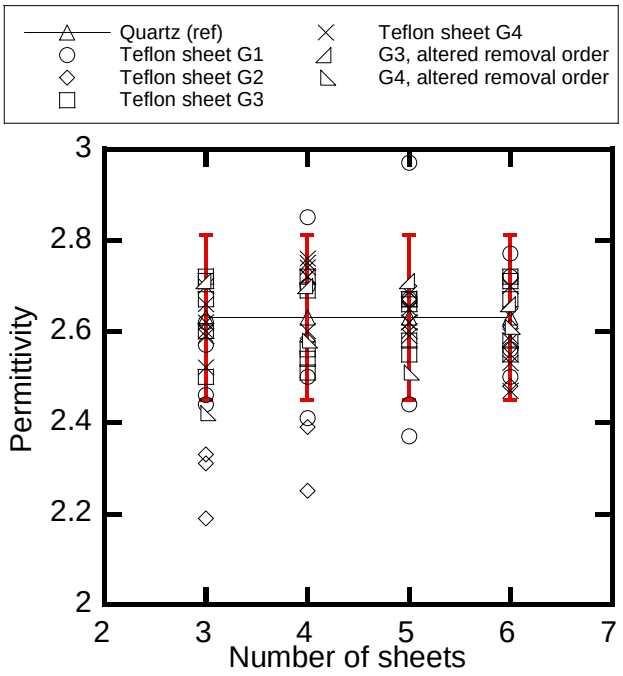

Figure A3: 20 GHz Permittivity data, all Teflon sheet samples

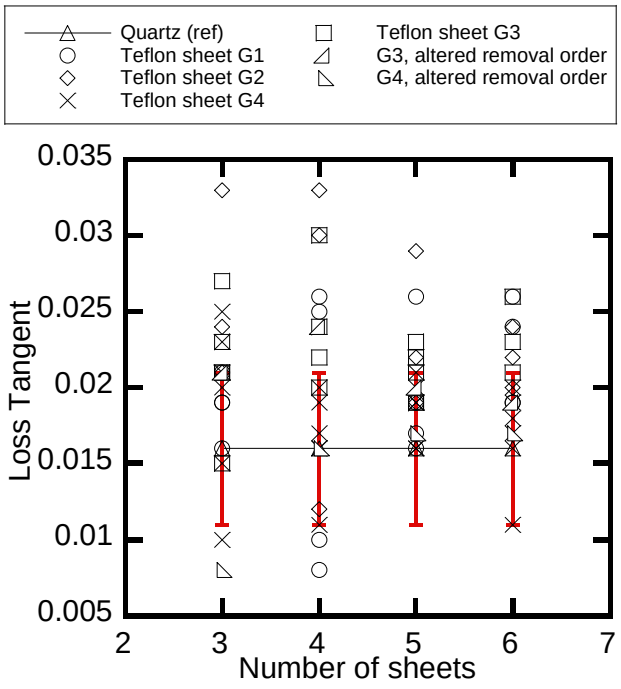

Figure A4: 20 GHz Loss Tangent data, all Teflon sheet samples

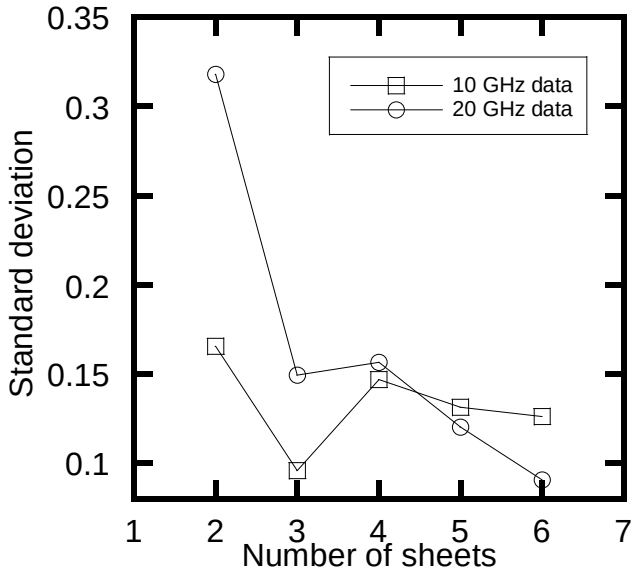

Figure A5: Standard deviation of the permittivity for all 10 GHz and 20 GHz measurements for samples on Teflon sheets.

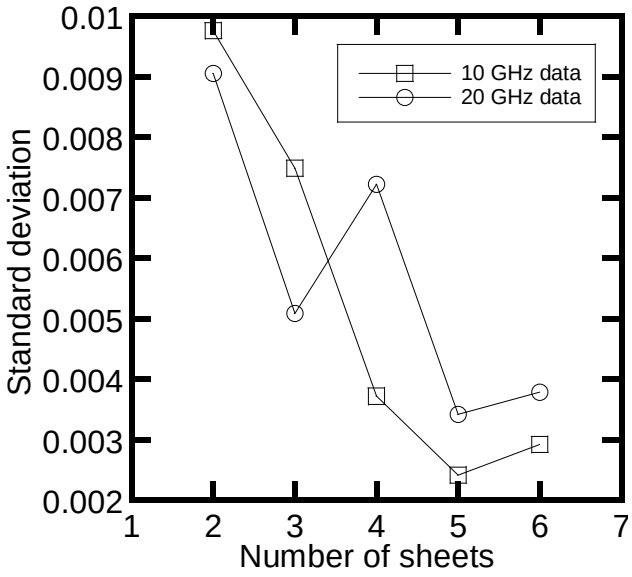

Figure A6: Standard deviation of the loss tangent for all 10 GHz and 20 GHz measurements for samples on Teflon sheets.

Table A1: 10GHz complex permittivity measurements for Group 1 samples (Temperature: 23 ˚C)

	Number of layers							
	6		5		4		3	
Trial number (dd/mm; time of measurement)	Permittivity (ε_f)	Loss Tangent ($\tan\delta_f$)	Permittivity (ε_f)	Loss Tangent ($\tan\delta_f$)	Permittivity (ε_f)	Loss Tangent ($\tan\delta_f$)	Permittivity (ε_f)	Loss Tangent ($\tan\delta_f$)
#1 (29/03; 08:20)	2.71 ± 0.22	0.026 ± 0.004	2.90 ± 0.24	0.019 ± 0.004	2.87 ± 0.25	0.024 ± 0.006	2.66 ± 0.24	0.026 ± 0.007
#4 (05/04; 08:40)	2.61 ± 0.21	0.021 ± 0.004	2.59 ± 0.21	0.017 ± 0.005	2.55 ± 0.21	0.026 ± 0.006	2.45 ± 0.22	0.010 ± 0.007

Table A2: 10GHz complex permittivity measurements for Group 3 samples (Temperature: 23 ˚C)

	Number of layers							
	6		5		4		3	
Trial number (dd/mm; time of measurement)	Permittivity (ε_f)	Loss Tangent ($\tan\delta_f$)	Permittivity (ε_f)	Loss Tangent ($\tan\delta_f$)	Permittivity (ε_f)	Loss Tangent ($\tan\delta_f$)	Permittivity (ε_f)	Loss Tangent ($\tan\delta_f$)
#1 (20/04; 09:10)	2.62 ± 0.20	0.025 ± 0.003	2.62 ± 0.21	0.022 ± 0.004	2.60 ± 0.21	0.024 ± 0.005	2.37 ± 0.21	0.029 ± 0.007
#2 (20/04; 13:10)	2.66 ± 0.21	0.021 ± 0.003	2.58 ± 0.20	0.022 ± 0.004	2.63 ± 0.22	0.028 ± 0.005	2.43 ± 0.21	0.037 ± 0.007
#3 (20/04; 15:00)	2.66 ± 0.21	0.017 ± 0.003	2.56 ± 0.20	0.023 ± 0.004	2.58 ± 0.21	0.025 ± 0.005	2.49 ± 0.22	0.026 ± 0.007
#4 (20/04; 16:15)	2.73 ± 0.21	0.021 ± 0.003	2.63 ± 0.21	0.021 ± 0.004	2.65 ± 0.22	0.018 ± 0.005	2.45 ± 0.21	0.013 ± 0.007
#5 (20/04; 20:35)	2.71 ± 0.21	0.023 ± 0.003	2.63 ± 0.21	0.024 ± 0.004	2.75 ± 0.23	0.023 ± 0.005	2.41 ± 0.21	0.020 ± 0.007

Table A3: 10GHz complex permittivity measurements for Group 4 samples (Temperature: 23 ˚C)

	Number of layers							
	6		5		4		3	
Trial number (dd/mm; time of measurement)	Permittivity (ε_f)	Loss Tangent ($\tan\delta_f$)	Permittivity (ε_f)	Loss Tangent ($\tan\delta_f$)	Permittivity (ε_f)	Loss Tangent ($\tan\delta_f$)	Permittivity (ε_f)	Loss Tangent ($\tan\delta_f$)
#1 (20/04; 09:55)	2.42 ± 0.18	0.021 ± 0.003	2.39 ± 0.18	0.022 ± 0.003	2.30 ± 0.18	0.021 ± 0.004	2.28 ± 0.18	0.016 ± 0.006
#2 (20/04; 14:00)	2.44 ± 0.18	0.019 ± 0.003	2.47 ± 0.19	0.017 ± 0.003	2.48 ± 0.19	0.022 ± 0.004	2.35 ± 0.19	0.024 ± 0.006
#3 (20/04; 15:55)	2.41 ± 0.17	0.019 ± 0.003	2.45 ± 0.18	0.023 ± 0.003	2.54 ± 0.20	0.016 ± 0.004	2.40 ± 0.20	0.018 ± 0.006
#4 (20/04; 19:45)	2.44 ± 0.18	0.016 ± 0.003	2.46 ± 0.19	0.023 ± 0.003	2.59 ± 0.21	0.017 ± 0.004	2.41 ± 0.20	0.017 ± 0.006
#5 (20/04; 21:15)	2.48 ± 0.18	0.021 ± 0.003	2.61 ± 0.20	0.019 ± 0.003	2.42 ± 0.19	0.020 ± 0.004	2.53 ± 0.21	0.023 ± 0.006

Table A4: 10GHz complex permittivity measurements for Group 3 and 4 where order of film removal from stack is altered to #3, #6, #2, #1 (Temperature: 23 ˚C)

	Number of layers							
	6		5		4		3	
Trial number (dd/mm; time of measurement)	Permittivity (ε_f)	Loss Tangent ($\tan\delta_f$)	Permittivity (ε_f)	Loss Tangent ($\tan\delta_f$)	Permittivity (ε_f)	Loss Tangent ($\tan\delta_f$)	Permittivity (ε_f)	Loss Tangent ($\tan\delta_f$)
Group 3								
#14 (03/05;10:30)	2.65 ± 0.21	0.020 ± 0.003	2.57 ± 0.20	0.025 ± 0.004	2.65 ± 0.22	0.020 ± 0.005	2.60 ± 0.23	0.033 ± 0.01
Group 4								
#14 (03/05; 11:30)	2.51 ± 0.18	0.016 ± 0.003	2.48 ± 0.19	0.015 ± 0.003	2.44 ± 0.19	0.019 ± 0.004	2.48 ± 0.20	0.016 ± 0.005

Table A5: 20GHz complex permittivity measurements for Group 1 samples (Temperature: 23 ˚C)

	Number of layers							
	6		5		4		3	
Trial number (date (dd/mm); time of measurement)	Permittivity (ε_f)	Loss Tangent ($\tan\delta_f$)	Permittivity (ε_f)	Loss Tangent ($\tan\delta_f$)	Permittivity (ε_f)	Loss Tangent ($\tan\delta_f$)	Permittivity (ε_f)	Loss Tangent ($\tan\delta_f$)
#3 (04/04; 14:00)	2.50 ± 0.18	0.026 ± 0.003	2.37 ± 0.17	0.026 ± 0.004	2.50 ± 0.18	0.026 ± 0.005	2.46 ± 0.19	0.019 ± 0.006
#5 (05/04; 21:15)	2.77 ± 0.20	0.019 ± 0.003	2.97 ± 0.23	0.017 ± 0.004	2.70 ± 0.20	0.008 ± 0.004	2.62 ± 0.20	0.021 ± 0.006
#9 (12/04; 20:30)	2.72 ± 0.20	0.024 ± 0.003	2.67 ± 0.20	0.019 ± 0.003	2.85 ± 0.22	0.010 ± 0.005	2.57 ± 0.20	0.019 ± 0.006
#?? (27/04; 10:10)	2.56 ± 0.18	0.019 ± 0.003	2.44 ± 0.17	0.016 ± 0.004	2.41 ± 0.18	0.025 ± 0.005	2.44 ± 0.18	0.016 ± 0.006

Table A6: 20GHz complex permittivity measurements for Group 2 samples (Temperature: 23 ˚C)

	Number of layers							
	6		5		4		3	
Trial number (dd/mm; time of measurement)	Permittivity (ε_f)	Loss Tangent ($\tan\delta_f$)	Permittivity (ε_f)	Loss Tangent ($\tan\delta_f$)	Permittivity (ε_f)	Loss Tangent ($\tan\delta_f$)	Permittivity (ε_f)	Loss Tangent ($\tan\delta_f$)
#2 (30/03; 15:30)	2.61 ± 0.19	0.022 ± 0.004	2.67 ± 0.20	0.022 ± 0.004	2.58 ± 0.20	0.030 ± 0.006	2.33 ± 0.18	0.033 ± 0.008
#9 (12/04; 21:10)	2.65 ± 0.19	0.020 ± 0.004	2.70 ± 0.20	0.029 ± 0.005	2.25 ± 0.16	0.012 ± 0.003	2.31 ± 0.18	0.024 ± 0.007
#10 (12/04; 21:55)	2.48 ± 0.18	0.024 ± 0.004	2.67 ± 0.20	0.019 ± 0.004	2.39 ± 0.18	0.033 ± 0.006	2.19 ± 0.16	0.021 ± 0.008

Table A7: 20GHz complex permittivity measurements for Group 3 samples (Temperature: 23 ˚C)

	Number of layers							
	6		5		4		3	
Trial number (dd/mm; time of measurement)	Permittivity (ε_f)	Loss Tangent ($\tan\delta_f$)	Permittivity (ε_f)	Loss Tangent ($\tan\delta_f$)	Permittivity (ε_f)	Loss Tangent ($\tan\delta_f$)	Permittivity (ε_f)	Loss Tangent ($\tan\delta_f$)
#7 (27/04; 13:35)	2.71 ± 0.20	0.021 ± 0.003	2.66 ± 0.19	0.022 ± 0.003	2.56 ± 0.19	0.024 ± 0.004	2.60 ± 0.20	0.021 ± 0.006
#8 (27/04; 15:20)	2.67 ± 0.19	0.023 ± 0.003	2.67 ± 0.20	0.019 ± 0.003	2.54 ± 0.19	0.030 ± 0.004	2.71 ± 0.21	0.027 ± 0.006
#9 (30/04; 10:45)	2.72 ± 0.20	0.023 ± 0.003	2.58 ± 0.19	0.021 ± 0.003	2.72 ± 0.20	0.022 ± 0.004	2.72 ± 0.21	0.015 ± 0.006
#10 (01/05; 9:10)	2.55 ± 0.18	0.023 ± 0.003	2.67 ± 0.20	0.019 ± 0.003	2.51 ± 0.18	0.022 ± 0.004	2.50 ± 0.19	0.023 ± 0.006
#15 (05/05; 9:10)	2.58 ± 0.18	0.026 ± 0.003	2.55 ± 0.18	0.023 ± 0.003	2.69 ± 0.20	0.020 ± 0.004	2.67 ± 0.21	0.021 ± 0.006

Table A8: 20GHz complex permittivity measurements for Group 4 samples (Temperature: 23 ˚C)

	Number of layers							
	6		5		4		3	
Trial number (dd/mm; time of measurement)	Permittivity (ε_f)	Loss Tangent ($\tan\delta_f$)	Permittivity (ε_f)	Loss Tangent ($\tan\delta_f$)	Permittivity (ε_f)	Loss Tangent ($\tan\delta_f$)	Permittivity (ε_f)	Loss Tangent ($\tan\delta_f$)
#6 (27/04; 10:50)	2.47 ± 0.17	0.017 ± 0.002	2.60 ± 0.19	0.016 ± 0.003	2.76 ± 0.21	0.020 ± 0.003	2.60 ± 0.19	0.010 ± 0.004
#7 (27/04; 14:30)	2.70 ± 0.19	0.011 ± 0.002	2.62 ± 0.19	0.021 ± 0.003	2.72 ± 0.20	0.019 ± 0.003	2.62 ± 0.20	0.015 ± 0.005
#8 (27/04; 16:15)	2.55 ± 0.18	0.020 ± 0.002	2.65 ± 0.19	0.016 ± 0.003	2.60 ± 0.19	0.016 ± 0.003	2.59 ± 0.19	0.025 ± 0.005
#9 (30/04; 13:05)	2.58 ± 0.18	0.018 ± 0.002	2.62 ± 0.19	0.019 ± 0.003	2.75 ± 0.20	0.011 ± 0.003	2.70 ± 0.21	0.023 ± 0.005
#10 (01/05; 10:30)	2.59 ± 0.18	0.016 ± 0.002	2.62 ± 0.19	0.020 ± 0.003	2.72 ± 0.20	0.017 ± 0.003	2.66 ± 0.20	0.020 ± 0.004
#11 (01/05; 11:15)	2.53 ± 0.18	0.019 ± 0.002	2.59 ± 0.18	0.019 ± 0.003	2.74 ± 0.20	0.016 ± 0.003	2.52 ± 0.19	0.021 ± 0.004

Table A9: 20GHz complex permittivity measurements for Group 3 and 4 where order of film removal from stack is altered to #3, #6, #2, #1 (Temperature: 23 ˚C)

	Number of layers							
	6		5		4		3	
Trial number (dd/mm; time of measurement)	Permittivity (ε_f)	Loss Tangent ($\tan\delta_f$)	Permittivity (ε_f)	Loss Tangent ($\tan\delta_f$)	Permittivity (ε_f)	Loss Tangent ($\tan\delta_f$)	Permittivity (ε_f)	Loss Tangent ($\tan\delta_f$)
Group 3								
#12 (01/05; 15:10)	2.66 ± 0.19	0.019 ± 0.003	2.71 ± 0.20	0.020 ± 0.003	2.70 ± 0.20	0.024 ± 0.004	2.71 ± 0.21	0.021 ± 0.005
Group 4								
#12 (01/05; 13:05)	2.61 ± 0.18	0.017 ± 0.002	2.51 ± 0.18	0.017 ± 0.003	2.58 ± 0.19	0.016 ± 0.003	2.42 ± 0.17	0.008 ± 0.003

References

[1] Courtney C C 1998 Time-Domain Measurement of the Electromagnetic Properties of Materials *IEEE Transactions on Microwave Theory and Techniques* **46** 517-22

[2] Yue H, Virga K L and Prince J L 1998 Dielectric Constant and Loss Tangent Measurement Using a Stripline Fixture *IEEE Transactions on Components, Packaging and Manufacturing Technology - Part B* **21**

[3] Afsar M N, Birch J R and Clarke R N 1986 The Measurement of the Properties of Materials *Proceedings of the IEEE* **74**

[4] Baker-Jarvis J, Vanzura E J and Kissick W A 1990 Improved Technique for Determining Complex Permittivity with the Transmission/Reflection Method *IEEE Transactions on Microwave Theory and Techniques* **38**

[5] Krupka J 2006 Frequency domain complex permittivity measurements at microwave frequencies *Meas. Sci. Technol.* **17** R55 - R70

[6] Murata K, Hanawa A and Nozaki R 2005 Broadband complex permittivity measurement techniques of materials with thin configuration at microwave frequencies *Journal of Applied Physics* **98**

[7] Courtney C C and Motil W 1999 One-Port Time-Domain Measurement of the Approximate Permittivity and Permeability of Materials *IEEE Transactions on Microwave Theory and Techniques* **47** 551-5

[8] Wang Z Y, Kelly M A, Shen Z X, Wang G, Xiang X D and Wetzel J T 2002 Evanescent microwave probe measurement of low-k dielectric films *Journal of Applied Physics* **92** 808-11

[9] Talanov V V, Scherz A, Moreland R L and Schwartz A R 2006 A near-field scanned microwave probe for spatially localized electrical metrology *Applied Physics Letters* **88**

[10] Talanov V V, Scherz A, Moreland R L and Schwartz A R 2006 Noncontact dielectric constant metrology of low-k interconnect films using a near-field scanned microwave probe *Applied Physics Letters* **88**

[11] Talanov V V, Scherz A and Schwartz A R 2006 Noncontact electrical metrology of Cu/low-k interconnect for semiconductor production wafers *Applied Physics Letters* **88**

[12] Krupka J, Geyer R G, Baker-Jarvis J and Ceremuga J 1996 Measurements of the complex permittivity of microwave circuit board substrates using split dielectric resonator and reentrant cavity techniques. In: *Seventh International Conference on Dielectric Materials Measurements & Applications,*

[13] Krupka J, Gregory A P, Rochard O C, Clarke R N, Riddle B and Baker-Jarvis J 2001 Uncertainty of Complex Permittivity Measurements by Split-Post Dielectric Resonator Technique *Journal of the European Ceramic Society* **21** 2673-6

[14] Krupka J, Huang W and Tung M 2005 Complex Permittivity Measurements of Thin Ferroelectric Films Employing Split Post Dielectric Resonator. In: *IMF11 Conference,* (Iguacu, Brasil

[15] Jacob M V, Krupka J, Derzakowski K and Mazierska J 2006 Measurement of thin polymer films employing split post dielectric resonator technique. In: *MIKON,* (Krakow pp 229 - 31

[16] Krupka J, Gabelich S A, Derzakowski K and Pierce B M 1999 Comparison of split post dielectric resonator and ferrite disc resonator techniques for microwave permittivity measurements of polycrystalline yttrium iron garnet *Meas. Sci. Technol.* **10** 1004 - 8

[17] Electrical Properties, GE Quartz Worldwide, http://www.gequartz.com/en/electric.htm.

CHAPTER 5 INVESTIGATION OF POLYMER STABILITY UNDER DIFFERENT ENVIRONMENTAL AND PHYSICAL CONDITIONS

This chapter presents two papers that describe the stability of the LAEO based polymer under different conditions. This knowledge can provide unique insight concerning the feasibility of employing the polymer, in addition to potential applications. Section 5.1 examines the stability of the polymer while in contact with various solvents in an attempt to determine the solubility characteristics, in addition to the adhesion properties of the films. The second paper presents the ageing and thermal stability of the polymers fabricated at varying RF powers.

5.1 SOLUBILITY AND ADHESION CHARACTERISTICS OF PLASMA POLYMERISED THIN FILMS DERIVED FROM LAVANDULA ANGUSTIFOLIA ESSENTIAL OIL

Adhesion and solubility characteristics of the LAEO based polymers are investigated in this paper. Contact angle data employing various solvents are used to provide information concerning the stability of the thin films. This data is used to obtain the surface tension (surface energy) of the polymer, which in turn can be used to determine the solubility of the polymer in various solvents. The adhesion of the polymer to commonly used substrates was examined using a crosshatch tape adhesion test. "Adhesion and solubility characteristics of plasma polymerised thin films derived from lavandula angustifolia essential oil" (Pub. 8.) at time of print is currently under review for publication in Journal of Applied Polymer Science (Wiley InterScience).

ADHESION AND SOLUBILITY CHARACTERISTICS OF PLASMA POLYMERISED THIN FILMS DERIVED FROM *LAVANDULA ANGUSTIFOLIA* ESSENTIAL OIL

Christopher D Easton and Mohan V Jacob*

Electronic Materials Research Lab, School of Engineering and Physical Sciences, James Cook University, Townsville, 4811, Australia

*Corresponding author. Tel.: +61 7 47814379; fax: +61 7 47815177; Email: Mohan.Jacob@jcu.edu.au

Abstract

Integration and implementation of organic polymer thin films often requires knowledge of the stability when in contact with solvents and the adhesion quality when applied to different substrates. This paper describes the solubility and adhesion characteristics of organic polymer thin films produced from lavandula angustifolia essential oil using radio frequency plasma polymerisation at four RF power levels. Contact angle data was obtained for various solvents and employed to determine the surface tension values for the polymer using three established methods. A relatively strong electron donor component and a negligible electronic acceptor component for the polymers indicate that they are monopolar in nature. Solubility data derived from interfacial tension values suggests the polymers would resist solubilisation from the solvents explored. The strongest solvophobic response was assigned to water, while diiodomethane demonstrated the weakest solvophobic response, with $\Delta G_{121} > 0$ in some instances depending on the surface tension values employed. The adhesion tests of the polymers deposited on glass, PET and PS indicated that the adhesion quality of the thin film improved with RF power, and was associated with an improvement in interfacial bonding.

Keywords: plasma polymerization, thin films, adhesion, solubility, contact angle

1. Introduction

Plasma polymerisation has gained significant attention in recent years for the fabrication of polymer thin films and plasma modification of surfaces. This technique is a luminous

chemical vapour deposition method that typically takes place in a low-temperature thermally non-equilibrium plasma. Polymer thin films produced via this method exhibit thickness homogeneity, physical and chemical stability, with smooth, pinhole free surfaces.[1,2] The properties of the polymers can be tuned by altering the deposition conditions, including RF power.[3] Such tuning can be employed during deposition to induce affects such as an optical gradient in the film.[4] Plasma polymers have been implemented in a number of applications involving electronics,[5] photonics,[6] and the biomedical[7,8] fields as protective coatings or functional thin films.

Polymer thin films fabricated from *Lavandula angustifolia* essential oil (LAEO)[9] and the resultant properties[10-12] have been reported previously. *Lavandula angustifolia* is one of three major commercial species of the Spica group, from the genus Lavandula; the other two species from the Spica group are *lavandula intermedia* and *lavandula latifolia.*[13] LAEO contains more than 80 components, including a number of hydrocarbon based components, in addition to metabolites that consist of ester, ketone and ether groups. The major components of LAEO are linalool (approx. 23 – 57 %) and linalyl acetate (approx. 4 – 35 %).[14] Herein the LAEO based polymer films will be referred to as polyLA. These polymer films were derived from a non-synthetic, natural source that is environmentally friendly. The resultant polymer is primarily hydrocarbon based with oxygen containing functional groups including hydroxyl and ketone. PolyLA has the potential to be implemented in biomedical and optoelectronic applications.

The adhesion and solubility characteristics of a thin film coating are important when considering implementation of the polymer in many applications. The chosen application will determine the conditions that it is subjected to during its life span, including device fabrication. For example, the properties of a sacrificial material for use in air gap fabrication can be dependent on the intended application and processing restrictions. The required properties of a thermally degradable sacrificial material for use in the fabrication of nanofluidic channels can include stability in solvents,[15] as acetone can be employed to remove photoresist rather than using plasma ashing. However within the microelectronics field, where air gaps are used to obtain structures with low dielectric constant, selective removal of a thermally degradable placeholder

material can been performed without the use of wet etching.[16,17] In addition, sacrificial materials that are removed through wet etching rather than thermal processing have been used with the aim of lowering the total thermal budget of IC fabrication.[18,19] A previous study[12] has indicated that polyLA is a potential candidate for use as a sacrificial polymer, therefore knowledge of the adhesion and solubility characteristics are important for this and other potential applications.

The aim is to characterise the adhesion and solubility properties of polyLA produced via RF plasma polymerisation. Contact angle (CA) measurement will be employed to determine the interfacial tension and thus the solubility of the polymer in various solvents. Adhesion tests will be performed on films fabricated at the various input power levels and substrate types. Samples fabricated at RF power levels of 10, 25, 50 and 75 W will be compared to determine the deviation in these properties as a function of deposition parameters.

2. Theory

Solubility of the polymer in different solvents can be determined using surface tension components employing the procedure outlined by Wu and Shanks.[20] The solubility of solute 1 (the polymer) in solvent 2 (the solvent) can be derived from their interfacial tension (γ_{12}):[20,21]

$$\Delta G_{121} = -2\gamma_{12} \quad (1),$$

where ΔG_{121} represents the free energy change. For $\Delta G_{121} >> 0$, solute 1 is solvophilic for solvent 2; $\Delta G_{121} << 0$, solute 1 is solvophobic for solvent 2; $\Delta G_{121} \approx 0$, solute 1 is partially dissolved in solvent 2.

To determine the interfacial tension for a polymer and solvent system, the surface tension of both parts is required. Wu and Shanks[20] employed the surface tension component theory of Van Oss, Chaudhury and Good (VCG) (also referred to as the Lifshitz-van der Waals / acid-base approach)[22] to obtain the surface tension values from CA measurements. However, there are several methods for obtaining surface tension values. The two main approaches are the VCG approach and the equation of state (EOS)

approach (ref[23,24] and references therein).There is much debate concerning the use of such methods to find the surface energy and the most appropriate method to employ. As such, there have been many publications addressing the validity of the methods,[24-28] accuracy,[29] and reviews of the available methods.[30,31] For this study, three approaches were chosen to provide a basis of comparison; the VCG approach, the EOS approach and the Fowkes approach.[32]

2.1 VCG approach

The VCG approach involves considering the total surface tension of a surface as a sum of components. The γ^{LW} component is assigned to Lifshitz-van der Wall interactions, including dispersion, dipolar and induction forces, and γ^{AB} is assigned to acid-base interactions, including electron donor-accepter interactions such as hydrogen bonding.[20] The total surface tension for a substance *i* is thus given by:[33]

$$\gamma_i = \gamma_i^{LW} + \gamma_i^{AB} = \gamma_i^{LW} + 2\sqrt{\gamma_i^+ \gamma_i^-} \quad (2),$$

where γ_i^+ represents the electron-acceptor parameters and γ_i^- the electron-donor parameter.

To determine the surface tension components for a solid, the following Young-Dupre equation for solid-liquid systems can be employed:[22]

$$(1+\cos\theta)\gamma_L = 2(\sqrt{\gamma_S^{LW}\gamma_L^{LW}} + \sqrt{\gamma_S^+\gamma_L^-} + \sqrt{\gamma_S^-\gamma_L^+}) \quad (3)$$

Therefore employing the known surface tension components for three liquids (L) and their corresponding CAs, the three surface tension parameters for the solid (S) can be determined. When choosing the three liquids to employ, one should be a high-energy apolar liquid such as diiodomethane where γ_L^+ and γ_L^- are zero, and the remaining two should be polar liquids.[22]

2.2 EOS approach

This approach derives the surface tension from a purely thermodynamic point of view, and therefore neglects the molecular origins of surface tension. The following equation

provides a method for calculating the surface energy of a solid from a single CA value (ref[23,24] and references therein):

$$\cos\theta_Y = -1 + 2\sqrt{\frac{\gamma_{sv}}{\gamma_{lv}}}e^{-\beta(\gamma_{lv}-\gamma_{sv})^2} \quad (4),$$

where the constant $\beta \approx 0.0001247$.[31]

2.3 Fowkes Approach

Surface free energy of a solid can be calculated from the following equation:[31,32]

$$\left[\frac{1+\cos\theta}{2}\right]\times\left[\frac{\gamma_l}{\gamma_l^d}\right] = \sqrt{\gamma_s^p}\times\sqrt{\frac{\gamma_l^p}{\gamma_l^d}} + \sqrt{\gamma_s^d} \quad (5),$$

where γ^p is the polar component and γ^d is the disperse component. It is recognised that γ^p can be replaced by γ^{AB}, and γ^d replaced by γ^{LW}. Employing the procedure outlined by Deshmukh and Shetty,[31] interpreting equation 5 as Y(LHS) = mX(RHS) + C and plotting LHS vs RHS for at least 3 solvents provides a straight line with a Y-axis intercept. The slope ($[\gamma^p]^{1/2}$) and intercept ($[\gamma^d]^{1/2}$) are used to determine the total surface energy.

2.4 Interfacial tension calculation

Once the surface tension values for the solid and liquid are known, the interfacial tension and thus the solubility can be determined. For a completely immiscible solid-liquid system, the interfacial tension is given by (ref[20]and references therein):

$$\gamma_{SL} = \gamma_S - \gamma_L\cos\theta \quad (6)$$

For a completely miscible system however, the interfacial tension cannot be measured directly, though can be obtained from the individual surface tension components based on the VCG approach (ref[20] and references therein):

$$\gamma_{12} = (\sqrt{\gamma_1^{LW}} - \sqrt{\gamma_2^{LW}})^2 + 2(\sqrt{\gamma_1^+\gamma_1^-} + \sqrt{\gamma_2^+\gamma_2^-} - \sqrt{\gamma_1^+\gamma_2^-} - \sqrt{\gamma_1^-\gamma_2^+}) \quad (7)$$

Therefore use of equation 7 is restricted to the surface tension components obtained using the VCG approach, however equation 6 can be applied using the value of surface tension for the solid obtained from any of the methods.

3. Experimental

L. angustifolia monomer obtained from G. R. Davis Pty Ltd was employed in the fabrication of plasma polymer films using the experimental apparatus detailed previously.[9] The thin films were fabricated at a pressure of approximately 250 mTorr, and RF energy (13.56 MHz) was delivered to the deposition chamber via external copper electrodes separated by a distance of 11 cm. The deposition time was varied (2.5 to 12 min) in conjunction with the applied RF power (10 to 75 W) to produce films of approximately the same thickness. Approximately 1 mL of the monomer was placed into the holder for each successive deposition. The monomer inlet valve opened briefly to evacuate the holder prior to placing the substrate within the polymerisation cell. During deposition, the monomer inlet was again opened and the vapour released into the chamber, where the flow rate was controlled via a vacuum stopcock. Three different types of substrate were used in this study; glass slides for the solubility and adhesion tests, and poly(ethylene terephthalate) (PET) and polystyrene (PS) (City Plastics Pty Ltd) for adhesion testing. Refer to ref[12] for substrate cleaning procedure.

CA measurements were performed using a KSV 101 system. The height of each drop was confirmed using a CCD camera prior to each measurement to ensure consistency in drop volume (8 μL). 6 to 8 drops were used to determine the average CA for each solvent-polymer combination. The solvents employed in this study are listed in Table 1. Once the drop was placed on the surface, the KSV CAM software was triggered to begin recording. An image was recorded every second for 30 s in order to monitor the CA as a function of time. CA values were derived from the raw data via image processing software by fitting the measured drop profile with the Young-Laplace equation.

Adhesion studies were performed using an Elcometer crosshatch tape adhesion test kit, complying with standard ASTM D3359. Similar adhesion studies have been performed previously on plasma polymers.[4,34] Using the cutting tool (6 teeth, 1 mm spacing), crosshatch patterns were made in the polymer films. Tape was then applied on top of the lattice followed by a pencil eraser across the surface to smooth out the tape. The tape was then removed by pulling at an angle of 180º and the results analysed using a template of images to provide a qualitative value for adhesion. The adhesion was rated on a scale between 5 to 0, with 5 representing no delamination, 4 representing less than 5 % delamination area, 3 representing 5 – 15 % delamination area, 2 representing 15 to 35 % delamination area, 1 representing 35 to 65 % delamination area, and 0 representing greater than 65% delamination area. 3 samples were fabricated for each applied RF power and substrate combination, with 3 crosshatch tests performed on each sample, therefore a total of 9 tests were performed for each applied RF power and substrate combination. Images of the tests were recorded using an optical microscope and CCD camera.

Table 1: Solvents employed in solubility study.

Solvent	Grade	Supplier
Ethylene Glycol (EG)	Laboratory	Ajax Finechem Pty Ltd
Glycerol	Analytical (99.5%)	Ajax Finechem Pty Ltd
Formamide	Laboratory (99.5%)	Ajax Finechem Pty Ltd
Dimethyl sulfoxide (DMSO)	Analytical (≥99.7%)	Ajax Finechem Pty Ltd
Diiodomethane (DIM)	≥ 98%	Merck Chemicals

4. Results and Discussion

4.1 Contact angle

The KSV 101 system employed in this study provided an equilibrium CA. The CA was measured at 1 second intervals to monitor any dynamic changes at the liquid-solid interface, including swelling or dissolution of the solid by the liquid.[24,35] As the measured CA has the potential to change as a function of time, these angles are then considered to be at instantaneous equilibrium with the surface and as such provide a representation of the surface state at each recorded point in time.[36]

As outlined previously,[10] the experimental procedure was confirmed by performing water CA measurements on PTFE. A linear fit was obtained from time dependant data using the equation y = -0.01t +119.95 and R^2 = 0.97, where t represents time. Extrapolating to t = 0 gives a water CA for PTFE of 119.95º and was comparable to the result reported by Alexander and Duc (y = -0.05t +119).[36]

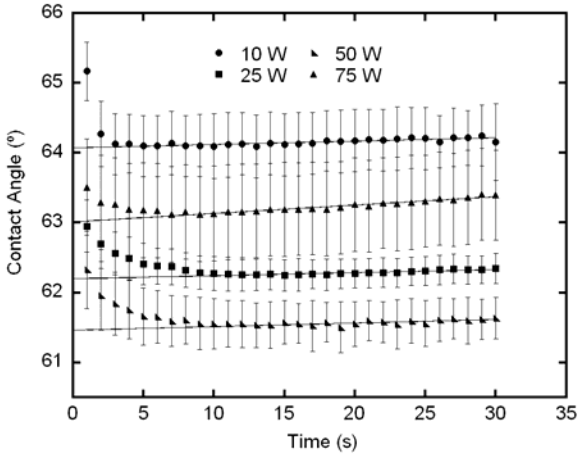

Figure 1: CA versus time for ethylene glycol.

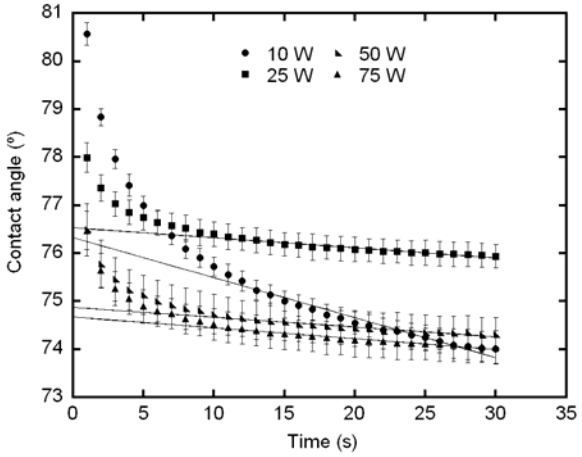

Figure 2: CA versus time for glycerol.

CA data for the polyLA thin films fabricated at various power levels are presented in Figures 1 to 5, where the error bars represent the 95 % confidence levels at each time

interval. Table 2 contains the equation that provides the linear fit to each data set, where 'm' also represents the rate of change of the CA, and 'c' represents the extrapolated value for CA at t = 0 for each polymer and solvent combination. The water CA values have been reported previously[10] and are included to aid in determining the surface energy of the polymer.

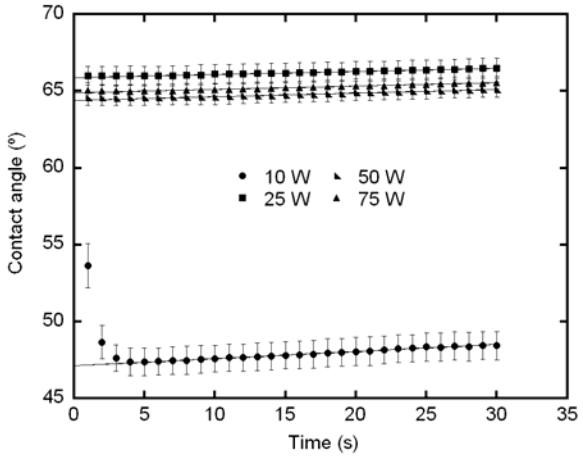

Figure 3: CA versus time for formamide.

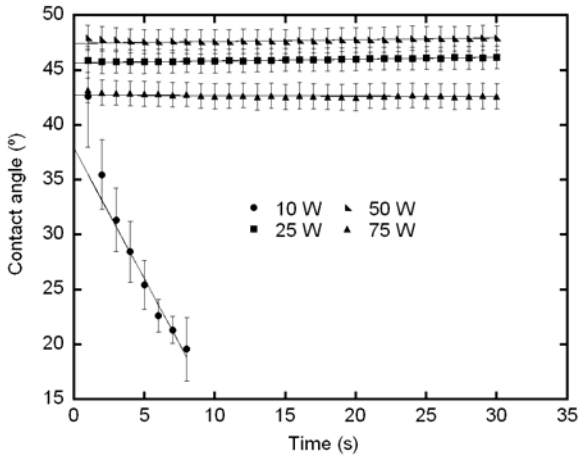

Figure 4: CA versus time for DMSO.

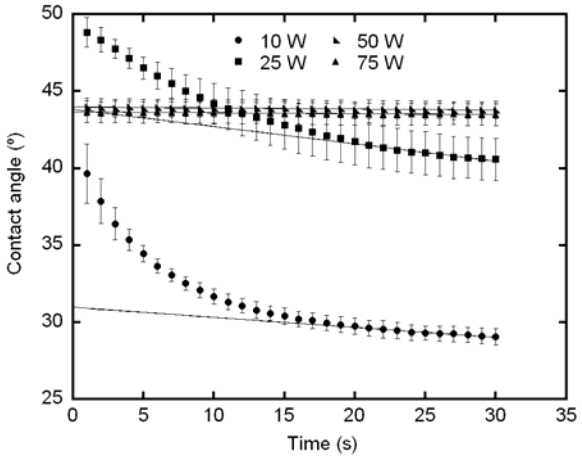

Figure 5: CA versus time for DIM.

The raw CA data presents useful information concerning interactions between the surface and liquid system. An initial rapid decrease in the contact angle has been used to identify absorption of the solvent into the sample, furthermore, a relatively large rate of change in the contact angle has been attributed to reorientation of functionalities at the solid-liquid interface.[36] For example, the rate of change in CA reported by Alexander and Duc for water on PTFE (0.05º s^{-1}) was considered small enough to be negligible. While the origin of this rate of change was not clarified by the authors, it was considered to be most likely occurring due to reactions between the solid-liquid interface, evaporation, or a combination of the two processes. Both of these trends in the raw CA data provide an indication of the stability of the polymer while in contact with the applied solvents.

From the raw CD data for ethylene glycol (Figure 1), an initial rapid drop in CA before stabilising for all polymer samples was found, thus indicating absorption of the solvent into thin film. The rate of change of CA was relatively small (~ 0.005º s^{-1}), however exhibited a positive gradient. While this rate of change was considered insignificant, the positive gradient suggested the occurrence of reorientation of functionalities at the interface. For glycerol, there was also an initial rapid decrease of CA before stabilising; however the magnitude of the drop decreased with increased applied RF power during fabrication. A similar situation occurred with the formamide and DMSO data, where an initial rapid drop in CA occurs for the 10 W sample, though was not present for the

other samples. Also for the DIM data, the 10 and 25 W samples both exhibited the initial rapid drop, while the 50 and 75 W data were relatively stable with time. These results indicated that the polymer was more stable as the RF power was increased, which was expected as an increase in RF power during fabrication typically results in an increase in cross link density for this form of polymerisation. It also signifies that the 10 W, and to a lesser extent the 25 W CA data may not produce reliable surface energy results due to the significant error introduced by the rapid decrease.

Table 2: Equations for line of best fit and corresponding CA data for polyLA deposited at four RF power levels for the solvents examined.

		Equation (mx +C)	
Liquid	Sample (W)	m / rate of change (º s^{-1})	C / CA (º)
Water[10]	10	-0.0048	81.93
	25	-0.0062	83.64
	50	-0.0086	84.46
	75	-0.014	91.95
Ethylene glycol	10	0.0048	64.074
	25	0.0044	62.199
	50	0.0052	61.462
	75	0.0044	62.199
Glycerol	10	-0.0833	76.329
	25	-0.021	76.543
	50	-0.0204	74.877
	75	-0.0224	74.673
Formamide	10	0.0464	47.119
	25	0.0197	65.892
	50	0.0236	64.407
	75	0.0218	64.893
DMSO	10	-2.3732	37.848
	25	0.0161	45.692
	50	0.0157	47.469
	75	-0.004	42.73
DIM	10	-0.0645	30.965
	25	-0.1129	43.853
	50	-0.0063	43.981
	75	-0.0059	43.668

It was reported previously[10] for the water CA measurements on polyLA that an increase in the fabrication RF power resulted in an increase in the CA value and thus a decrease in the polarity of the polymer. The increase in CA was found to be the result of a decrease in the oxygen content of the resultant polymers, where the hydroxyl group

diminished in intensity as RF power increased. Such a clear trend in the CA data was not present for the remaining solvents employed in this study (see Table 2). This was most likely due to interactions occurring between the solvent-solid interface and was further indication that the data sets for the lower RF power level samples may produce unreliable surface energy results.

4.2 Calculation of surface tension (surface energy)

Surface tension values for polyLA fabricated at different RF powers were calculated using the three methods outlined in the theory section. The contact angle data obtained for the solvents, together with the surface tension parameters outlined in Table 3 were employed in this study. The surface tension results from the VCG, EOS and Fowkes approaches are presented in Tables 4, 5, and 6 respectively, and the graphs used to determine the values for the Fowkes approach are shown in Figure 6.

Table 3: Surface tension parameters for the solvents employed.

Solvent	γ	γ^{LW}	γ^{AB}	γ^{+}	γ^{-}
Water[b]	72.8	21.8	51.0	25.5	25.5
EG[a]	47.99	28.99	19.0	1.92	47.0
Glycerol[a]	64	34	30.0	3.92	57.4
Formamide[a]	57.49	38.49	19.0	2.28	39.6
DMSO[a]	43.58	35.58	8.0	0.5	32.0
DIM[b]	50.8	50.8	0	0	0
Hexane[c]	18.4	-	-	-	-
Chloroform[c]	27.32	-	-	-	-
Ethanol[c]	22.39	-	-	-	-
Acetone[c]	24.02	-	-	-	-

[a]Taken from ref [26]. [b]Taken from ref [20]. [c]Taken from [37].

Table 4: Surface tension components obtained for polyLA using VCG approach[a]

Sample	Liquid combination	γLW	γ+	γ-	γS
10 W	G:W:DIM	43.82	0.33	7.17	40.72
	EG:W:DIM	43.82	0.55	8.08	39.59
	F:W:DIM	43.82	0.72	1.56	45.94
	DMSO:W:DIM	43.82	0.16	6.24	41.82
	G:EG:DIM	43.82	1.34	24.00	32.47
	G:F:DIM	43.82	161.10	2313.50	-1177.10
	G:DMSO:DIM	43.82	0.08	2.33	42.97
	EG:F:DIM	43.82	52.00	1214.40	-458.80
	EG:DMSO:DIM	43.82	0.00	1.13	43.72
	F:DMSO:DIM	43.82	2.05	115.71	13.03
25 W	G:W:DIM	37.62	0.03	6.33	36.71
	EG:W:DIM	37.62	0.04	6.41	36.63
	F:W:DIM	37.62	0.05	6.57	36.45
	DMSO:W:DIM	37.62	0.06	6.67	36.34
	G:EG:DIM	37.62	0.06	7.44	36.33
	G:F:DIM	37.62	0.39	17.70	32.38
	G:DMSO:DIM	37.62	0.09	8.68	35.89
	EG:F:DIM	37.62	0.00	3.57	37.37
	EG:DMSO:DIM	37.62	0.10	9.70	35.66
	F:DMSO:DIM	37.62	0.07	7.35	36.19
50 W	G:W:DIM	37.55	0.00	4.94	37.63
	EG:W:DIM	37.55	0.01	5.54	37.01
	F:W:DIM	37.55	0.00	5.23	37.33
	DMSO:W:DIM	37.55	0.11	6.58	35.88
	G:EG:DIM	37.55	0.20	16.12	33.92
	G:F:DIM	37.55	0.36	20.95	32.07
	G:DMSO:DIM	37.55	0.31	19.57	32.61
	EG:F:DIM	37.55	0.15	13.67	34.69
	EG:DMSO:DIM	37.55	0.36	22.45	31.88
	F:DMSO:DIM	37.55	0.31	19.32	32.67
75 W	G:W:DIM	37.72	0.13	0.85	38.38
	EG:W:DIM	37.72	0.00	1.63	37.73
	F:W:DIM	37.72	0.04	1.20	38.13
	DMSO:W:DIM	37.72	0.00	1.52	37.84
	G:EG:DIM	37.72	0.79	32.41	27.63
	G:F:DIM	37.72	1.52	49.35	20.38
	G:DMSO:DIM	37.72	0.02	8.44	36.80
	EG:F:DIM	37.72	0.54	24.41	30.46
	EG:DMSO:DIM	37.72	0.01	0.59	37.89
	F:DMSO:DIM	37.72	0.00	4.58	37.45

[a]Key: W, Water; EG, Ethylene Glycol; G, Glycerol; F, Formamide;

Table 5: Surface tension values obtained for polyLA using EOS approach[a]

	γs			
Solvent	10 W	25 W	50 W	75 W
Water	34.27	33.20	32.69	28.00
EG	27.52	28.39	28.74	28.01
Glycerol	31.72	31.60	32.55	32.67
Formamide	42.82	33.08	33.87	33.61
DMSO	35.47	32.42	31.70	33.60
DIM	44.28	38.96	38.90	39.04

[a]Key: W, Water; EG, Ethylene Glycol; G, Glycerol; F, Formamide;

Table 6: Surface tension values obtained for polyLA using the Fowkes approach.

γs			
10 W	25 W	50 W	75 W
39.66	33.93	34.26	36.61

4.2.1 VCG approach

All possible solvent combinations involving 1 apolar liquid (DIM) and 2 polar liquids were employed in the VCG approach to provide 10 iterations per sample. As predicted, some of the data obtained for the 10 W sample appears to contain significant error, with large negative values derived for some liquid combinations. However, not all of the surface tension data for the 10 W was affected.

From all the CA data obtained, the measurements for the solvent water[10] are the most stable, with no initial rapid drop in CA value, a small rate of change, and minor values for the 95% confidence limits. These results indicated that it was highly unlikely that any interactions are occurring between the surface-liquid interface and that the polymer was stable while in contact with water. Due to these favourable conditions, these CA values are expected to be accurate. Thus it was not surprising that the stability in water CA values has transferred into the surface tension data calculated using the VCG approach. The surface tension components calculated employing water as one of the solvents demonstrated the least variance when compared to values calculated without the use of water. Therefore emphasis will only be given to the surface tension values obtained using water as a solvent (see highlighted values in Table 4).

The γ^{LW} values calculated for the solid provides a benchmark for the lowest value of γ of a liquid that can be used to obtain CA values. In the case of the 10 W sample, γ^{LW} = 43.82, thus for a liquid, the lowest value of γ that can be successfully employed in CA measurement is 43.82. In this study, DMSO has the lowest value of γ (43.58). As this value of γ was (slightly) smaller than the γ^{LW} value of the solid, the CA should not be measurable. As can be seen in Figure 4, the CA measurement for the 10 W sample demonstrates a rapid decrease with time, and in under 10 s becomes unmeasurable. For the remaining samples (25, 50 and 75 W), the CA data for DMSO was relatively stable and measurable. For these samples, $\gamma^{LW} \sim 37.63$ and thus was lower than the quoted value of γ for DMSO. Therefore the raw CA vs. time data suggests that the calculated results of γ^{LW} were accurate.

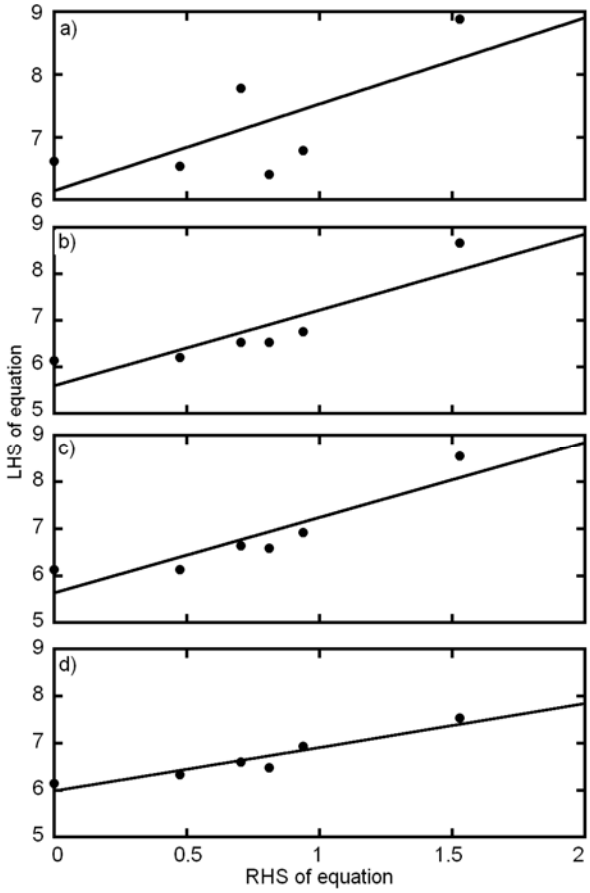

Figure 6: Graphs used to obtain surface tension values from the Fowkes approach using equation 5 for samples a) 10 W (R2 = 0.52), b) 25 W (R2 = 0.78), c) 50 W (R2 =0.82), and d) 75 W (R2 = 0.90).

Values for γ^+ and γ^- provide information concerning polar interactions with the surface. For this polymer, $\gamma^- >> \gamma^+$ and thus was considered monopolar. Most monopolar materials however are water soluble[20] as their value of γ^- are relatively large. It is possible to use this value of γ^- to determine an upper limit for which if exceeded, solubility will occur. Van Oss et. al.[21] demonstrated that for a γ^- monopole surface (substance 1) and water which is bipolar (substance 2), the following equation can provide that limit:

$$\gamma_{12}^{TOT} = (\sqrt{\gamma_1^{LW}} - \sqrt{\gamma_2^{LW}})^2 + 2(\sqrt{\gamma_2^+\gamma_2^-} - \sqrt{\gamma_1^-\gamma_2^+}) \quad (8)$$

Employing $\gamma_2^{LW} \approx 40$ mJ/m^2, it was found that equation 8 becomes negative and thus the interfacial tension becomes negative for $\gamma_1^- > 28.31$ mJ/m^2. A negative interfacial tension between the material and water indicates that the water will tend to penetrate the material, leading to repulsion between the molecules or particles and promote solubilisation.[21] As seen in Table 4, $\gamma^- < 28.31$ mJ/m^2 for all polymers, and thus indicates that they are not water soluble. It can also be seen that as the RF power was increased during deposition, the magnitude of γ^- tended to decrease, therefore providing another indicator that the hydrophobicity of the polymer increased with RF power.

4.2.2 EOS approach

For the EOS approach, the CA obtained for each solvent provides a unique result for the surface tension. There was some variance in the surface tension value between different solvents for each polymer (Table 5). With the exception of the surface tension results from DIM, the values obtained using the EOS approach are smaller than those obtained with the VCG approach. Employing the same assumption that was used for the VCG approach that the water CA values are the most accurate, then the values of surface tension derived using water should best represent the polymer. Therefore, the surface tension from the EOS approach for the polymer ranges from 34.27 to 28.00 mJ/m^2 for a RF power range of 10 to 75 W.

4.2.3 Fowkes approach

All 6 contact angle values were used for each sample in the Fowkes approach to derive a single value of surface tension. From the plots used to derive the surface tension values (Figure 6), it was apparent that the linear fit to the data improved with increasing RF power during deposition. Thus this result demonstrated that the 10 W CA data contains a significant degree of error, and that the stability of the polymer while in contact with the solvents improved with increasing RF power. The results obtained with the Fowkes approach roughly compare with those obtained by the VCG and EOS methods. Overall however, the results produced using the Fowkes and VCG methods are expected to be a more accurate representation of the polymer as they require more than one CA measurement to derive the surface tension values.

4.3 Calculation of solubility

The results of the solubility calculations using equations 6, 7 and 1 are presented in Table 7. ΔG_{121} values for the solvents employed for CA measurement were calculated, as well as for some common solvents including hexane, chloroform, ethanol and acetone. Due to the relatively low surface tension values for these solvents, it was not possible to obtain CA data and thus their CA was taken as 0º. In the instances where both equation 6 and 7 were used to obtain the interfacial tension for the solvent-solid system, in most cases the results were roughly equivalent, where the difference between the two values tended to decrease for increasing RF power.

ΔG_{121} values obtained suggest that the polymer would resist solubilisation from the solvents examined. These results indicated that the strongest solvophobic response was assigned to water, which was expected as the CA values for water proved to be the most stable. ΔG_{121} derived for DIM demonstrated the weakest solvophobic response, with $\Delta G_{121} > 0$ for the results calculated using the EOS and Fowkes surface tension values.

Table 7: ΔG121 values obtained for each solvent-sample combination under consideration using equations 7 and 6 from the derived surface tension data.

		Sample							
		10 W		25 W		50 W		75 W	
Solvent[a]	γ_s data[b]	equ 7	equ 6	equ 7	equ 6	equ 7	equ 6	equ 7	equ 6
W	A	-50.07	-61.00	-53.71	-57.29	-61.36	-61.20	-81.76	-81.74
	B	-45.65	-58.74	-53.14	-57.13	-57.63	-59.96	-80.55	-80.44
	C	-71.48	-71.44	-52.29	-56.77	-60.06	-60.60	-81.05	-81.24
	D	-55.07	-63.20	-51.71	-56.55	-51.15	-57.70	-81.43	-80.66
	E		-48.10		-50.27		-51.32		-60.98
	F		-58.88		-51.73		-54.46		-78.20
EG	A	-16.61	-39.47	-22.17	-28.66	-26.78	-29.40	-25.48	-33.22
	B	-13.39	-37.21	-21.63	-28.50	-24.26	-28.16	-32.07	-31.92
	C	-15.10	-49.91	-21.07	-28.14	-26.43	-28.80	-28.47	-32.72
	D	-20.23	-41.67	-20.62	-27.92	-19.19	-25.90	-32.31	-32.14
	E		-26.57		-21.64		-19.52		-12.46
	F		-37.35		-23.10		-22.66		-29.68
G	A	-28.78	-51.19	-36.75	-43.60	-42.58	-41.87	-43.30	-42.92
	B	-24.69	-48.93	-36.10	-43.44	-39.45	-40.63	-50.08	-41.62
	C	-29.88	-61.63	-35.40	-43.08	-42.07	-41.27	-46.33	-42.42
	D	-33.34	-53.39	-34.84	-42.86	-33.21	-38.37	-50.43	-41.84
	E		-38.29		-36.58		-31.99		-22.16
	F		-49.07		-38.04		-35.13		-39.38
F	A	-13.87	-3.20	-20.21	-26.45	-24.60	-25.60	-24.70	-27.97
	B	-10.95	-0.94	-19.72	-26.29	-22.23	-24.36	-30.30	-26.67
	C	-13.69	-13.64	-19.20	-25.93	-24.21	-25.00	-27.24	-27.47
	D	-17.19	-5.40	-18.78	-25.71	-17.58	-22.10	-30.57	-26.89
	E		9.70		-19.43		-15.72		-7.21
	F		-1.08		-20.89		-18.86		-24.43
DMSO	A	-2.44	-12.62	-6.76	-12.54	-9.77	-16.34	-6.63	-12.74
	B	-0.47	-10.36	-6.40	-12.38	-8.07	-15.10	-12.45	-11.44
	C	1.64	-23.06	-6.04	-12.02	-9.58	-15.74	-9.32	-12.24
	D	-4.74	-14.82	-5.74	-11.80	-4.70	-12.84	-12.58	-11.66
	E		0.28		-5.52		-6.46		8.02
	F		-10.50		-6.98		-9.60		-9.20
DIM	A	-6.67	5.68	-3.72	-0.15	-2.00	-2.15	-3.27	-3.27
	B	-8.95	7.94	-4.00	0.01	-2.94	-0.91	-1.94	-1.97
	C	-4.75	-4.76	-4.27	0.37	-2.00	-1.55	-2.82	-2.77
	D	-4.51	3.48	-4.51	0.59	-5.40	1.35	-1.94	-2.19
	E		18.58		6.87		7.73		17.49
	F		7.80		5.41		4.59		0.27
Hex	A		-44.64		-36.62		-38.46		-39.96
	B		-42.38		-36.46		-37.22		-38.66
	C		-55.08		-36.10		-37.86		-39.46
	D		-46.84		-35.88		-34.96		-38.88
	E		-31.74		-29.60		-28.58		-19.20
	F		-42.52		-31.06		-31.72		-36.42
Chl	A		-26.80		-18.78		-20.62		-22.12
	B		-24.54		-18.62		-19.38		-20.82
	C		-37.24		-18.26		-20.02		-21.62
	D		-29.00		-18.04		-17.12		-21.04
	E		-13.90		-11.76		-10.74		-1.36
	F		-24.68		-13.22		-13.88		-18.58

Eth	A	-36.66	-28.64	-30.48	-31.98
	B	-34.40	-28.48	-29.24	-30.68
	C	-47.10	-28.12	-29.88	-31.48
	D	-38.86	-27.90	-26.98	-30.90
	E	-23.76	-21.62	-20.60	-11.22
	F	-34.54	-23.08	-23.74	-28.44
Ac	A	-33.40	-25.38	-27.22	-28.72
	B	-31.14	-25.22	-25.98	-27.42
	C	-43.84	-24.86	-26.62	-28.22
	D	-35.60	-24.64	-23.72	-27.64
	E	-20.50	-18.4	-17.34	-7.96
	F	-31.28	-19.8	-20.48	-25.18

[a]Key: W, Water; EG, Ethylene Glycol; G, Glycerol; F, Formamide; Hex, Hexane; Chl, Chloroform; Eth, Ethanol; Ac, Acetone.

[b]Key: A, G:W:DIM (VCG); B, EG:W:DIM (VCG); C, F:W:DIM (VCG); D, DMSO:W:DIM (VCG); E, Water (EOS); F, Fowkes data.

Chloroform has been used to dissolve the polymer fabricated at 10 W in order to perform NRM spectroscopy[10], however dissolution of the polymer fabricated at higher power levels was not possible. Thus, there appears to be a contradiction between the calculated solvophobic response for the 10 W sample and experimental result. Results obtained at 10 W should then be considered a rough estimate at best. These results demonstrate the importance of determining CA values using solvents that are inert with the material under test. Interactions between the solvent and solid under test result in false CA values and thus an incorrect representation of the surface free energy of the solid.

The solubilisation of the polymer in ethanol is important when considering implementing the film in biomedical applications. Ethanol was used previously to sterilise plasma polymers prior to implementation,[38] therefore stability of the sample whilst immersed was necessary. The solubility data obtained indicated that the polymers would resist solubilisation from ethanol and as such can be sterilised in this manner.

4.4 Adhesion study

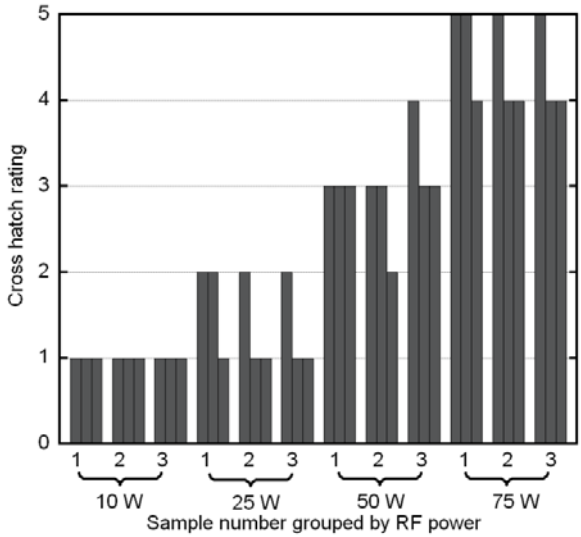

Figure 7: Adhesion data for polyLA deposited on glass at various RF power levels.

The adhesion data obtained using the cross hatch test for polyLA deposited on glass, PET and PS are presented in Figures 7, 8 and 9 respectively. A general trend was observed for all three substrate types where as the RF power during deposition was increased, the quality of the adhesion improved. In all cases, the 10 W samples demonstrated relatively poor adhesion, with the tape test removing a majority of the sample. The adhesion results for PET and PS were poor for the 25 W samples, however a sharp improvement was observed for these substrates at 50 and 75 W. At the high RF powers, no delamination from the substrate was observed for PS, while minor (< 5%) delamination was observed for a PET sample at 50 W and none at 75 W. An increase in adhesion quality was expected for increasing RF powers, as an increase in energy input into a plasma and an associated increase in ion bombardment can improve interfacial bonding.[39] Examples of the adhesion results obtained using the optical microscope for PS (Figure 10), glass (Figure 11), and PET (Figure 12) are presented.

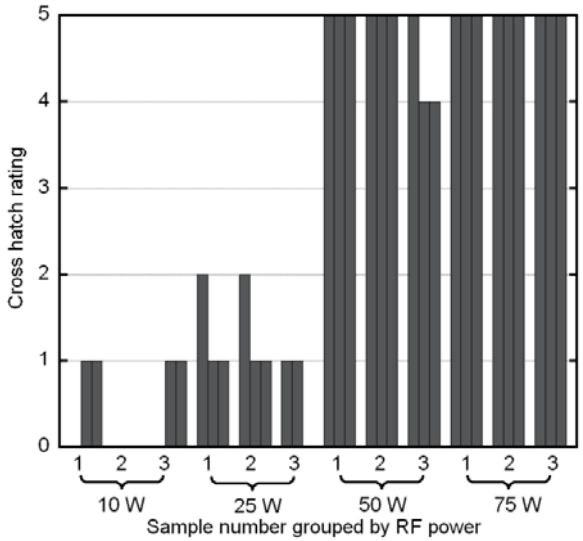

Figure 8: Adhesion data for polyLA deposited on PET at various RF power levels.

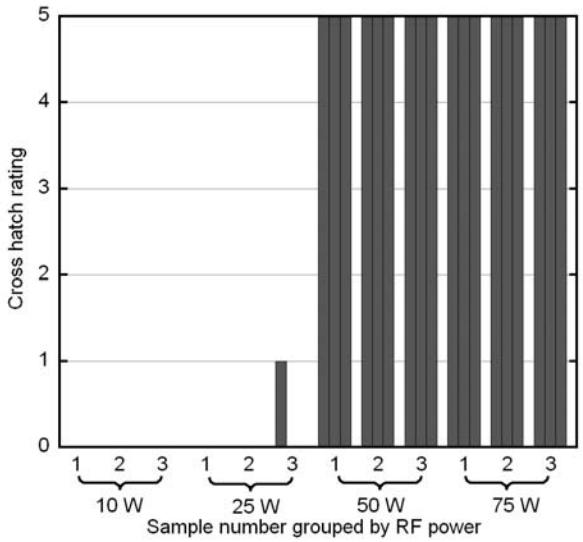

Figure 9: Adhesion data for polyLA deposited on PS at various RF power levels.

While the adhesion results of the polymer films fabricated at high RF power demonstrated good adhesive properties, at low RF power further improvement is possible. It is known that plasma-assisted surface modification of substrates by means of surface cross-linking, surface activation, or deposition of adhesion layers can improve the adhesion quality of thin films to these substrates.[7] Plasma pre-treatment using Ar or an Ar-N_2 mixture has been shown to improve adhesion of plasma deposits

to polymers.[40] All substrates employed in this study were plasma pre-treated with Ar. It is clear that additional work is required for improving the adhesion quality of the films deposited at low RF power levels.

The optical images obtained for the 10 W samples suggest a difference in the hardness of these samples in comparison to the films deposited at higher RF power levels. For the thin films deposited at an RF power of 25 W or higher, the areas which were not affected by the tape test appear uniform (see Figure 10 and 11), however for the 10 W samples (Figure 13), a significant amount of deformation, in addition to adhesion failing, occurred to the sample upon applying and subsequent removal of the tape. An increase in hardness for an increase in RF power has been reported previously for plasma polymers.[39,41,42] This trend is typically attributed to an increase in cross link density associated with increasing applied RF power, and would account for the apparent change in hardness observed.

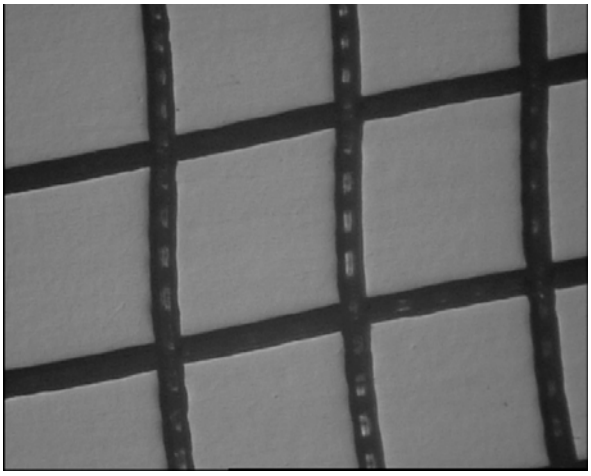

Figure 10: Sample 3 deposited at 75 W on PS (Example of cross hatch rating of 5). Cross hatch represents 1 x 1 mm.

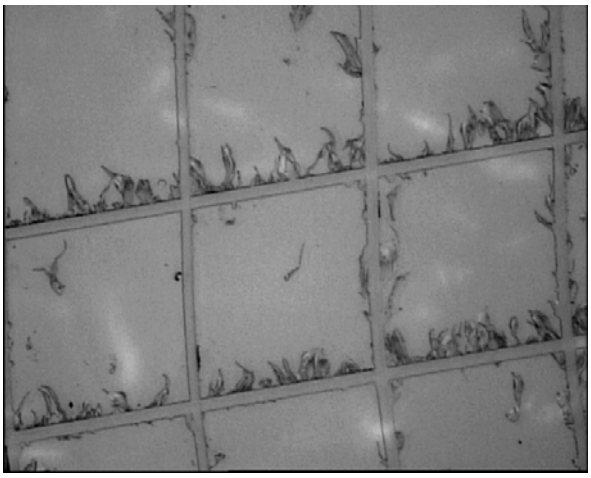

Figure 11: Sample 3 deposited at 25 W on glass (Example of cross hatch rating of 2). Cross hatch represents 1 x 1 mm.

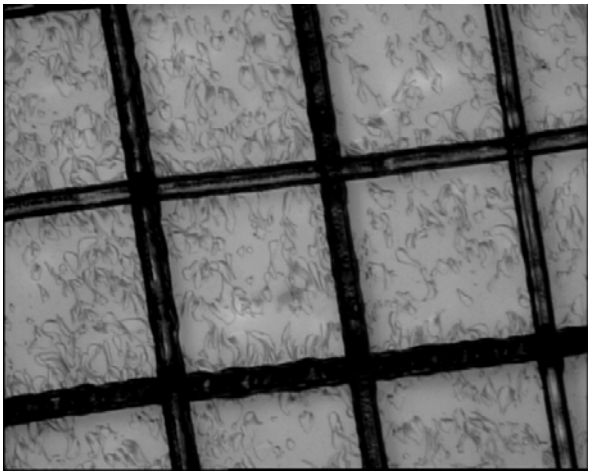

Figure 12: Sample 2 deposited at 25 W on PET (Example of cross hatch rating of 0). Cross hatch represents 1 x 1 mm.

It was evident from the experimental data that there was some variation in the quality of adhesion within sample groups. The crosshatch tape adhesion test provides a qualitative result for adhesion, and as such the accuracy of the test is dependent on correctly identifying the degree of delamination from optical images. A difference of approximately 5% between samples can potentially result in a difference in ratings. As such, there is a limitation as to the usefulness of such a test and should be used as an approximate result.

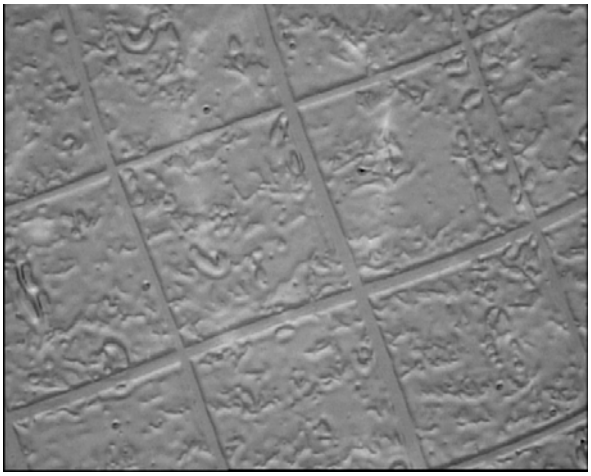

Figure 13: Sample 1 deposited at 10 W on glass (Example of cross hatch rating of 0). Cross hatch represents 1 x 1 mm.

5. Conclusion

Thin films have been fabricated from LAEO using RF plasma polymerisation and their solubility and adhesion characteristics determined. CA data has been obtained for the polymer fabricated at four different RF power levels using six solvents. For the 10 W sample, evidence of adsorption of the solvent into the polymer and reorientation of functionalities at the solid-liquid interface was present for all solvents, with the exception of water. For the polymers deposited at high RF power levels, the magnitude at which these reactions occurred decreased, with the exception for ethylene glycol, where the magnitude appeared unchanged with respect to RF power. The CA data was used to determine the surface tension values of the polymers employing three approaches; the VCG, EOS and Fowkes methods. For the VCG and EOS approaches, only surface tension data obtained from water CA values was considered. Results obtained from the VCG and Fowkes approach are believed to represent the polymer more accurately as they require more than one CA value to determine the surface tension. Based on these criteria, surface tension ranges have been established for the polymers fabricated at 10 W (39.53 – 45.94), 25 W (33.93 – 36.34), 50 W (34.26 – 37.63), and 75 W (36.61 – 38.38). The polymer demonstrated a relatively strong electron donor component and a negligible electronic acceptor component and was therefore monopolar in nature. Solubility results obtained from interfacial tension values

indicate that the polymer would resist solubilisation from the solvents examined. However, the dissolution of the 10 W sample in chloroform demonstrated the importance of a stable solvent-solid interface when obtaining CA data. An adhesion study established that for all substrates employed, the films deposited at high RF powers provided the best adhesion quality, while the films produced at low RF powers adhered poorly to the substrates. This trend was attributed to an improvement in interfacial bonding as a result of the increase in RF power and associated ion bombardment during deposition.

Acknowledgements

The authors are grateful to the financial support provided under the RIRDC and ARC LIEF and DP schemes. CDE is grateful to the APA and RIRDC scholarships. We are grateful to Ms Ruilan Liu for access to the solvent DMSO and to the Advanced Analytical Centre at JCU for use of the optical microscope.

References

1. Kim, M. C.; Cho, S. H.; Han, J. G.; Hong, B. Y.; Kim, Y. J.; Yang, S. H.; Boo, J. H., Surface & Coatings Technology 169, 595 2003.

2. Sajeev, U. S.; Mathai, C. J.; Saravanan, S.; Ashokan, R. R.; Venkatachalam, S.; Anantharaman, M. R., Bulletin of Materials Science 29, 159 2006.

3. Shi, F. F., Surface & Coatings Technology 82, 1 1996.

4. Muir, B. W.; Thissen, H.; Simon, G. P.; Murphy, P. J.; Griesser, H. J., Thin Solid Films 500, 34 2006.

5. Sohn, S.; Kim, K.; Kho, S.; Jung, D.; Boo, J. H., J. Alloy. Compd. 449, 191 2008.

6. Begou, T.; Beche, B.; Goullet, A.; Landesman, J. P.; Granier, A.; Cardinaud, C.; Gaviot, E.; Camberlein, L.; Grossard, N.; Jezequel, G.; Zyss, J., Opt. Mater. 30, 657 2007.

7. Forch, R.; Chifen, A. N.; Bousquet, A.; Khor, H. L.; Jungblut, M.; Chu, L. Q.; Zhang, Z.; Osey-Mensah, I.; Sinner, E. K.; Knoll, W., Chem. Vapor Depos. 13, 280 2007.

8. Siow, K. S.; Britcher, L.; Kumar, S.; Griesser, H. J., Plasma Processes and Polymers 3, 392 2006.

9. Jacob, M. V.; Easton, C. D.; Woods, G. S.; Berndt, C. C., Thin Solid Films 516, 3884 2008.

10. Easton, C. D.; Jacob, M. V.; Shanks, R. A.; Bowden, B. F., Chem. Vapor Depos. 2009, doi:10.1002/cvde.200806719.

11. Easton, C. D.; Jacob, M. V., Thin Solid Films 517, 4402 2009.

12. Easton, C. D.; Jacob, M. V., Polymer Degradation and Stability 94, 597 2009.

13. Peterson, L.; Rural Industries Research & Development Corporation: 2002.

14. Shellie, R.; Mondello, L.; Marriott, P.; Dugo, G., Journal of Chromatography A 970, 225 2002.

15. Li, W. L.; Tegenfeldt, J. O.; Chen, L.; Austin, R. H.; Chou, S. Y.; Kohl, P. A.; Krotine, J.; Sturm, J. C., Nanotechnology 14, 578 2003.

16. Park, S.; Allen, S. A. B.; Kohl, P. A., J. Electron. Mater. 37, 1524 2008.

17. Park, S.; Allen, S. A. B.; Kohl, P. A., J. Electron. Mater. 37, 1534 2008.

18. Gaillard, F.; de Pontcharra, J.; Gosset, L. G.; Lyan, P.; Bouchu, D.; Daamen, R.; Louveau, O.; Besson, P.; Passemard, G.; Torres, J., Microelectron. Eng. 83, 2309 2006.

19. Gosset, L. G.; Farcy, A.; de Pontcharra, J.; Lyan, P.; Daamen, R.; Verheijden, G.; Arnal, V.; Gaillard, F.; Bouchu, D.; Bancken, P. H. L.; Vandeweyer, T.; Michelon, J.; Hoang, V. N.; Hoofman, R. M.; Torres, J., Microelectron. Eng. 82, 321 2005.

20. Wu, S. H.; Shanks, R. A., Journal of Applied Polymer Science 93, 1493 2004.

21. Vanoss, C. J.; Chaudhury, M. K.; Good, R. J., Advances in Colloid and Interface Science 28, 35 1987.

22. Vanoss, C. J.; Chaudhury, M. K.; Good, R. J., Chemical Reviews 88, 927 1988.

23. Tavana, H.; Neumann, A. W., Advances in Colloid and Interface Science 132, 1 2007.

24. Kwok, D. Y.; Neumann, A. W., Advances in Colloid and Interface Science 81, 167 1999.

25. Wu, W.; Giese, R. F.; Vanoss, C. J., Langmuir 11, 379 1995.

26. Kwok, D. Y.; Li, D.; Neumann, A. W., Langmuir 10, 1323 1994.

27. Kwok, D. Y.; Lin, R.; Mui, M.; Neumann, A. W., Colloids and Surfaces a-Physicochemical and Engineering Aspects 116, 63 1996.

28. Johnson, R. E.; Dettre, R. H., Langmuir 5, 293 1989.

29. Shalel-Levanon, S.; Marmur, A., Journal of Colloid and Interface Science 262, 489 2003.

30. Balkenende, A. R.; van de Boogaard, H.; Scholten, M.; Willard, N. P., Langmuir 14, 5907 1998.

31. Deshmukh, R. R.; Shetty, A. R., Journal of Applied Polymer Science 107, 3707 2008.

32. Fowkes, F. M., The Journal of Physical Chemistry 67, 2538 1963.

33. Vanoss, C. J.; Good, R. J.; Chaudhury, M. K., Langmuir 4, 884 1988.

34. Yasuda, H. K.; Yu, Q. S.; Reddy, C. M.; Moffitt, C. E.; Wieliczka, D. M., Journal of Applied Polymer Science 85, 1443 2002.

35. Sedev, R. V.; Petrov, J. G.; Neumann, A. W., Journal of Colloid and Interface Science 180, 36 1996.

36. Alexander, M. R.; Duc, T. M., Polymer 40, 5479 1999.

37. Speight, J. G., Lange's Handbook of Chemistry; The McGraw-Hill Companies, Inc.: New York, 2005.

38. Detomaso, L.; Gristina, R.; Senesi, G. S.; d'Agostino, R.; Favia, P., Biomaterials 26, 3831 2005.

39. Cech, V., IEEE Trans. Plasma Sci. 34, 1148 2006.

40. Vallon, S.; Hofrichter, A.; Drevillon, B.; KlembergSapieha, J. E.; Martinu, L.; PoncinEpaillard, F., Thin Solid Films 291, 68 1996.

41. Cech, V.; Studynka, J.; Conte, N.; Perina, V., Surface and Coatings Technology 201, 5512 2007.

42. Bae, I. S.; Cho, S. J.; Choi, W. S.; Cho, H. J.; Hong, B.; Jeong, H. D.; Boo, J. H., Progress in Organic Coatings 61, 245 2008.

5.2 AGEING AND THERMAL DEGRADATION OF PLASMA POLYMERISED THIN FILMS DERIVED FROM LAVANDULA ANGUSTIFOLIA ESSENTIAL OIL

This paper examines the properties of the polymers while exposed to ambient conditions for an extended period (ageing), in addition to the exposure to elevated temperatures. For both studies, the thin films were monitored using spectroscopic ellipsometry and FTIR, which allowed for the monitoring of the thickness, optical constants and chemical structure of the polymers during the course of the experiments. "Ageing and thermal degradation of plasma polymerised thin films derived from Lavandula angustifolia essential oil" (Pub. 5.) is published in Polymer Degradation and Stability (Elsevier).

AGEING AND THERMAL DEGRADATION OF PLASMA POLYMERISED THIN FILMS DERIVED FROM *LAVANDULA ANGUSTIFOLIA* ESSENTIAL OIL

C D Easton and M V Jacob*

Electronic Materials Research Lab, School of Engineering, James Cook University, Townsville, 4811, Australia

*Corresponding author. Tel.: +61 7 47814379; fax: +61 7 47815177; Email: Mohan.Jacob@jcu.edu.au

Abstract

The ageing and thermal degradation of polymer thin films derived from the essential oil of *Lavandula angustifolia* (LA) fabricated using plasma polymerisation were investigated. Spectroscopic ellipsometry and Fourier transform infra-red (FTIR) spectroscopy were employed to monitor the optical parameters, thickness and chemical structure of the polyLA films fabricated at various RF powers over a period of 1400 hours. The bulk of the degradation under ambient conditions was found to occur within the first 100 hours after fabrication. The thermal degradation of the polyLA films was also investigated using the ellipsometry and FTIR. An increase in thermal stability was found for films fabricated at increased RF power levels. Between 200 to 300 ºC, the properties indicate a phase change occurs in the material. Samples annealed upto 405 ºC demonstrated minimal residue, with retention ranging between 0.47 – 2.2 %. A tuneable degradation onset temperature and minimal residue post anneal demonstrates that the polyLA films are an excellent candidate as a sacrificial material for air gap fabrication.

Keywords: Plasma polymer, ellipsometry, FTIR, oxidation, sacrificial material

1. Introduction

Production of polymer thin films from organic materials has gained significant attention, in particular for implementation in organic electronics[1] due to the advent of new thin film technologies. Plasma polymerisation is a luminous CVD process and provides a method for fabricating organic thin films using materials that do not normally polymerise using conventional techniques[2]. Polymers fabricated using this process have been proposed for implementation or implemented in electrical, optical and biomedical fields in a wide variety of applications including sensors or as a sacrificial material[2-5].

The stability of a plasma polymer under ambient conditions is an important parameter when considering implementation. The usefulness of the material is dependent on whether the intended properties can be maintained during the intended lifetime. Ageing in plasma polymers exposed to ambient conditions occurs via oxidation due to free radicals in the polymer structure. The uptake of oxygen is typically extremely rapid during the first few days after deposition associated with a high radical density, followed by a decline and eventual termination[6]. In some cases the time period of ageing can exceed 1 year for plasma polymers[7].

Fabrication of closed cavity, air gap structures at micro and manometer scales have the potential of providing significant technological advances. Applications include use in photonics and in semiconductor devices as ultra low-k dielectrics[5], and nanofluidic channels in chip based bio/chemical analysis[8]. Formation techniques for air gap structures can be classified into two groups; 1) formation between metal lines via CVD deposition[9], and 2) use of sacrificial materials as "place-holders" providing a temporary support layer for the interlevel dielectric and is subsequently removed either by etching or thermodecomposition[10]. The use of sacrificial materials is the preferred method as it allows for the complete removal of the intermetal dielectric within the gap and provides greater control of the gap shape.

Fabrication of an organic polymer based on *Lavandula angustifolia* essential oil (LAEO) was reported[11]. These polymer films were fabricated from a natural, non-

synthetic source that is environmentally friendly. The chemical structure of the monomer[12-14] and resulting polymer[15] has been described elsewhere. It was shown that the LAEO monomer contains a number of components including hydrocarbons, in addition to metabolites that contain ester, ketone and ether groups, while the polymer was primarily hydrocarbon based with oxygen containing groups such as ketone and hydroxyl. As outlined in the previous study, the optical properties of these films were promising, with a refractive index and extinction coefficient at 500 nm of 1.565 and 0.01 respectively. It was reported that these polymers possess an optical band gap value within the range of semiconductors. In addition to the possible electrical and optical applications, this polymer has the potential to be implemented in the biomedical field either as a fouling or non-fouling material depending on its properties.

The aim of this paper is to determine the ageing and thermal degradation of polymer thin films derived from LAEO through RF plasma polymerisation. Herein the LAEO based polymer films will be referred to as polyLA. Samples fabricated at varying RF power levels will be compared to determine the deviation in these properties as a function of deposition parameters. The stability of the polyLA films stored in ambient conditions will be monitored using spectroscopic ellipsometry and Fourier transform infrared (FTIR) spectroscopy. The thermal degradation of the polymer films will also be investigated via spectroscopic ellipsometry and FTIR.

2. Experimental

L. angustifolia monomer obtained from G. R. Davis Pty. Ltd. was used for fabricating the plasma polymer films using the experimental arrangement outlined previously[11]. The polymer films were fabricated at a starting pressure of approximately 250 mTorr. RF energy (13.56 MHz) was delivered to the deposition chamber via external copper electrodes separated by a distance of 11 cm. Approximately 5 mL of the monomer is placed into the holder and replaced after each subsequent deposition. Prior to placement of substrate within the polymerisation cell, the monomer inlet is opened briefly to evacuate the monomer container. During deposition, the monomer inlet is again opened and the vapour is released into the chamber, where the flow rate is controlled via a vacuum stopcock. Two different types of substrate were employed in this study; glass

slides for the optical characterisation, and KBr discs were deposited onto directly for the FTIR analysis. The glass slides were cleaned first with a solution of Extran and distilled water, then ultrasonically cleaned for 15 min, rinsed with Propan-2-ol and air-dried. The wet cleaning procedure was not employed for the KBr discs. Prior to fabrication, all substrates were pre-treated with Ar plasma in order to produce an oxygen-free surface[16].

The ellipsometric parameters phi (Ψ) and delta (Δ) are related to the Fresnel coefficients (*Rp* and *Rs*) and the complex reflection coefficient (ρ) by the following equation[17]:

$$\rho = \frac{R_p}{R_s} = \tan(\Psi)e^{i\Delta} \quad (1),$$

where *Rp* and *Rs* represents the Fresnel coefficient for the p- and s- directions, respectively. Parameters Ψ and Δ were obtained over the wavelength range of 200 – 1000 nm (6.199– 1.239 eV) using a variable angle spectroscopic ellipsometer (model M-2000, J. A. Woollam Co., Inc.).

For the ageing samples, data was obtained at three different angles of incidence, φ = 55º, 60º, and 65º. It is important to collect data near the Brewster angle of the material in order to minimise noise and systematic errors in the measured data[18]. Transmission data was also collected for each sample using the ellipsometer. The position of the glass slide on the ellipsometry stage for the first measurement was recorded and used for each subsequent measurement to minimise sample error. Samples fabricated at various input RF power levels (10 W, 25 W, 50 W and 75 W) were measured to determine the effect of RF power on the stability of the polymer. These samples were produced at increasing deposition times in order to produce thin films of approximately the same thickness of 800 nm. Samples produced at a constant RF power level (25 W) and varying deposition times were also measured to determine whether the ageing rate was thickness dependent. Samples were stored in ambient conditions at room temperature (22 ºC) for the duration of the measurements.

The thermal degradation studies were performed using the temperature stage attachment of the ellipsometer. Samples of approximately the same thickness (350 nm) fabricated at 10 W, 25 W, 50 W and 75 W were left at room temperature in ambient conditions for at least 5 days post fabrication to allow the polymers to stabilise. The temperature of the stage was increased in steps of 5 ºC every 5 mins upto 405 ºC to ensure thermal equilibrium between heater and sample. Dynamic ellipsometric measurements were performed using the CompleteEASE software which measures Ψ and Δ as a function of time at a fixed angle, 70º in this case. The data can then be imported into the WVASE32 software package for analysis.

Experimentally obtained Ψ and Δ are used to derive the optical constants based on a model of the sample built in the J. A. Woollam Inc. analysis software (WVASE32) via regression analysis. A quantitative measure of the quality of the fit is then derived, where the mean-squared error (MSE) is defined as[19]:

$$MSE = \frac{1}{2N - M} \sum_{i=1}^{N} \left[\left(\frac{\Psi_i^{\mathrm{mod}} - \Psi_i^{\mathrm{exp}}}{\sigma_{\Psi i}^{\mathrm{exp}}} \right)^2 + \left(\frac{\Delta_i^{\mathrm{mod}} - \Delta_i^{\mathrm{exp}}}{\sigma_{\Delta i}^{\mathrm{exp}}} \right)^2 \right] \quad (2),$$

where N is the number of Ψ and Δ pairs, M is the number of fit parameters used in the model, and σ is the standard deviation of the experimental data points. Ideally a MSE value of zero is desired after performing the regression analysis, however this value is dependent on the amount of information available, the quality of the data, and how accurately the model reflects the sample.

In order to create a model to relate the measured ellipsometric parameters to the optical properties of the material under test, oscillators are implemented. These oscillators represent the dielectric function of the material as a linear summation of real and complex terms as a function of wavelength, inverse wavelength or photon energy[20]. A Gaussian and Tauc-Lorentz oscillator were employed which produced the best fit to the data, with a lower MSE and lower average correlation between fitting terms. The Tauc-Lorentz oscillator term, derived by Jellison and Modine[21], is based on the Tauc joint density of states[22] and the Lorentz calculation[23] for the imaginary part of the dielectric function (ε_2):

$$\varepsilon_2(E) = \left[\frac{AE_0C(E-E_g)^2}{(E^2-E_0^2)^2 + C^2E^2} \times \frac{1}{E} \right], E > E_g$$
$$= 0, E \le E_g \quad (3),$$

A is a constant, E_g is the optical band gap, E_0 is the peak transition energy and C is the broadening term. The real part of the dielectric function (ε_1) can be found using Kramers-Kronig integration:

$$\varepsilon_1(E) = \varepsilon_1(\infty) + \frac{2}{\pi} P \int_{E_g}^{\infty} \frac{\xi \varepsilon_2(\xi)}{\xi^2 - E^2} d\xi \quad (4),$$

where P represents the Cauchy principal part of the integral and $\varepsilon 1(\infty)$ is an additional fitting parameter. This equation can be solved in closed form and can be found in an erratum by Jellison and Modine [24].

As for the Gaussian oscillator, the formulas for the real and imaginary part of the dielectric function are as follows [25, 26]:

$$\varepsilon_2(E) = Ae^{-\left(\frac{E-E_n}{\sigma}\right)^2} - Ae^{-\left(\frac{E+E_n}{\sigma}\right)} \quad (5),$$

$$\varepsilon_1(E) = \frac{2}{\pi} P \int_{E_g}^{\infty} \frac{\xi \varepsilon_2(\xi)}{\xi^2 - E^2} d\xi \quad (6),$$

where A represents the amplitude, En the peak position, and σ the full width at half maximum.

FTIR was employed to determine the chemical structure of the polymer thin films deposited on KBr employing the Nicolet Maxim system. Spectra were obtained in transmission mode in the region of 4000 – 400 cm^{-1}, where 32 scans were acquired for each sample at a resolution of approximately 2 cm^{-1}. CO_2 and H_2O were accounted for in the spectra by the background substraction procedure, where the background was recorded under the same atmospheric conditions.

3. Results and Discussion

3.1 Ageing of polymer

PolyLA samples fabricated at 10, 25, 50 and 75 W and stored in ambient conditions were monitored for upto approximately 1400 hours or 58 days via ellipsometry. The optical properties were studied over a wavelength range of 200 – 1000 nm. The change in refractive index at 300, 600 and 900 nm for the polymers is presented in Figure 1, Figure 2, and Figure 3 respectively. The percentage change in refractive index for the duration of the ageing period is detailed in Table 1. For the 25, 50 and 75 W samples, the refractive index increases for approximately the first 100 hours after deposition, then remains constant for the remainder of the measurement period. Therefore the bulk of the degradation in the polyLA samples fabricated at these RF power levels occurs within the first 100 hours after deposition. However, the refractive index of the 10 W sample at all three wavelengths is still increasing. A shift to higher values of refractive index with an increase of thickness over the measured wavelength range for thicknesses upto approximately 1000 nm have been observed as shown in Figure 4. Clearly this opposes the trend observed for the 10 W sample, thus it is unlikely that the increase in refractive index is the result of the decrease in thickness.

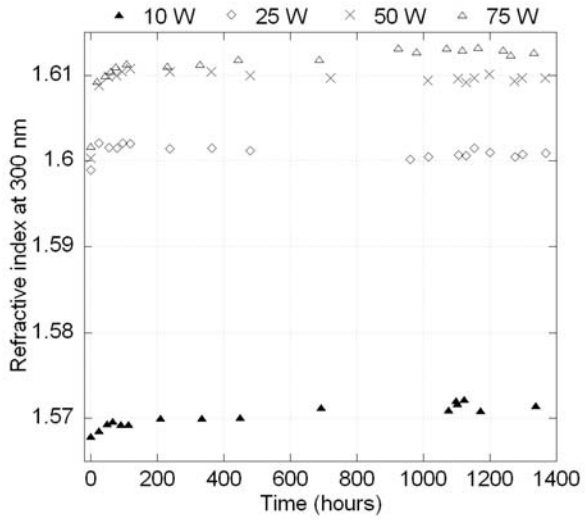

Figure 1: Refractive index at 300 nm as a function of time for polyLA films deposited at 10, 25, 50 and 75 W.

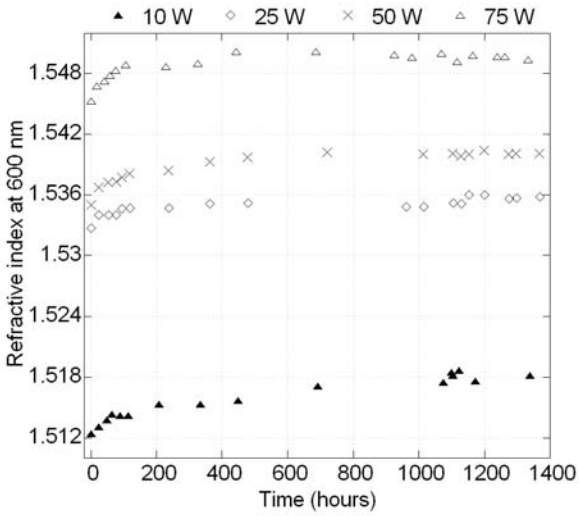

Figure 2: Refractive index at 600 nm as a function of time for polyLA films deposited at 10, 25, 50 and 75 W.

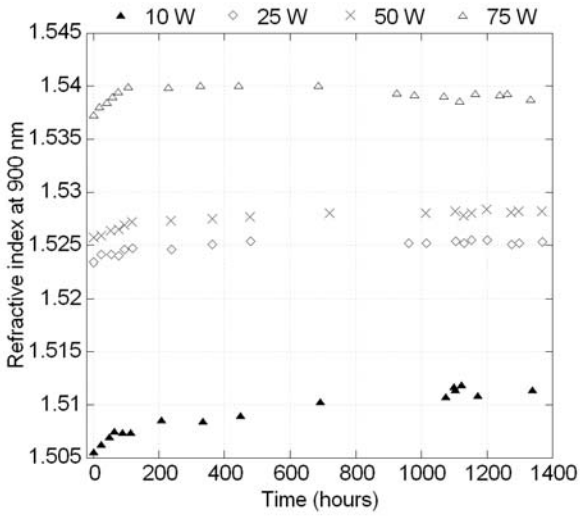

Figure 3: Refractive index at 600 nm as a function of time for polyLA films deposited at 10, 25, 50 and 75 W.

Table 1: Change in refractive index (%) at 300, 600 and 900 nm after approximately 1400 hrs after deposition

	Change in refractive index (%) after approx. 1400 hrs at:		
Sample	300 nm	600 nm	900 nm
10 W	0.26	0.4	0.41
25 W	0.13	0.2	0.13
50 W	0.59	0.33	0.16
75 W	0.69	0.27	0.1

The effect of thickness on the ageing for samples fabricated at 25 W was also examined. Samples of thicknesses 548, 831 and 1048 nm were monitored for upto approximately 1400 hours. The change in refractive index at 300, 600 and 900 nm are presented in Figure 4, Figure 5, and Figure 6 respectively. As previously noted, a small increase in refractive index exists for an increase in thickness. The results reveal that the ageing rate is independent of the film thickness.

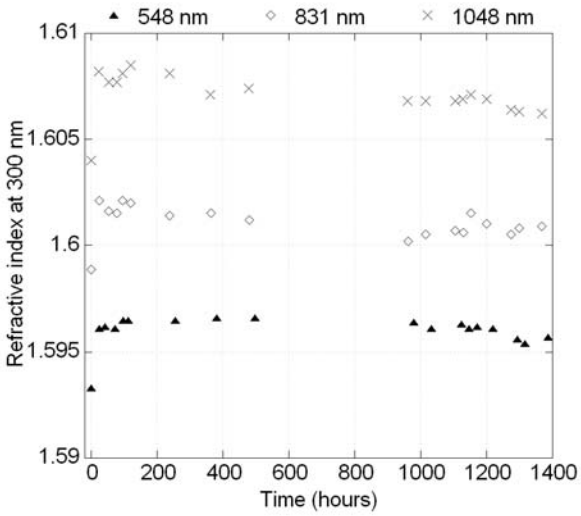

Figure 4: Refractive index at 300 nm as a function of time for polyLA films deposited at 25 W and various thicknesses.

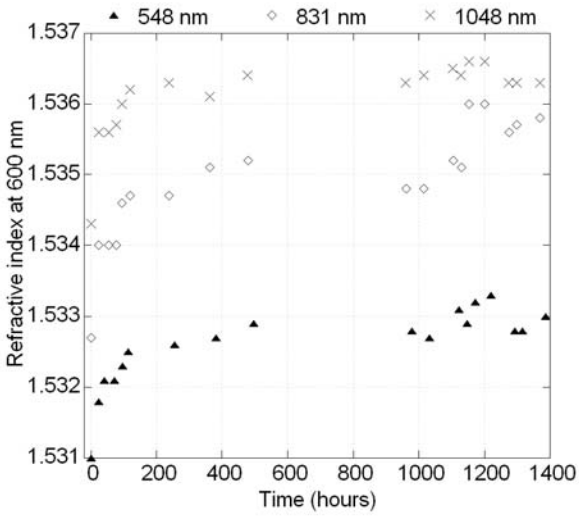

Figure 5: Refractive index at 600 nm as a function of time for polyLA films deposited at 25 W and various thicknesses.

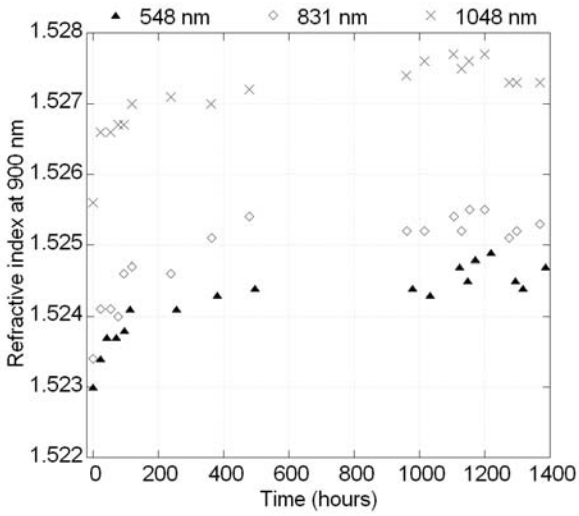

Figure 6: Refractive index at 900 nm as a function of time for polyLA films deposited at 25 W and various thicknesses.

The thickness of each of the samples stayed approximately constant for the duration of the experiment, with the exception of the 10 W sample (Figure 7). The decrease in thickness shown has two regimes, where the rate of change of thickness decreases after approximately 70 hours. After almost 1400 hours the thickness is still not at equilibrium, with a total change of thickness of almost 13 % for the time period

measured. Decrease in polymer thickness has been reported previously for glassy polymers such as polysulfone[27], however in this case the change in thickness was significantly smaller, ~0.8 % over 6000 hrs. The change in thickness for polysulfone was comparable to the change in density calculated from refractive index using the Lorentz-Lorenz equation and as such it was suggested that the ageing process had no effect on the lateral dimensions of the film. The Lorentz-Lorenz equation is expressed as[27]:

$$\frac{n^2-1}{n^2+2}=\frac{\rho N_{av}\alpha}{3M_0\varepsilon_0} \quad (9),$$

where ρ is the density of the polymer, ε_0 the permittivity of free space, α the average polarizability of the polymer repeating unit, N_{av} is Avogadro's number and M_0 is the molecular weight of the polymer repeat unit. Employing the Lorentz-Lorenz equation to determine the change in density for the polyLA polymer from the change in refractive index results in a 1 % change in density for the 10 W sample. Clearly in this case the change in thickness is not comparable to the change in density. This suggests that the primary cause for the loss of thickness is not the change in density, but rather some other mechanism. As outlined in Figure 8, there is no apparent change in the chemical structure of the 10 W sample over a 40 day period. The most likely explanation is that the polymer is being effectively etched when exposed to the atmosphere. The rate of change in thickness loss at approximately 70 hours indicates that the etching rate is dependent on the stability of the polymer.

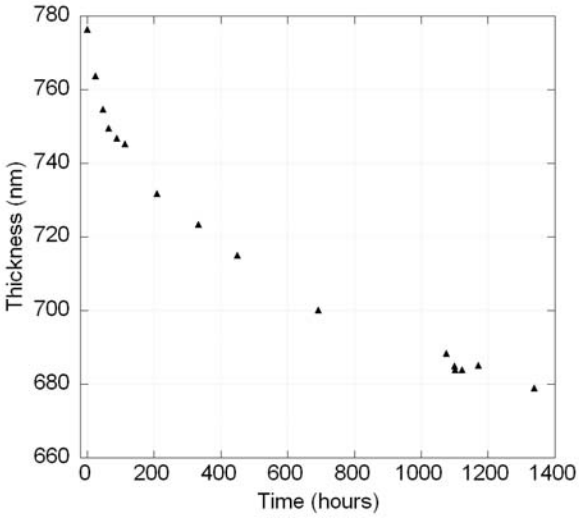

Figure 7: Thickness of the 10 W polyLA sample as a function of time.

Figure 8 and Figure 9 demonstrate the FTIR spectra within 24 hours of deposition and after 40 days for the 10 W and 75 W samples respectively. The peaks seen in the figures at approximately 2350 cm^{-1} are associated with the removal of CO_2 from the spectrum and thus can be ignored. The peak assignments for the polyLA films have been reported previously[15]. It has been shown that the difference in the IR spectra for the polyLA films fabricated at varying RF power levels is associated with the magnitude of the spectra peaks, and as such in this case the samples were produced at the extremes of the applied RF power range, 10 and 75 W respectively. After 40 days, there is no apparent change in the 10 W sample spectra. For the 75 W spectra, the broad peak centred around 3460 cm^{-1} assigned to OH stretch has increased in intensity, indicating an uptake of oxygen into the chemical structure of the polymer.

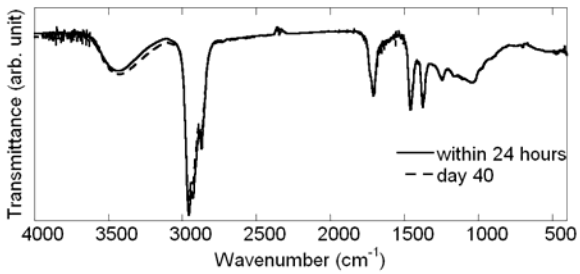

Figure 8: FTIR spectra of the 10 W sample within 24 hours of deposition and after 40 days.

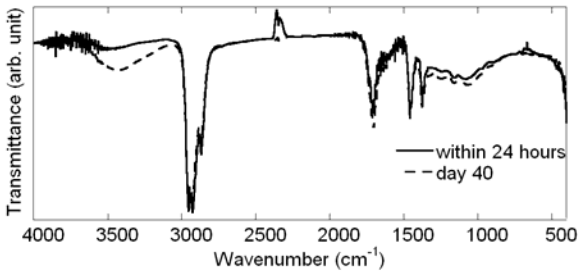

Figure 9: FTIR spectra of the 75 W sample within 24 hours of deposition and after 40 days.

Based on the results obtained from ellipsometry and FTIR spectroscopy, the ageing mechanism of the 25, 50 and 75 W samples follows the oxidation path typically seen in plasma polymers. The uptake of oxygen into the polymer structure is not as strong in comparison to other plasma polymers[28] where the inclusion of additional hydroxyl (C-O, 1205 – 1125 cm^{-1}) and carbonyl (C=O, ~1700 cm^{-1}) groups have been reported for plasma polymerised α-methylstyrene for similar ageing periods. Additionally, from the ellipsometry measurements the bulk of the ageing in these films occurs within the first 5 days after fabrication. The ageing mechanism for the 10 W sample is however different. According to the FTIR results, there is no apparent uptake of oxygen into the chemical structure. However, if the surface is being etched, the bulk of polymer undergoing oxidation is also being etched. The difference between the 10 W sample and the samples fabricated at higher powers is attributed to the increased temperatures that the polymers are exposed to during fabrication with increased RF power.

3.2 Thermal degradation

Thermal stability of polyLA samples fabricated at 10, 25, 50 and 75 W were monitored via ellipsometry up to a maximum temperature of 405 ºC. Figure A1 to Figure A8 located in the supplementary information section show the Ψ and Δ data for the samples examined. A few attributes of the polyLA samples can be uncovered from this raw data. An increase in RF power results in a reduction in the oscillations in the phi data up to approximately 200 ºC, suggesting an increase in thermal stability within this temperature range. Between 200 – 300 ºC, both the phi and delta data for all samples

undergo large changes with temperature. This is indicative to a phase change in the material. Another trend can be seen in the delta data (wavelength 192 nm), where an increase in RF power results in a broadening of the shoulder above 220 ºC. The peak of the shoulder also shifts to higher temperatures with increased RF power. This is attributed to a greater retention of the polymer after undergoing the phase change. Above 380 ºC however, both the phi and delta data for all samples is approximately equal. In addition, the phi and delta data at these temperatures for the 200 – 1000 nm wavelength band are essentially identical to the data for an uncoated substrate (data not shown). Hence each polyLA film examined undergoes full thermal degradation within the measured temperature range leaving minimal residue.

The Ψ and Δ data was imported into the WVASE analysis software where the thickness and optical properties of the samples was derived at each temperature interval. Refractive index and thickness as a function of temperature are presented in Figure 10 and Figure 11 respectively. Up to approximately 200 ºC the refractive index of all samples is relatively stable, however between 200 to 300 ºC it undergoes a large rate of change coinciding to the phase change identified from the phi and delta data.

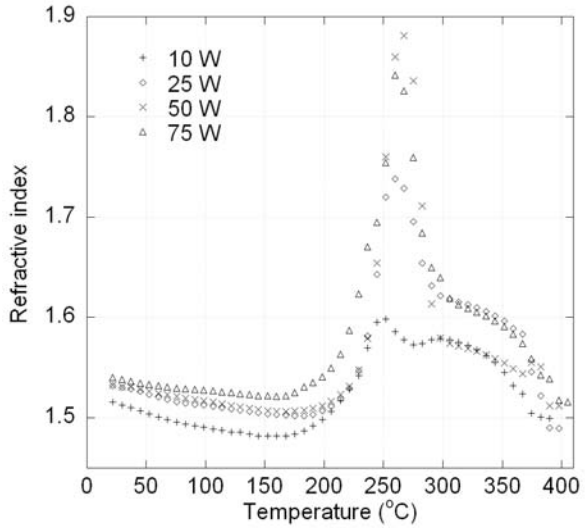

Figure 10: Refractive index vs. temperature for polyLA films deposited at 10, 25, 50 and 75 W.

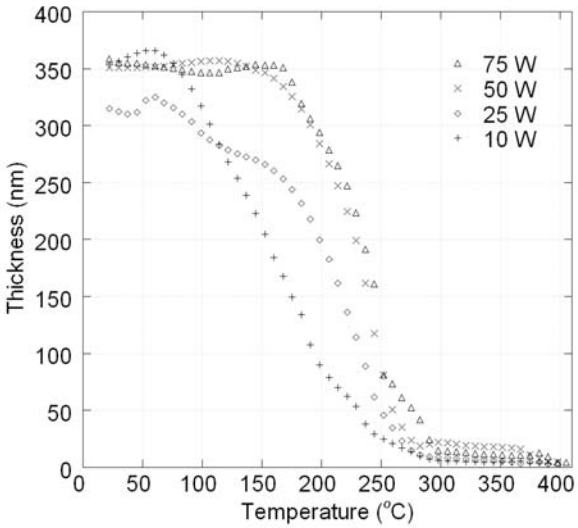

Figure 11: Thickness vs. temperature for polyLA films deposited at 10, 25, 50 and 75 W.

In general, an increase in the RF power during fabrication results in an increase in the thermal degradation onset temperature of the polyLA films. For the 10 W sample, thermal degradation begins to occur at approximately 60 ºC. The 25 W sample also begins degradation at the same temperature, however has two regimes with the second commencing at approximately 170 ºC. The same phenomena has been observed for plasma polymerised α-methylstyrene and was credited to the desorption of low molecular weight species before the onset of bulk decomposition[28]. Onset for thermal degradation for the 50 and 75 W samples occurs at approximately 130 and 170 ºC respectively. This increase in the degradation onset temperature for increasing RF power is attributed to a higher degree of cross-linking in the polymer structure. The amount of residue remaining post anneal ranges from 0.47 – 2.2 % which is favourable when compared to reported values of 3.0 – 5.8 % for hydrogen-terminated and 2,2-diphenyl hexyl group-terminated poly(methyl methacrylate) (PMMA) [29] and 0.8 – 5.2 % for low power plasma polymerised PMMA [5]. The results are summarised in Table 2. These results confirm the observations made from the raw Ψ and Δ data. Within the span of deposition conditions studied, a range of degradation temperatures have been acquired which could prove to be vital when integrating into a multi-component system. With the ability to obtain low degradation temperatures and minimal residue, the polyLA films are excellent candidates for sacrificial layers.

Table 2: Thermal stability results for the polyLA films

Sample	As-deposited thickness (nm)	Post anneal (405 ºC) thickness (nm)	Degradation onset (ºC)	Retention (%)
10 W	354.39 ± 0.35	6.95 ± 1.2	~ 60	1.96
25 W	315.13 ± 0.4	5.03 ± 1.1	~60, 170	1.6
50 W	350.70 ± 0.3	7.7 ± 2.3	~130	2.2
75 W	358.53 ± 0.32	1.7 ± 0.3	~170	0.47

In order to understand the degradation mechanisms occurring during heat treatment of the polyLA films, the FTIR spectra of a 25 W sample was obtained after subsequent heat treatments at increasing temperatures. The FTIR spectra for the as deposited film and the spectra after heat treatment upto 150 ºC presented in Figure 12 are essentially identical. Therefore in this region, thermal degradation is associated primarily with weight loss. As noted previously, between approximately 200 to 300 ºC the optical parameters of the polyLA films undergo a large rate of change suggesting a phase change. The FTIR spectra of the polyLA film after heating to 245 ºC is also shown. Peaks assigned to stretching (ν) and bending (δ) of C-H have all reduced in intensity [2962 cm^{-1} (ν_a(C-H)), 2933 cm^{-1} (ν_a(C-H)), 2873 cm^{-1} (ν_s(C-H)), 1457 cm^{-1} (δ_a(C-H)) and 1374 cm^{-1} (δ_s(C-H))]. In addition, the peaks assigned to carbon-oxygen stretching [1706 cm^{-1} (ν(C=O)) and 1236 cm^{-1} (ν(C-O))] have increased in intensity, while a new peak is now present [1610 cm^{-1} (ν(C=C))] which could have been previously obscured by the relatively strong peak at 1706 cm^{-1}. C=C at approximately 1600 cm^{-1} indicates an increase of aromatic structures in the polymer, however there is no accompanied increase in aromatic C-H at > 3000 cm^{-1} or in the regions 700-1000 cm^{-1}. The reduction in magnitude of all peaks associated with carbon-hydrogen bonding indicates that heating the polyLA films to this temperature range results in a major change in the chemical structure. The C-H peaks in the untreated polyLA films were previously assigned to either methyl (CH_3) or methylene (CH_2) bands. The scission of the C-H bonds in the methyl and methylene groups has however not resulted in the formation of methyne (CH) bands in the FTIR spectra. Therefore upon heating at high temperatures, the polymer undergoes hydrogen abstraction, most likely by the elimination of water, and the subsequent formation of either C-O or C=C bonds, resulting in a less

hydrocarbon dense polymer. Polyvinylalcohol (PVA) undergoes a similar process where it beings to eliminate water above 220 ºC[30].

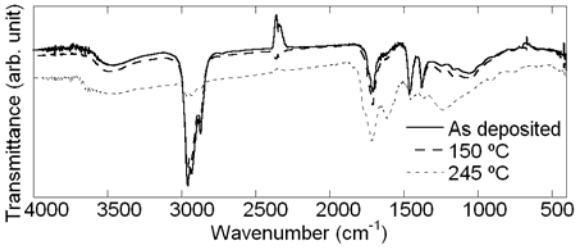

Figure 12: FTIR spectra of 25 W polyLA sample as deposited and after successive heat treatments to 150 and 245 ºC.

Conclusion

Ageing and thermal degradation of polyLA films fabricated from plasma polymerisation at various input RF power levels has been investigated. Ellipsometry and FTIR measurements indicate that the samples fabricated at low power age differently to those produced at higher power levels. Samples fabricated at 25, 50 and 75 W age via oxidation, specifically increase of hydroxyl inclusion (OH, ~ 3460 cm^{-1}), where the bulk of the ageing occurs within the first 5 days after fabrication. The 10 W sample however demonstrated no apparent increase of hydroxyl inclusion, while undergoing ~13 % thickness loss over a 1400 hour period attributed to etching of the surface.

Thermal degradation results obtained via ellipsometry indicate that an increase in RF power results in an increase in the thermal stability of the polyLA films. Both the raw phi and delta data and the refractive index values signify a phase change in the material between 200 to 300 º C for all samples. FTIR spectra of the polyLA film heated upto this temperature range indicates loss of hydrogen from the chemical structure via elimination of water and the subsequent formation of C-O or C=C bonds. Below this temperature range, no change is recorded in the FTIR spectra compared to the as deposited polymer. Samples annealed upto 405 º C demonstrated minimal residue, with retention ranging between 0.47 – 2.2 %. With the ability to tune the degradation onset temperature and minimal residue post anneal, the polyLA films are an excellent candidate as a sacrificial material for air gap fabrication.

Acknowledgements

The authors are grateful to the financial support provided under the RIRDC and ARC LIEF and DP schemes. CDE is grateful to the APA and RIRDC scholarships. We are thankful to A./ Prof B. Bowden for assistance in obtaining the FTIR spectra and Prof. R. Shanks for his valuable comments.

Supplementary Information

Raw spectrometric ellipsometry (Ψ and Δ) data as a function of time and temperature for samples fabricated at RF power levels 10, 25, 50 and 75 W heated upto 405 ºC are presented in Figure A1 – Figure A8.

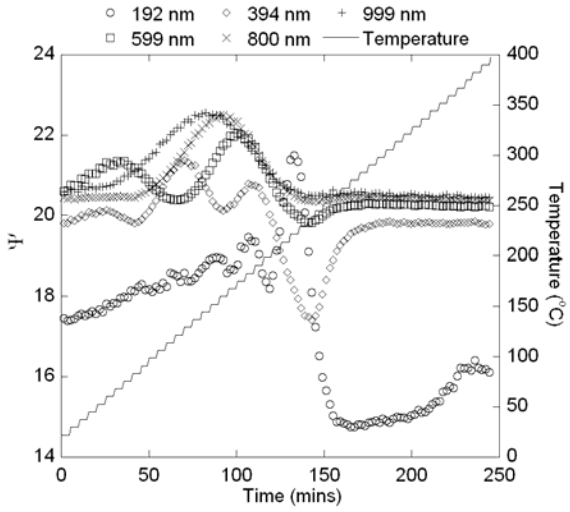

Figure A1: Ψ data as a function of temperature and time for the 10 W sample.

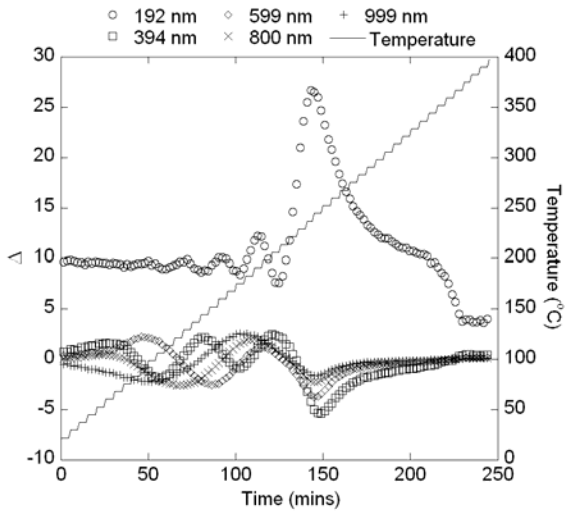

Figure A2: Δ data as a function of temperature and time for the 10 W sample.

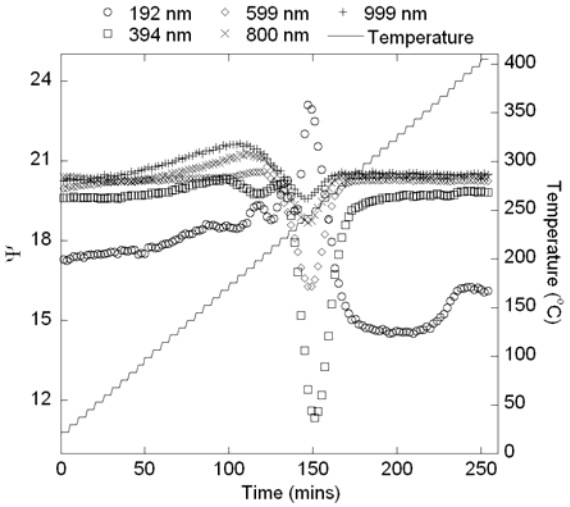

Figure A3: Ψ data as a function of temperature and time for the 25 W sample.

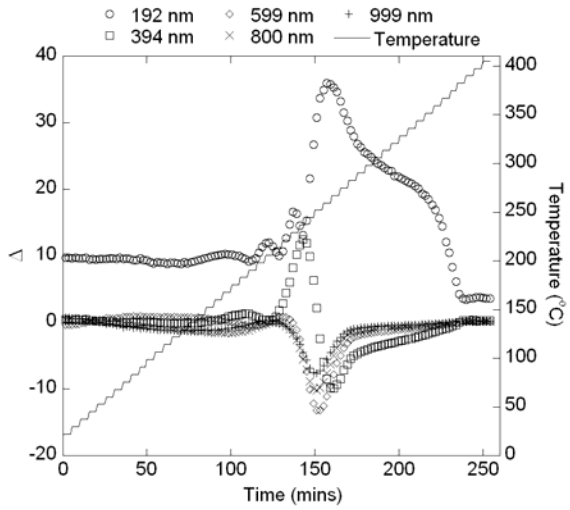

Figure A4: Δ data as a function of temperature and time for the 25 W sample.

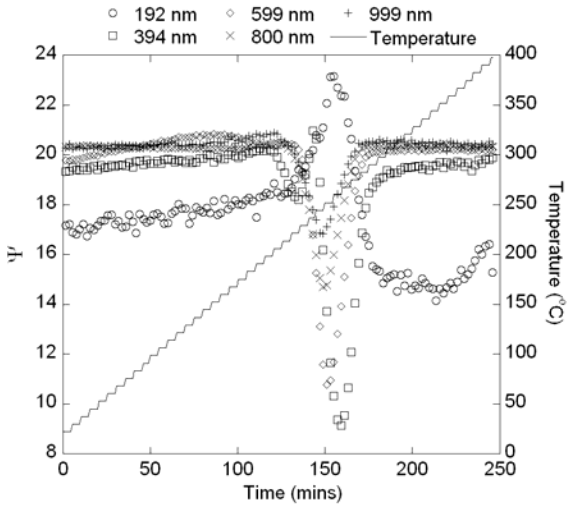

Figure A5: Ψ data as a function of temperature and time for the 50 W sample.

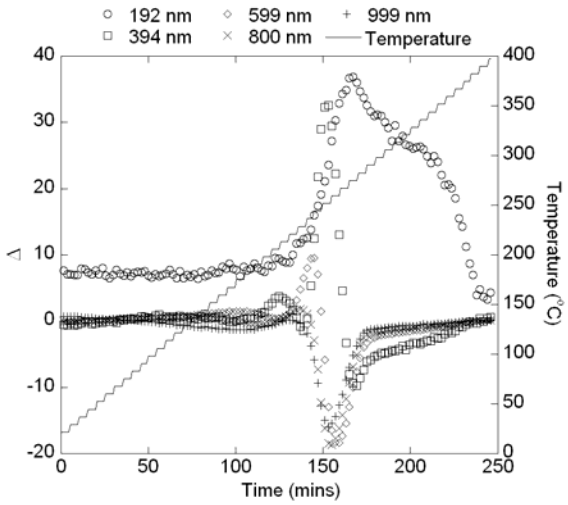

Figure A6: Δ data as a function of temperature and time for the 50 W sample.

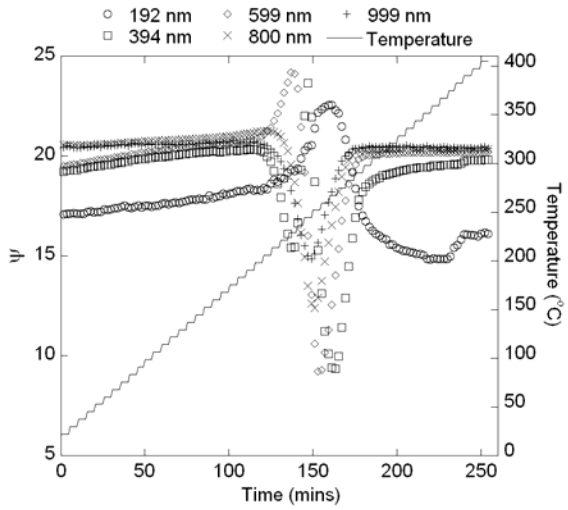

Figure A7: Ψ data as a function of temperature and time for the 75 W sample.

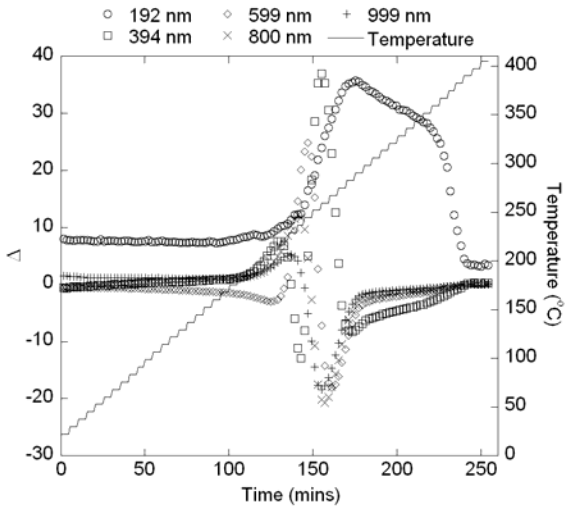

Figure A8: Δ data as a function of temperature and time for the 75 W sample.

References

[1] Z. V. Vardeny, A. J. Heeger, and A. Dodabalapur. Fundamental research needs in organic electronic materials. Synthetic Metals 2005;148(1):1-3.

[2] A. Hiratsuka and I. Karube. Plasma polymerized films for sensor devices. Electroanalysis 2000;12(9):695-702.

[3] R. Forch, A. N. Chifen, A. Bousquet, H. L. Khor, M. Jungblut, L. Q. Chu, Z. Zhang, I. Osey-Mensah, E. K. Sinner, and W. Knoll. Recent and expected roles of plasma-polymerized films for biomedical applications. Chemical Vapor Deposition 2007;13(6-7):280-294.

[4] F. F. Shi. Recent advances in polymer thin films prepared by plasma polymerization Synthesis, structural characterization, properties and applications. Surface & Coatings Technology 1996;82(1-2):1-15.

[5] T. B. Casserly and K. K. Gleason. Effect of substrate temperature on the plasma polymerization of poly(methyl methacrylate). Chemical Vapor Deposition 2006;12(1):59-66.

[6] T. R. Gengenbach and H. J. Griesser. Deposition conditions influence the postdeposition oxidation of methyl methacrylate plasma polymer films. Journal of Polymer Science Part a-Polymer Chemistry 1998;36(6):985-1000.

[7] T. R. Gengenbach and H. J. Griesser. Post-deposition ageing reactions differ markedly between plasma polymers deposited from siloxane and silazane monomers. Polymer 1999;40(18):5079-5094.

[8] W. L. Li, J. O. Tegenfeldt, L. Chen, R. H. Austin, S. Y. Chou, P. A. Kohl, J. Krotine, and J. C. Sturm. Sacrificial polymers for nanofluidic channels in biological applications. Nanotechnology 2003;14(6):578-583.

[9] B. Shieh, K. C. Saraswat, J. P. McVittie, S. List, S. Nag, M. Islamraja, and R. H. Havemann. Air-gap formation during IMD deposition to lower interconnect capacitance. IEEE Electron Device Letters 1998;19(1):16-18.

[10] P. A. Kohl, D. M. Bhusari, M. Wedlake, C. Case, F. P. Klemens, J. Miner, B. C. Lee, R. J. Gutmann, and R. Shick. Air-gaps in 0.3 mu m electrical interconnections. IEEE Electron Device Letters 2000;21(12):557-559.

[11] M. V. Jacob, C. D. Easton, G. S. Woods, and C. C. Bemdt. Fabrication of a novel organic polymer thin film. Thin Solid Films 2008;516(12):3884-3887.

[12] R. Shellie, L. Mondello, P. Marriott, and G. Dugo. Characterisation of lavender essential oils by using gas chromatography-mass spectrometry with correlation of linear retention indices and comparison with comprehensive two-dimensional gas chromatography. Journal of Chromatography A 2002;970(1-2):225-234.

[13] T. J. Morgan, W. E. Morden, E. Al-Muhareb, A. A. Herod, and R. Kandiyoti. Essential oils investigated by size exclusion chromatography and gas chromatography-mass spectrometry. Energy & Fuels 2006;20(2):734-737.

[14] R. Shellie, P. Marriott, and C. Cornwell. Characterization and comparison of tea tree and lavender oils by using comprehensive gas chromatography. Hrc-Journal of High Resolution Chromatography 2000;23(9):554-560.

[15] C. D. Easton, M. V. Jacob, R. A. Shanks, and B. F. Bowden. Surface and chemical characterisation of polyLA thin films fabricated using plasma polymerisation. Chemical Vapor Deposition in press.

[16] M. C. Kim, S. H. Cho, J. G. Han, B. Y. Hong, Y. J. Kim, S. H. Yang, and J. H. Boo. High-rate deposition of plasma polymerized thin films using PECVD method and characterization of their optical properties. Surface & Coatings Technology 2003;169(595-599.

[17] J. A. Woollam Co., Inc. Guide to Using WVASE32, A Short Course in Ellipsometry. 2001, p.

[18] H. A. Al-Attar and A. D. Telfah. Optical constants of polyaniline/poly(methylmethacrylate) blend. Optics Communications 2004;229(1-6):263-270.

[19] J. A. Woollam Co., Inc. Guide to Using WVASE32, A Short Course in Ellipsometry. 2001, p. 50.

[20] J. A. Woollam Co., Inc. Guide to Using WVASE32, WVASE32 Addendum E: General Oscillator Layer. 2001, p. 11.

[21] G. E. Jellison and F. A. Modine. Parameterization of the optical functions of amorphous materials in the interband region. Applied Physics Letters 1996;69(3):371-373.

[22] J. Tauc, Grigorov.R, and A. Vancu. Optical Properties and Electronic Structure of Amorphous Germanium. Physica Status Solidi 1966;15(2):627-&.

[23] F. Wooton. Optical Properties of Solids. New York: Academic, 1972.

[24] G. E. Jellison and F. A. Modine. Parameterization of the optical functions of amorphous materials in the interband region (vol 69, pg 371, 1996). Applied Physics Letters 1996;69(14):2137-2137.

[25] D. D. Meneses, M. Malki, and P. Echegut. Structure and lattice dynamics of binary lead silicate glasses investigated by infrared spectroscopy. Journal of Non-Crystalline Solids 2006;352(8):769-776.

[26] J. A. Woollam Co., Inc. Guide to Using WVASE32, WVASE32 Addendum E: General Oscillator Layer. 2001, p. 25.

[27] Y. Huang and D. R. Paul. Physical aging of thin glassy polymer films monitored by optical properties. Macromolecules 2006;39(4):1554-1559.

[28] D. D. Burkey and K. K. Gleason. Structure and thermal properties of thin film poly(alpha-methylstyrene) deposited via plasma-enhanced CVD. Chemical Vapor Deposition 2003;9(2):65-71.

[29] B. J. Holland and J. N. Hay. The kinetics and mechanisms of the thermal degradation of poly(methyl methacrylate) studied by thermal analysis-Fourier transform infrared spectroscopy. Polymer 2001;42(11):4825-4835.

[30] A. Hollander and J. Thome. In: H. Biederman, editor. Plasma Polymer Films: Degradation and Stability of Plasma Polymers. London: Imperial Collage Press, 2004. p. 252

CHAPTER 6 INVESTIGATION OF POLYMERS FABRICATED FROM THE MAJOR COMPONENTS OF LAEO

LAEO has been reported to contain approximately 80 components [37-39]. Therefore without the appropriate investigation, it is unclear which components are contributing to the polymerisation process. In addition, variation exists in the content of these components between different sources of the same material, thus casting doubt on the repeatability of polymer fabrication when employing different sources. This chapter presents a paper where the major components of LAEO are polymerised and the resultant properties are compared with the established LAEO based polymer. A list of the major components of LAEO and their typical content is presented in Table 1.

Table 1: The major components found in lavender oil

Compound	Content (%)
1,8-cineole	0.1 – 20
Limonene	0.2 – 3.9
Trans-β-ocimene	2 – 6
Cis- β-ocimene	4 – 10
3-octanone	0.3 – 3.5
Camphor	0.1 – 5
Linalool	23 – 57
Linalyl acetate	4 – 35
Terpinene-4-ol	2 – 6
Lavandulol	0.05 – 3.3
Lavandulyl acetate	0.7 – 6.2
α-terpineol	0.9 – 6

6.1 PLASMA POLYMERISATION OF THE CONSTITUENTS OF LAVANDULA ANGUSTIFOLIA ESSENTIAL OIL

To obtain a better understanding of which components of the LAEO contribute to the polymerisation process, the major components were polymerised and the properties of the resultant films contrasted. The LAEO obtained from the same supplier and batch was analysed using gas chromatography – mass spectrometry and the major components identified. A deposition rate study for the different monomers was performed. In

addition, the properties of the resultant polymers were analysed using FTIR, spectroscopic ellipsometry, AFM and water contact angle. The properties of the films were compared between the different monomers and with the properties of the LAEO based polymer. “Plasma polymerisation of the constituents of *Lavandula angustifolia* essential oil” (Pub. 6.) at time of print is currently under review for publication in Chemical Vapor Deposition (Wiley InterScience). This paper involved collaboration with Prof. Robert Shanks.

PLASMA POLYMERISATION OF THE CONSTITUENTS OF *LAVANDULA ANGUSTIFOLIA* ESSENTIAL OIL

Christopher D Easton[1], Mohan V Jacob[1]* and Robert A Shanks[2]

[1]Electronic Materials Research Lab, School of Engineering, James Cook University, Townsville, 4811, Australia

[2]Applied Sciences, RMIT University, GPO Box 2476V, Melbourne, 3001, Australia

*Corresponding author. Tel.: +61 7 47814379; fax: +61 7 47815177; Email: Mohan.Jacob@jcu.edu.au

Abstract

Fabrication of *Lavandula angustifolia* essential oil (LAEO) based polymer films has been reported previously. However, LAEO is comprised of a number of components. The aim of this paper is to compare the LAEO based polymer films with polymer films fabricated from the major components using RF plasma polymerisation. The properties of these materials was examined and compared with the characteristics of the LAEO based polymers described previously. FTIR spectra of the polymers demonstrate that irrespective of the starting monomer, the resultant polymers are almost the same, with only the cis-β-ocimene based polymer exhibiting a significant difference. All films were shown to be optically transparent, with refractive index values ranging between 1.539 – 1.57 at 500 nm. Average roughness values obtained from AFM were less than 0.8 nm indicating a very smooth surface, with the exception of the cis-β-ocimene based polymer which had a much higher value. Water contact angle results demonstrated that the surfaces range from hydrophilic to mildly hydrophobic and are stable while in contact with water.

Keywords: Plasma polymer, FTIR, AFM, ellipsometry, contact angle.

1. Introduction

Plasma polymerisation is a luminous CVD process that can be employed to alter the surface properties of a material and to fabricate polymer thin films. This technique provides a method for fabricating organic thin films using materials that do not normally polymerise under conventional techniques, due to the reactions that occur within the plasma phase that are unique to this process.[1] The development of organic polymers has gained significant interest in recent years due to increase of production of organic electronics [2] and bioelectronics.[3] In addition, plasma polymerisation has gained attention for use in the biomedical field.[4]

Lavandula angustifolia essential oil (LAEO) typically contains approximately 80 different components that have been identified previously using gas chromatography.[5-7] Some variation in the content of these compounds can exist between different sources of LAEO, however the two major components are linalool and linalyl acetate.[5] LAEO is produced from a natural, non-synthetic source that is environmentally friendly.

Recently, fabrication of an organic polymer based on LAEO was reported.[8] An in-depth analysis of the chemical and surface properties [9] has been undertaken in addition to the optical properties of the polymer.[10] However, as LAEO is a mixture of a number of components with different vapour pressures, it is uncertain which components contributed to the formation of the polymer during the polymerisation process. Within the plasma phase there are a number of components that are contributing to the formation of the polymer including ions, radicals, electrons, metastable species and photons.[11] In addition to this, the monomer undergoes fragmentation once released into the plasma phase; therefore there are a potentially large number of components contributing to the composition of the resultant polymer.

The aim of this paper is to fabricate polymer thin films from the major components of LAEO and determine the chemical, optical, surface and physical properties of the resultant materials. The measured properties of these materials will then be compared with those of the established LAEO based polymer film in order to provide some insight into the deposition process. The chemical structure of the polymers will be examined

using Fourier transform infra-red (FTIR) spectroscopy. Spectroscopic ellipsometry will be used to determine the thickness and optical constants of the thin films, including refractive index, extinction coefficient and transmission. The surface of the polymers will be investigated by atomic force microscope (AFM), and water contact angle (WCA) measurements.

2. Results and Discussion

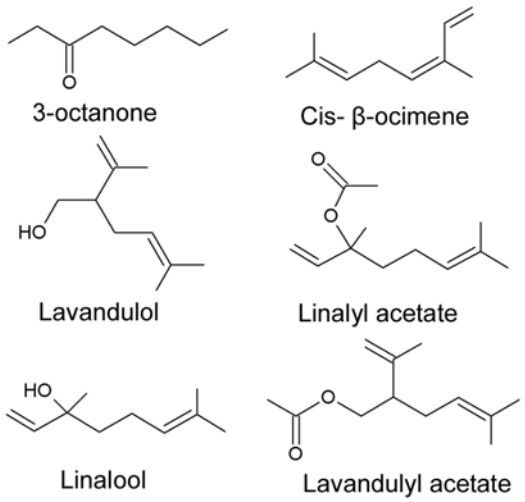

Figure 1: Compounds referred to in *Lavandula angustifolia* essential oil

LAEO based polymer films have been fabricated and their properties including chemical and optical been examined in detailed.[8-10, 12] LAEO is comprised of a number of components. Gas chromatography – mass spectrometry (GC-MS) was employed to determine the major constituents (Table 1) of the LAEO (*L. angustifolia* – G. R. Davis Pty. Ltd.) that has been implemented in the fabrication of LAEO based polymer films. The purpose of the GC-MS study was to determine the major components present in this particular oil, and as such the spectra were interpreted using the spectral database rather than using authentic reference standards. As such, the proportions obtained for the minor components of LAEO should only be taken as approximate values. From Table 1, it is apparent that linalool and linalyl acetate are the most abundant compounds in this particular oil. The components chosen for this study are indicated below (Figure

1). Cis-β-ocimene was chosen over trans-β-ocimene due to its availability, however the only difference between the two components is the geometry of the C=C. Even though it was not possible to detect lavandulol in the oil without the use of an authentic reference, it was still chosen as this component is a requisite for LAEO. As seen from the structures, all of the components contain oxygen functional groups such as ketones or esters, with the exception of cis- β-ocimene which is a pure hydrocarbon.

Table 1: Content of the individual components found in the LAEO monomer employed in previous studies

Compound	ISO Standard 3515[5] (%)	Actual (%)
Trans-β-ocimene	2 – 6	4.32
Cis- β-ocimene[1]	4 – 10	0.1
3-Octanone[1]	0 -2	3.2
Camphor	0 – 0.5	0.28
Linalool[1]	25 - 38	37.91
Linalyl acetate[1]	25 - 45	31.06
Terpinene-4-ol	2 - 6	3.69
Lavandulol[1]	min 0.3	0
Lavandulyl acetate[1]	min 2	2.27
α-Terpineol	0 - 1	0.9

[1]Components chosen for study

2.1 Deposition rate

Polymer thin films were successfully fabricated from all six components using the deposition parameters employed previously for the LAEO based polymer. Thickness of the resultant polymers was determined using spectroscopic ellipsometry, where the thickness of the films as a function of time is demonstrated in Figure 2 and the corresponding deposition rates in Table 2. Employing identical deposition conditions as the current study, deposition rates of up to 120 nm/min have been obtained for the LAEO based polymer films. Therefore in comparison, the deposition rates of the components were lower than that of the LAEO polymer. This result indicated that deposition of the LAEO polymer occurred via an additive nature between more than just one or two components, and likely a number of components are contributing to the deposition.

Table 2: Deposition rate, roughness (AFM) and water contact angle values of the fabricated polymer thin films.

Component	Deposition rate (nm/min)	Roughness (nm)	WCA (º)
3-Octanone	28	0.6	85.72
Cis- β-ocimene	94	14.82	94.14
Linalool	64	0.73	89.92
Linalyl acetate	26	0.46	81.9
Lavandulol	29	0.77	83.45
Lavandulyl acetate	18	0.39	76.85

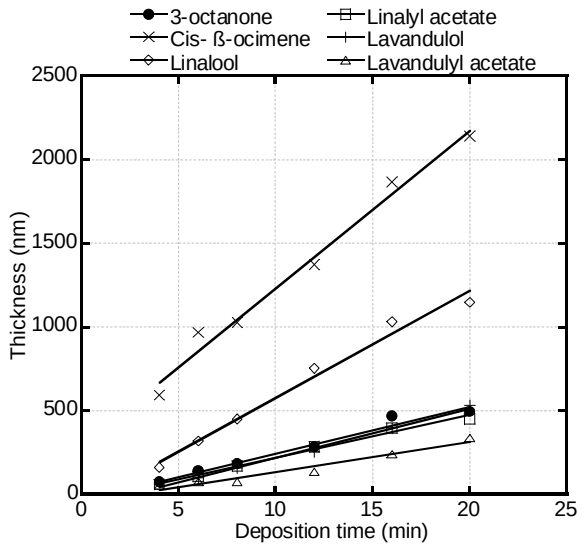

Figure 2: Film thickness of resultant polymers as a function of time

2.2 Chemical structural analysis

FTIR spectra of the monomer (top panel) and resultant polymer (bottom panel) for the six components are presented in Figure 3, the corresponding FTIR assignments for the monomer are listed in Tables A1 to A6 (appendix), and the assignments for the polymers shown in Table 3 based on the peak assignments presented in reference.[13] It is apparent that irrespective of the starting monomer, the spectra of the resultant polymers are similar. The majority of the same spectral peaks are found in each polymer, with some variation in the relative intensity of the peaks. All polymers demonstrate peaks associated with the presence of alcohol (~3460 cm^{-1}, O-H), and methyl (2956 cm^{-1}, 2871 cm^{-1}, 1457 cm^{-1}, 1376 cm^{-1}) and methylene (2930 cm^{-1}, 1457

cm^{-1}) groups. A large number of strong methyl peaks suggests that the thin films are comprised of a large number of short polymer chains, which is characteristic of plasma polymers.[14] A C=O peak associated with a ketone can be identified in the spectra of all the polymers with the exception of the cis-β-ocimene based polymer.

Table 3: FTIR assignments for the polymer thin films fabricated from the six identified components. Vibrational modes: νa ≡ asymmetrical stretching, νs ≡ symmetrical stretching, ν ≡ stretching, δa ≡ asymmetrical bending, δs ≡ symmetrical bending.

Wavenumber (cm^{-1})	Relative intensity	Assignment
~3460 (broad)[g]	medium[f]; weak[a,c,d,e]; v. weak[b]	ν(OH)
~3020[b]	v. weak	ν(C-H)
~2956[g]	v. strong[a,b,c,d,e]; strong[f]	ν_a(C-H)
~2930[g]	v. strong[a,b,d,e,f]; strong[c]	ν_a(C-H)
~2871[g]	strong[d,e]; medium[a,b,c,f]	ν_s(C-H)
2727[b]	v. weak	ν(C-H)
~1708[a,c,d,e,f]	v. strong[f]; strong[d]; medium[a,e,]; weak[c]	ν(C=O)
1604[b]	v. weak	ν(C=C)
~1457[g]	medium[d,e]; weak[a,b,c,f]	δ_a(C-H) OR δ(C-H)
~1376[g]	Medium[d,e]; weak[a,b,c,f]	δ_s(C-H)
1244[d]	v. weak	ν(C-O)
~1161[a,c,d,e,f]	v. weak	ν(C-O)
~1065[e]	v. weak	ν(C-O)
969[b,c], 884[b,c], ~750[b], 700[b]	Weak to v. weak	CH deformation

[a]3-octanone; [b]cis- β-ocimene; [c]linalool; [d]linalyl acetate; [e]lavandulol; [f]lavandulyl acetate; [g]all polymers

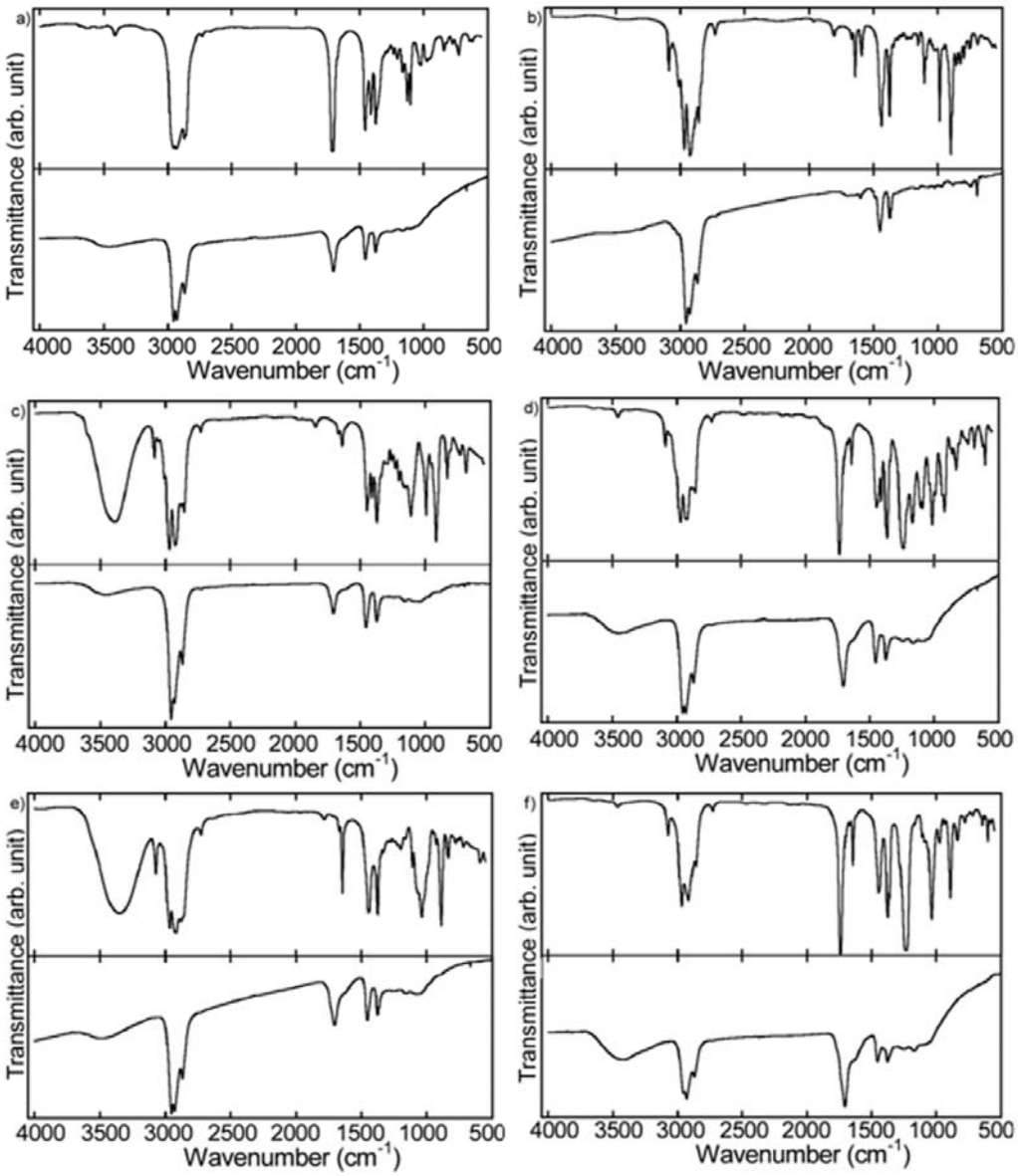

Figure 3: FTIR spectra for the components in monomer form (top panel) and resultant polymer thin films (bottom panel) fabricated from a) 3-octanone, b) cis-β-ocimene, c) linalool, d) linalyl acetate, e) lavandulol, f) lavandulyl acetate

We can infer from this information that for the ketone peak to be present in the resulting polymer, the monomer must contain an oxygen functional group. However, as the O-H peak is present for all polymers then it is likely that incorporation of O-H into the polymer structure is resulting from multiple sources, most likely due to oxygen uptake and the subsequent radical termination post deposition regardless of the chemical composition of the monomer. It has been shown for the LAEO based polymers that such

physical aging occurs via oxygen uptake and the subsequent increase in the O-H stretch,[12] and thus confirms the current observations. As expected there is a correlation between oxygen content of monomer and content in resultant polymers, with the lavandulyl acetate monomer containing a strong C=O (ester) and the resultant polymer exhibiting strong C=O (ketone) and O-H peaks. Special consideration should be given to the cis-β-ocimene based polymer. With the exception of the very weak O-H peak which is likely the result of radical termination, the structure consists of peaks allocated to C=C stretching (1604 cm^{-1}) and C-H stretching connected to C=C bonding (3020 cm^{-1}). Therefore, in addition to the lack of ketone peak, the chemical structure of the cis-β-ocimene based polymer is the only spectra to exhibit any significant deviation compared to the other samples.

Comparing the FTIR spectra of the polymers obtained in this study with that obtained for the LAEO based polymer,[9] with the exception of the cis-β-ocimene based polymer, the spectra of all the polymers are similar. The only significant different occurs in the intensity of the O-H and C=O peaks.

3.3 Optical properties

The refractive index and extinction coefficient of the polymers in addition to the transmission of the polymer + glass slide were examined by employing spectroscopic ellipsometry (Figure 4). The optical properties shown are for the films fabricated for 20 mins and thus under identical conditions. Therefore the thicknesses of the films are not equal, however their exposure time to UV irradiation and ion bombardment within the plasma phase was equal. The optical parameters of each polymer were compared as a function of thickness (data not shown). The largest difference in refractive index with respect to thickness was found for the linalool based polymer with a difference of 0.027 at long wavelengths for a thickness range of 719 nm. While for extinction coefficient, the largest difference was for the 3-octanone based polymer with a change of 0.01 at short wavelengths for a thickness range of 350 nm. These changes are comparable with those found by Gaynor et al.[15] for polyparaxylylene films grown by chemical vapour deposition, as well as the LAEO based polymer film,[10] where both polymers were deemed to not have significant thickness dependence on the refractive index.

Comparing the optical constants of all six resultant polymers, it is apparent that the refractive index and extinction coefficient of the films, with the exception of the cis-β-ocimene based polymer, were approximately equal and were slightly greater than that of glass. These results were comparable to those found for the LAEO based polymer.[10] The refractive index and extinction coefficient of the cis-β-ocimene based polymer however were greater than the other polymers, especially at higher wavelengths. For this polymer, there was no measurable change in extinction coefficient over a thickness range of 1500 nm (data not shown), thus the significantly higher value of extinction coefficient is a product of the difference in optical constant and not due to a weak thickness dependence. The transmission measurements confirmed that all the polymers were optically transparent. The deviation at shorter wavelengths of the cis-β-ocimene and linalool based polymers is a result of a thickness dependence of transmission (data not shown) rather than a difference in the optical properties.

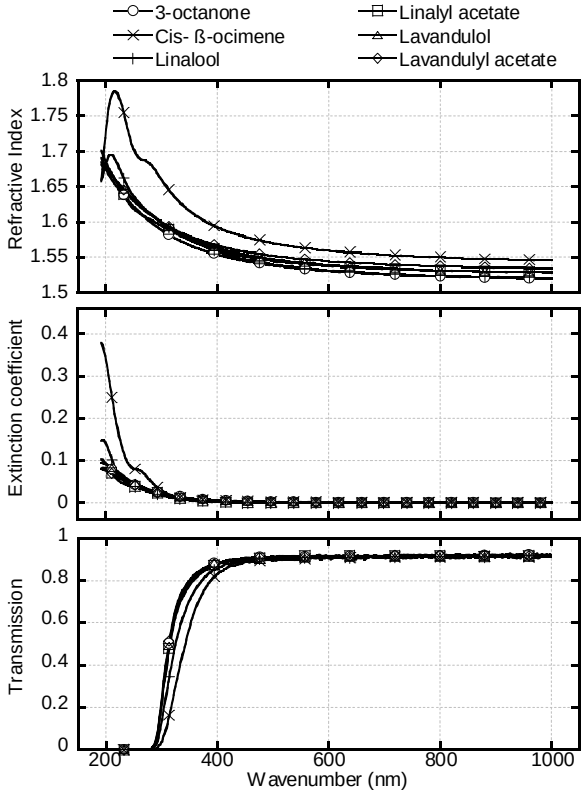

Figure 4: Optical properties of the resultant polymer films

3.4 Surface topology analysis

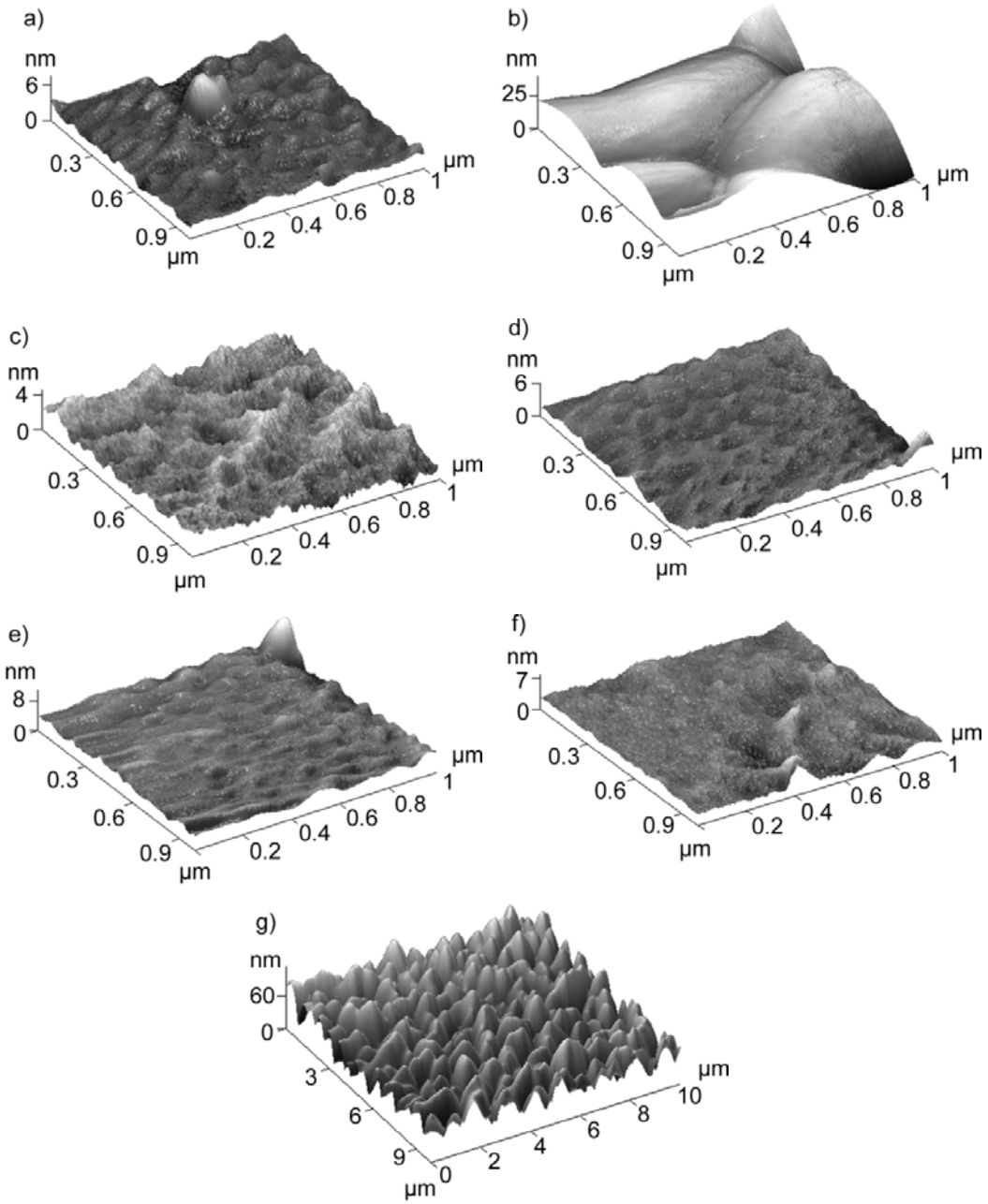

Figure 5: AFM images of the polymer films in semi-contact mode: a) 3-octanone, b) cis-β-ocimene, c) linalool, d) linalyl acetate, e) lavandulol, f) lavandulyl acetate, g) cis-β-ocimene (10 x 10 μm).

AFM images of the resultant polymers were obtained in semi-contact mode in order to obtain an understanding of the surface topology. Images of the films of scan size 1 x 1 μm are presented in Figure 5 a)- f), and a 10 x 10 μm image of cis-β-ocimene is shown Figure 5 g). Scan sizes of 10 x 10 μm were used to determine the average roughness of the surface of the polymers (Table 2).

From these images it is apparent that the surface topologies of all the films, with exception of cis-β-ocimene based polymer, were similar. The lavandulyl acetate and linalyl acetate based polymers produced the smoothest surfaces, with a roughness comparable with that of the LAEO based polymer fabricated under the same conditions (0.42).[9] The 3-octanone, linalool and lavandulol based polymers demonstrated a very smooth surface, however small mounds of approximately 6 – 10 nm in height were evenly distributed over the surface. One such mound can be seen in each of the figures corresponding to the identified polymers. The cis-β-ocimene based polymer resulted in a surface roughness much higher than the other polymers (14.82 nm). A 10 x 10 μm was also included for this polymer as the structure of the surface was much larger comparatively and thus was necessary to provide an adequate representation. This image looked to be very similar to that obtained for LAEO,[9] except that the Z scale was significantly larger. Given that the height from the baseline to the top of the peaks was less than 100 nm, this film still provides a uniform coating as the actual thickness of this film is 1867 nm.

2.5 Water contact angle

Equilibrium water contact angle values were obtained for the fabricated polymers (Figure 6). The error bars in the plot represent the 95% confidence levels at each time interval. The experimental procedure has been confirmed previously [9] using polytetrafluoroethylene where the data was represented by a linear fit with equation $y = -0.01t + 119.95$ and $R^2 = 0.97$, where t represents time. From Table 2, the WCA ranges from 76.85 (lavandulyl acetate) to 94.14 (cis-β-ocimene). Referring back to the FTIR analysis, as expected the polymers with strong peaks assigned to oxygen resulted in low WCA values, while the cis-β-ocimene based polymer with very little oxygen measured the highest WCA value. The contact angle observed for the cis-β-ocimene based

polymer could also be attributed to the relatively large average roughness of the film. An increase in surface roughness has been previously associated with an increase in hydrophobicity.[16] The polymer with a WCA closest to the LAEO based polymer (83.64) is the lavandulol based polymer (83.45), followed by the 3-octaneone based polymer (81.9), and then the linalyl acetate polymer (85.72).

An initial rapid rate of change in contact angle typically represents an absorption of water by the sample.[17] From Figure 6, there is no apparent rapid rate of change in contact angle for most of the polymers. However, the lavandulyl acetate based polymer data demonstrates a small deviation from the line of best fit at time less than 5 s. Due to the magnitude of the deviation, the amount of water absorption into the polymer was expected to be minimal.

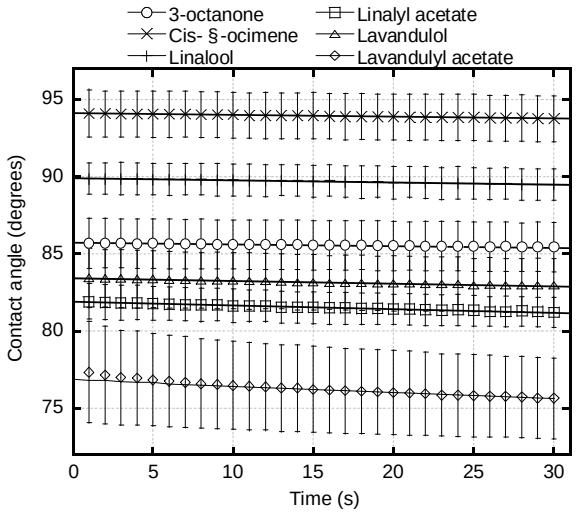

Figure 6: Equilibrium water contact angle of the resultant films as a function of time.

WCA as a function of time can provide information concerning reactions between the liquid and the polymer, where a large rate of change is associated with reorientation of functionalities at the solvent-surface interface. In this study, the highest rate of change was for lavandulyl acetate at -0.04º s^{-1}, where the rate of change for the remaining polymers was between -0.009º s^{-1} to -0.023º s^{-1}. These results are slightly greater than that obtained for LAEO based polymer (-0.006º s^{-1}), however are much lower than that

obtained for poly(acrylic acid) (-0.2º s^{-1}).[17] The WCA results demonstrate that it is highly unlikely that interactions such as swelling (with the exception of the lavandulyl acetate based polymer) or reorientation of polar groups are occurring at the liquid-solid interface, and as such these polymers are stable while in contact with water. In addition, the WCA for the polymers, with the exception of cis-β-ocimene, fall within the demonstrated range for plasma polymers that provide favourable dose response of ^{125}I-protein A uptake to human immunoglobulin G (hIgG).[18] It has also be shown that linalool can induce a decrease in biofilm metabolic activity.[19] Therefore these materials have the potential to be implemented in biomedical applications as either bio-reactive or bio-non-reactive coatings.

3. Conclusion

Plasma polymer thin films have been fabricated from the constituents of LAEO and the properties of these materials have been examined. Using GC-MS, the major components were identified. The deposition rate of the polymers was found to range between 18 to 94 nm/min, which is lower than that obtained for the LAEO based polymer (120 nm/min). FTIR spectra of the polymers have been obtained for both the monomers and resulting polymers. It is apparent that irrespective of the starting monomer, the spectra of the resultant polymers are very similar. The cis-β-ocimene based polymer exhibited the most significant deviation as the spectral peak for ketone at approximately 1710 cm^{-1} was absent, and peaks associated with C=C were present. The results indicate that an oxygen functional group contained in the monomer was required in order to obtain a ketone peak in the resulting polymer; however this requirement was not necessary for the O-H stretch. Therefore alcohol inclusion into the polymer structure resulted from multiple sources, most likely through radical termination post deposition. The optical properties were examined via ellipsometry. All polymers were proven to be optically transparent. Refractive index of the polymers was only slightly greater than that of glass, with the exception of the cis-β-ocimene based polymer which was greater still. The extinction coefficient demonstrated that there was negligible absorption at wavelengths greater than 400 nm. AFM investigation of the polymers demonstrated some variation in the surface topology between the thin films. The average roughness of most of the polymers was less than 0.8 nm indicating a very smooth surface. The cis-β-ocimene based polymer however has a surface topology that results in a much higher

average roughness (14.82 nm). WCA values ranged from 76.85º to 94.14º indicating that the polymers ranged from hydrophilic to mildly hydrophobic. The WCA results demonstrated that the polymer thin films were stable while in contact with water. These results indicate that the LAEO based polymer is the result of the polymerisation of a number of the constituents within the plasma phase. Overall, there were similarities between the properties of these polymers and the LAEO based polymer. This indicated that polymers of similar characteristics could be fabricated from LAEO irrespective of the composition of the LAEO monomer.

4. Experimental

LAEO components were obtained from Australian Botanic Products, with the exception of lavandulyl acetate ((±)-lavandulol acetate; assay ≥ 98.5%; Fluka) and lavandulol (assay ≥ 98.5%; Aldrich) from Sigma Aldrich and used without further purification. Employing the experimental apparatus described,[8] polymer thin films were fabricated. Deposition parameters including RF power (25 W) were kept constant and the deposition time (4, 6, 8, 12, 16, and 20 min) varied to obtain films of various thicknesses. Fabrication was performed at a pressure of approximately 300 mTorr. RF energy (13.56 MHz) was delivered to the deposition chamber via external copper electrodes separated by a distance of 11 cm. For all monomers employed, approximately 1 mL was placed into the holder and replaced after each subsequent deposition. Prior to placement of substrate within the polymerisation cell, the monomer inlet was opened briefly to evacuate the monomer container. During deposition, the monomer inlet was again opened and the vapour was released into the chamber, where the flow rate was controlled via a vacuum stopcock. Three different types of substrate were employed in this study; glass slides for AFM, ellipsometry and WCA experiments, KBr discs were deposited onto directly for the FTIR analysis, and NaCl disks were used for the FTIR analysis of the monomers. The glass slides were cleaned first with a solution of Extran and distilled water, then ultrasonically cleaned for 15 min, rinsed with propan-2-ol and air-dried. The wet cleaning procedure was not employed for the KBr discs. The NaCl disks were cleaned with dichloromethane after measurement of each monomer. Prior to fabrication, the glass slides and KBr were pre-treated with Ar plasma in order to produce an oxygen-free surface.[20]

Gas chromatography – mass spectrometry (GC-MS) was performed using the Varion GC 3800 and the Varion 1200 Mass Spectrometer, respectively. The measurement was performed at Advanced Analytical Centre (AAC), James Cook University (JCU), where the LAEO was diluted in hexane prior to analysis.

A Perkin-Elmer Spectrum 2000 FTIR Spectrometer (RMIT) was employed to determine the chemical structure of the polymer thin films. Spectra were obtained in transmission mode in the region of 4000 – 500 cm^{-1}. A total of 32 scans were acquired for each film at a resolution of 1 cm^{-1}. CO_2 and H_2O were accounted for in the spectra by a background substraction procedure using a pre-recorded background under the same atmospheric conditions.

Spectroscopic ellipsometry was used to determine the thickness and optical properties of the polymer thin films including refractive index, extinction coefficient and transmission. Measurements were performed in the wavelength range 190 – 1000 nm using a variable angle spectroscopic ellipsometer (model M-2000, J. A. Woollam Co., Inc.). Ellipsometric parameters Ψ and Δ were obtained at three different angles of incidence, φ = 55º, 60º, and 65º, in addition to transmission data. These measured parameters were used to derive the optical constants based on a model of the sample built in the J. A. Woollam Inc. analysis software (WVASE32) via regression analysis. A single Gaussian oscillator (3-octanone, lavandulol, lavandulyl acetate) or a Gaussian and Tauc-Lorentz oscillator (cis-β-ocimene, linalool, linalyl acetate) were employed within the model providing the best possible fit to the data, with a lower mean-squared error and lower average correlation between fitting terms. See reference [10] for a more detailed review of the experimental procedure.

Analysis of the surface morphology was undertaken at the AAC, JCU using the NT-MDT NTEGRA Prima AFM in semi-contact mode.

A KSV 101 system was implemented for the water contact angle measurements. Drop volume of approximately 8 μL was employed, where 8 drops were used to determine the WCA for each film. Double distilled water produced using a Labglass Delta system (Labglass Pty Ltd) was employed for the measurements. Once the drop was placed on the surface, the software (KSV CAM software) was triggered and an image was recorded every second for 30 s in order to monitor the contact angle as a function of time. Using image processing software, contact angle values were obtained by fitting the measured drop profile with the Young-Laplace equation.

Acknowledgements

The authors are grateful to the financial support provided under the RIRDC and ARC LIEF and DP schemes. CDE is grateful to the APA, RIRDC and GRS (JCU) scholarships. We are thankful to Dr B. Rengarajan and Mr K. Frost (RMIT) for assistance in obtaining the FTIR spectra, and Dr S. Askew (AAC – JCU) for assistance in obtaining the AFM images and the GC-MS analysis. We acknowledge the AAC for use of their characterisation facilities.

Appendix

Table A 1: FTIR assignments for 3-octanone monomer

Wavenumber (cm^{-1})	Relative intensity	Assignment
3415	v. weak	ν(O-H)
~2961	v. strong	ν_a(C-H)
~2934	v. strong	ν_a(C-H)
~2873	v. strong	ν_s(C-H)
~2861	v. strong	ν_s(C-H)
1713	v. strong	ν(C=O)
1460	Strong	δ(C-H)
1412	Strong	δ_a(C-H)
1374	Strong	δ_s(C-H)
1286, 1240, 1207, 1165, 1131, 1106	Strong to weak	ν(C-C)
1039, 1023, ~975, ~963, 844, 822, 766, 728, 644, 620	Medium to v. weak	CH deformation

Table A 2: FTIR assignments for cis-β-ocimene monomer

Wavenumber (cm^{-1})	Relative intensity	Assignment
3091	Medium	ν(C-H)
~3009	Medium	ν(C-H)
2970	v. strong	ν_a(C-H)
~2928	v. strong	ν_a(C-H)
~2916	v. strong	ν_a(C-H)
2858	Strong	ν_s(C-H)
~2836	Medium	ν_s(C-H)
2730	Weak	ν(C-H)
1806	v. weak	ν(C=O)
1672	v. weak	ν(C=C)
1645	Medium	ν(C=C)
1594	Weak	ν(C=C)
1438	Medium	δ(C-H)
1376	Medium	δ_s(C-H)
1345, 1155, 1107, 1090, 1051, 1036	Medium to v. weak	ν(C-C)
986, 957, 901, 887, 858, 828, 798, 754, 692	v. strong to weak	CH deformation

Table A 3: FTIR assignments for linalool monomer

Wavenumber (cm^{-1})	Relative intensity	Assignment
~3400 (broad)	Strong	ν(O-H)
3087	Weak	ν(C=C)
3007	Medium	ν(C=C)
2970	v. strong	ν_a(C-H)
~2928	v. strong	ν_a(C-H)
2857	Strong	ν_s(C-H)
2729	Weak	ν(C-H)
1843	v. weak	ν(C=O)
1676	v. weak	ν(C=C)
1643	Weak	ν(C=C)
1452	Medium	δ_a(C-H)
1410	Medium	δ(O-H)
1375	Medium	δ_s(C-H)
~1338, 1264, 1234, 1206	Weak	ν(C-C)
~1165	Medium	ν(C-O)
1114	Medium	ν(C-C)
996, 919, 834, 736, 690	Strong to weak	CH deformation

Table A 4: FTIR assignments for linalyl acetate monomer

Wavenumber (cm^{-1})	Relative intensity	Assignment
3452	v. weak	ν(O-H)
3088	Weak	ν(C=C)
2970	Strong	ν_a(C-H)
~2925	Strong	ν_a(C-H)
2858	Medium	ν_s(C-H)
2730	v. weak	ν(C-H)
1737	v. strong	ν(C=O)
1673	v. weak	ν(C=C)
1645	Weak	ν(C=C)
1449	Medium	δ(C-H)
1412	Medium	δ(C-H)
1367	Strong	δ_s(C-H)
1243, 1171, 1111, 1091	v. strong to medium	ν(C-O)
1041	Medium	ν(C-C) OR CH deformation
1019, 997, 940, 922, 863, 833, 739, 691, 624, 609	Strong to weak	CH deformation

Table A 5: FTIR assignments for lavandulol monomer

Wavenumber (cm^{-1})	Relative intensity	Assignment
~3350 (broad)	Strong	ν(O-H)
3073	Medium	ν(C=C)
2969	v. strong	ν_a(C-H)
2920	v. strong	ν_a(C-H)
2880	Strong	ν_s(C-H)
2860	Strong	ν_s(C-H)
2726	Weak	ν(C-H)
1784	v. weak	ν(C=O)
1673	v. weak	ν(C=C)
1644	Medium	ν(C=C)
1445	Strong	δ(C-H)
1375	Strong	δ_s(C-H)
1199, 1160, 1111	Medium to v. weak	ν(C-C)
1039	Strong	ν(C-O) (primary alcohol)
930, 889, 837, 780, 720, 593	Strong to v. weak	CH deformation

Table A 6: FTIR assignments for lavandulyl acetate monomer

Wavenumber (cm^{-1})	Relative intensity	Assignment
3462	v. weak	ν(O-H)
3075	Weak	ν(C=C)
2969	Strong	ν_a(C-H)
2916	Strong	ν_a(C-H)
2858	Medium	ν_s(C-H)
2729	v. weak	ν(C-H)
1743	v. strong	ν(C=O)
1671	v. weak	ν(C=C)
1647	Medium	ν(C=C)
1450	Strong	δ_a(C-H)
1378	Strong	δ_s(C-H)
1360	Strong	δ_s(C-H)
1236, 1114, 1091	v. strong to v. weak	ν(C-O)
1039, 972, 891, 839, 778, 723, 644, 604	Strong to v. weak	CH deformation

References

[1] A. Hiratsuka, I. Karube, *Electroanalysis* **2000**, *9*, 695.

[2] Z. V. Vardeny, A. J. Heeger, A. Dodabalapur, *Synthetic Metals* **2005**, *1*, 1.

[3] M. Berggren, A. Richter-Dahlfors, *Advanced Materials* **2007**, *20*, 3201.

[4] R. Forch, A. N. Chifen, A. Bousquet, H. L. Khor, M. Jungblut, L. Q. Chu, Z. Zhang, I. Osey-Mensah, E. K. Sinner, W. Knoll, *Chem. Vapor Depos.* **2007**, *6-7*, 280.

[5] R. Shellie, L. Mondello, P. Marriott, G. Dugo, *Journal of Chromatography A* **2002**, *1-2*, 225.

[6] T. J. Morgan, W. E. Morden, E. Al-Muhareb, A. A. Herod, R. Kandiyoti, *Energy & Fuels* **2006**, *2*, 734.

[7] R. Shellie, P. Marriott, C. Cornwell, *Hrc-Journal of High Resolution Chromatography* **2000**, *9*, 554.

[8] M. V. Jacob, C. D. Easton, G. S. Woods, C. C. Berndt, *Thin Solid Films* **2008**, *12*, 3884.

[9] C. D. Easton, M. V. Jacob, R. A. Shanks, B. F. Bowden, *Chem. Vapor Depos.* **In press**.

[10] C. D. Easton, M. V. Jacob, *Thin Solid Films* **In press**.

[11] M. E. Ryan, A. M. Hynes, S. H. Wheale, J. P. S. Badyal, C. Hardacre, R. M. Ormerod, *Chem. Mat.* **1996**, *4*, 916.

[12] C. D. Easton, M. V. Jacob, *Polymer Degradation and Stability* **In press**.

[13] J. Coates, in: *Encyclopedia of Analytical Chemistry* (Eds: R. A. Meyers), John Wiley & Sons Ltd, Chichester, UK **2000**, p. 10815.

[14] H. Biederman, in: *Plasma Polymer Films* (Eds: H. Biederman), Imperial College Press, London **2004**.

[15] J. F. Gaynor, S. B. Desu, *Journal of Materials Research* **1996**, *1*, 236.

[16] S. H. Gao, M. K. Lei, Y. Liu, L. S. Wen, *Appl. Surf. Sci.* **2009**, *11*, 6017.

[17] M. R. Alexander, T. M. Duc, *Polymer* **1999**, *20*, 5479.

[18] S. Kurosawa, N. Kamo, N. Minoura, M. Muratsugu, *Materials Science and Engineering: C* **1997**, *4*, 291.

[19] S. Dalleau, E. Cateau, T. Berges, J. M. Berjeaud, C. Imbert, *Int. J. Antimicrob. Agents* **2008**, *6*, 572.

[20] M. C. Kim, S. H. Cho, J. G. Han, B. Y. Hong, Y. J. Kim, S. H. Yang, J. H. Boo, *Surface & Coatings Technology* **2003**, 595.

CHAPTER 7 INVESTIGATION OF POLYMERS FROM CINEOLE

A great variety of essential oils are available that could be employed in plasma polymerisation. The properties of these resultant films could be beneficial for a number of applications. One possible route is to attempt to identify and maintain certain key properties of the monomer during the polymerisation process. 1,8-Cineole can be a major component of LAEO, however no detectable amount was found in the LAEO monomer employed in this thesis. It is also a major component of eucalyptus oil. The cineole monomer has been shown to have desirable properties for use in the medical field. This chapter presents a paper where 1,8-cineole was polymerised and the properties of the resultant films determined.

7.1 FABRICATION AND CHARACTERISATION OF POLYMER THIN-FILMS DERIVED FROM CINEOLE USING RADIO FREQUENCY PLASMA POLYMERISATION

This paper describes the fabrication and characterisation of polymer thin films fabricated from 1,8-cineole. The chemical structure of the resultant polymer was examined using FTIR, while the optical properties were investigated employing spectroscopic ellipsometry. The surface profile and roughness was measured using the AFM, and the stability and hydrophilicy of the surface determined using water contact angle. “Fabrication and characterisation of polymer thin-films derived from cineole using radio frequency plasma polymerisation” (Pub. 7.) at time of print is currently under review for publication in Polymer (Elsevier). This paper involved collaboration with Prof. Robert Shanks.

FABRICATION AND CHARACTERISATION OF POLYMER THIN-FILMS DERIVED FROM CINEOLE USING RADIO FREQUENCY PLASMA POLYMERISATION

Christopher D Easton[1], Mohan V Jacob[1]* and Robert A Shanks[2]

[1]Electronic Materials Research Lab, School of Engineering, James Cook University, Townsville, 4811, Australia

[2]Applied Sciences, RMIT University, GPO Box 2476V, Melbourne, 3001, Australia

*Corresponding author. Tel.: +61 7 47814379; fax: +61 7 47815177; Email: Mohan.Jacob@jcu.edu.au

Abstract

The development of organic polymer thin films is critical for the progress of many fields including organic electronics and biomedical coatings. This paper describes the fabrication of an organic polymer thin film produced from 1,8-cineole via radio frequency plasma polymerisation. A deposition rate of 55 nm/min was obtained under the polymerisation conditions employed. Infrared spectroscopic analysis demonstrated that some functional groups observed in the monomer were retained after the polymerisation process, while new functional groups were introduced. The refractive index and extinction coefficient were estimated to be 1.543 (at 500 nm) and 0.001 (at 500 nm) respectively. The polymers were shown to be optically transparent. AFM images of the polymer established a very smooth and uniform surface with average roughness of 0.39 nm. Water contact angle data demonstrated that the surface was weakly hydrophilic and was stable while in contact with water.

Keywords: Plasma polymerisation; 1,8-cineole; thin-film.

1. Introduction

The advent of thin-film applications stemming from new technologies including organic electronics [1] and bioelectronics [2] have resulted in an increase in attention in the development of polymer thin-films from organic resources. Plasma polymerisation is a method for fabricating organic thin-films for use in such applications using materials that do not normally polymerise using conventional techniques [3]. The resulting polymer is typically of a high quality, exhibiting properties including chemical and physical stability, film homogeneity and a smooth, pinhole free surface [4, 5]. In addition, it is possible to maintain a high degree of chemical functionality of the monomeric precursor through control of the deposition parameters [6]. As a result, plasma polymerisation has become popular for use in the biomedical field for the fabrication of bio-reactive and non-bio-reactive coatings [7].

1,8-Cineole, or Eucalyptol, is a saturated monoterpene and it is major component of Eucalyptus oil. The chemical structure of 1,8-Cineole is shown in Figure 1. This monomer is obtained from a natural, environmentally friendly, non-petrochemical resource. Use of both Eucalyptus oil and 1,8-cineole as monomers within medical research has gained considerable interest in recent years. Examples include use as an anti-inflammatory in bronchial asthma [8], inhibition of cytokine production [9], and induce activation of human monocyte derived macrophages, stimulating their phagocytic response and thus inducing an immune system response [10]. The antifungal activity of 1,8-cineole has been confirmed via biofilm experiments [11].

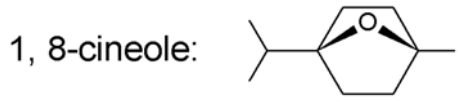

Figure 1: Chemical structure of 1,8-cineole

Plasma polymerisation has been implemented in the past to fabricate films from Eucalyptus oil [12], where the electrical and optical (optical band gap) properties of the films were examined. However, as Eucalyptus oil is a mixture of several components with different vapour pressures, it is not clear which components contributed to the formation of the polymer within the plasma phase. The plasma polymerisation process

involved fragmentation of the monomer molecules upon release into the plasma phase, and thus not only 1,8-cineole, but the additional components found in Eucalyptus oil will contribute to the composition of the resulting polymer.

The aim is to fabricate polymer thin-films from 1,8-cineole via plasma polymerisation and determine the chemical, optical, surface and physical properties of the resulting films. The chemical structure of the polymer will be investigated using Fourier transform infrared (FTIR) spectroscopy. Spectroscopic ellipsometry will be employed to determine the refractive index, extinction coefficient and optical transmission of the material. Ellipsometry will also be utilised to monitor the thickness of the resulting films and evaluate the deposition rate of the polymer thin-film. Atomic force microscope (AFM) will be used to study the surface profile of the polymer films, and the physical properties of the surface will be examined via water contact angle (WCA) measurements.

2. Experimental

1,8-Cineole monomer obtained from Australian Botanical Products was used for the fabrication of the plasma polymer thin-films at a radio frequency (RF) power level of 25 W and for various deposition times. The deposition parameters including RF power and pressure employed in this study were adapted from a previous study [13]. A diagram of the experimental apparatus is presented in Figure 2. The polymer films were fabricated at a pressure of approximately 33 Pa. RF energy (13.56 MHz) was delivered to the deposition chamber via external copper electrodes separated by a distance of 11 cm. The distance between the monomer inlet and the edge of the plasma excitation zone (edge of right electrode in Figure 2) was 12 cm. Approximately 1 mL of the monomer is placed into the holder and replaced after each subsequent deposition. The monomer inlet was opened in order to evacuate the monomer container prior to placement of substrate within the polymerisation cell. The monomer was released into the chamber throughout deposition, and the flow rate was controlled via a vacuum stopcock. It was found that for the cineole monomer addition, completely opening the monomer flow valve lead to saturation of the polymerisation cell and resulted in a pressure too high for polymerisation. Therefore greater control of the flow rate was

required when using this monomer compared with the previous study in order to achieve the same deposition pressure. To achieve this, the monomer flow rate was restricted by only opening the valve partially. The monomer flow rate was determined employing the procedure outlined by Gengenbach and Griesser[2]. Briefly, the flow rate (F; cm^3 (STP)/min) was determined using the following equation [3]:

$$F = \frac{dp}{dt} \times 16172 \frac{V}{T} \quad (1),$$

where p = pressure (mbar), t = time (s), V = volume of plasma reactor = 1.8 L, T = temperature = 295 K. The change in pressure as a function of time was determined by first evacuating the plasma reactor, then opening the monomer valve and allowing the pressure to stabilise. The valve to the vacuum pump was then closed and the pressure recorded every 5 s for 60 s. A flow rate of F= 1.5 cm^3/min was employed in this study.

Three different types of substrate were employed in this study; glass slides for AFM, Ellipsometry and WCA experiments, the films were deposited onto KBr directly for FTIR analysis, and NaCl disks were used for FTIR of the 1,8-cineole monomer. The glass slides were first cleaned with a solution of Extran and distilled water, then ultrasonically cleaned for 15 min, rinsed with propan-2-ol and air-dried. The wet cleaning procedure was not employed for the KBr discs. Prior to fabrication, all substrates were pre-treated with Ar plasma in order to produce an oxygen-free surface [4].

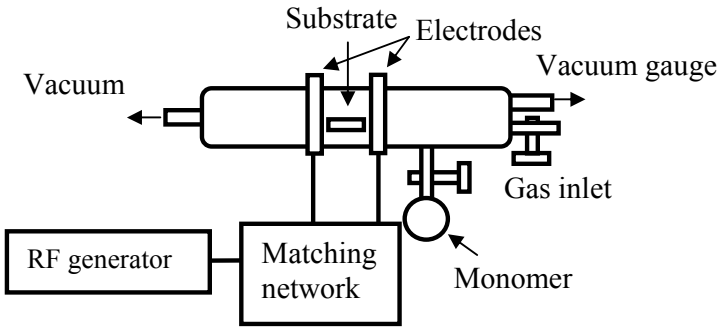

Figure 2: Experimental apparatus

FTIR spectroscopy was employed to determine the chemical structure of the polymer thin-films using a Perkin-Elmer Spectrum 2000 FTIR Spectrometer. Spectra were obtained in transmission mode in the region of 4000 – 500 cm^{-1}, where 32 scans were acquired for each sample at a resolution of 1 cm^{-1}. CO_2 and H_2O were eliminated from spectra by a background substraction procedure, where the background was pre-recorded under the same atmospheric conditions.

Optical properties and thickness of the resultant thin-film was examined over the wavelength range 190 – 1000 nm using a variable angle spectroscopic ellipsometer (model M-2000, J. A. Woollam Co., Inc.). Ellipsometric parameters Ψ and Δ were obtained at three different angles of incidence, φ = 55º, 60º, and 65º. In addition, the transmission data was also collected. Ψ and Δ were used to derive the optical constants based on a model of the sample built in the J. A. Woollam Inc. analysis software (WVASE32) via regression analysis. The quality of the fit was measured quantitatively by determining the mean-squared error and through the use of the correlation matrix. Gaussian and Tauc-Lorentz oscillators were employed within the model to provide an optimal fit of the data, with a lower mean square error and lower average correlation between fitting terms. A more detailed review of the procedure has been reported elsewhere [14].

Analysis of the surface morphology was undertaken using the NT-MDT NTEGRA Prima AFM in semi-contact mode.

Water contact angle measurements were performed using a KSV 101 system. The height of each drop is confirmed using a CCD camera prior to each measurement to ensure consistency in drop volume. Drop volumes of approximately 8 µL were employed, where 8 drops were used to determine the WCA. Double distilled water produced using a Labglass Delta system (Labglass Pty Ltd) was employed for the measurements. Once the drop was placed on the surface using a one-touch dispenser system, the KSV CAM software was triggered to begin recording. An image was recorded every second for 30 s in order to monitor the contact angle as a function of

time. Image processing software was used to determine the contact angle by fitting the measured drop profile with the Young-Laplace equation.

3. Results and Discussion

3.1 Deposition rate

Polymer thin-films were successfully fabricated from 1,8-cineole using an RF glow discharge. Spectroscopic ellipsometry was employed to determine the thickness of the polymer, and the estimated film thickness as a function of time is demonstrated in Figure 3. This study demonstrated that a deposition rate of approximately 55 nm/min was achieved, which is comparable to deposition rates for other monomer precursors employed in plasma polymerisation such as thiophene [15]. The rate of deposition of polymer could be adjusted by altering the deposition parameters such as RF power or pressure, however the parameters outlined in experimental were maintained to allow for reproducibility. The deposition rate obtained indicates that thin film coatings can be fabricated in a minimal amount of time, leading to fast production rates for implementation in applications.

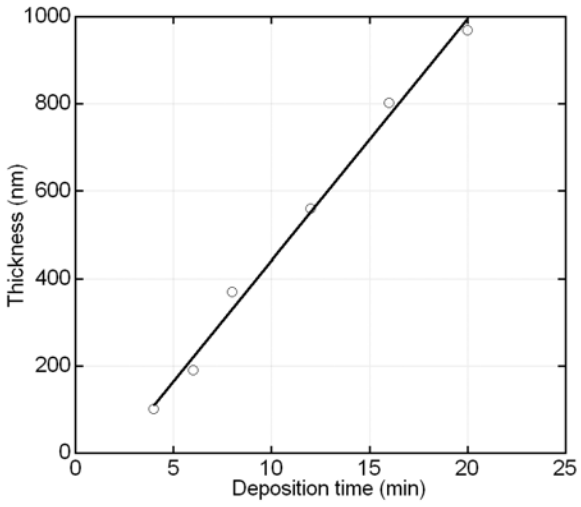

Figure 3: Thickness of 1,8-Cineole based polymer thin-film as a function of deposition time

3.2 Infrared spectroscopic analysis

FTIR spectra of 1,8-cinole monomer in addition to the 1,8-cineole based polymer films are presented in Figure 4 with the corresponding FTIR assignments listed in Table 1 based on the peak assignments presented in reference [16]. Considering first the spectrum for the monomer, the spectral allocation was expected to be straightforward as the chemical structure was known. Stretching of methyl (2985 cm^{-1}, 2968 cm^{-1}, 2945 cm^{-1}, and 2881 cm^{-1}) and methylene groups (2924 cm^{-1} and 2881 cm^{-1}) is indicated by strong bands in the spectrum, in addition to bending of C-H groups (1466 cm^{-1}, 1446 cm^{-1}, 1375 cm^{-1}, 1081 cm^{-1}, and 1052 cm^{-1}). Bands between 1359 cm^{-1} to 1214 cm^{-1} demonstrate stretching of carbon-carbon bonds. C-O stretching is represented by the peak at 1168 cm^{-1}, while the very weak peak at 3175 cm^{-1} assigned to O-H stretching could imply an impurity.

Comparison of the results for the 1,8-Cineole based polymer with that of the monomer, it is apparent that upon polymerisation the intensity of the bands within the fingerprint region have been reduced, however some functional groups of the monomer were maintained. The bands around 2900 cm^{-1} associated with methyl and methylene groups appear largely unaffected. The broad peak at 3469 cm^{-1} is associated with O-H stretching, while the peak at 1707 cm^{-1} is indicative of C=O of ketone, which was not present in the monomer spectra. An ether group is present in the monomer, and this can be converted to other oxygen containing species, such as a ketone group in the polymer. Within the plasma phase, fragmentation of parts of the monomer occurs. If one or both bonds of the between the oxygen and carbon in the ether group can be ruptured within the plasma, then this could lead to the oxygen forming a double bond with a single carbon group to become stable and thus form the ketone. As the ketone groups are present in the polymer, it would appear that this reaction path is favourable. Carbon-carbon bonds by analogy become unsaturated by plasma treatment. Therefore based on the assigned spectra, the resultant polymer was predominantly hydrocarbon dense with the presence of oxygen containing groups in the form of alcohol and ketone groups within the structure.

Table 1: FTIR spectra assignments for 1,8-Cineole monomer and 1,8-cineole based polymer.

Wavenumber (cm^{-1})	Relative intensity	Assignment
1,8-Cineole monomer:		
~3175 (broad)	very weak	ν(O-H)
~2985, ~2968, ~2945, ~2924	very strong	ν_a(C-H)
~2881	strong	ν_s(C-H)
~2853	medium	ν_s(C-H)
1466 and 1446	medium	δ(C-H)
1375	strong	δ_s(C-H)
1359	medium	δ(C-H)
1307	medium	ν(C-C)
1272	weak	ν(C-C)
1232	medium	ν(C-C)
1214	strong	ν(C-C)
1168	medium	ν(C-O)
1081	strong	δ(C-H)
1052	medium	δ(C-H)
1015, 986, 929, 921, 888, 864, 843, 812, 788, 765, 650, 576	very strong to very weak	C-H deformation
1,8-Cineole based polymer:		
~3469	weak	ν(O-H)
2958 and 2930	very strong	ν_a(C-H)
2872	medium	ν_s(C-H)
1707	weak	ν(C=O)
1456	weak	δ_a(C-H)
1375	weak	δ_s(C-H)
1213	very weak	ν(C-C)
1163	very weak	ν(C-O)
1059	very weak	δ(C-H)
986	very weak	CH deformation

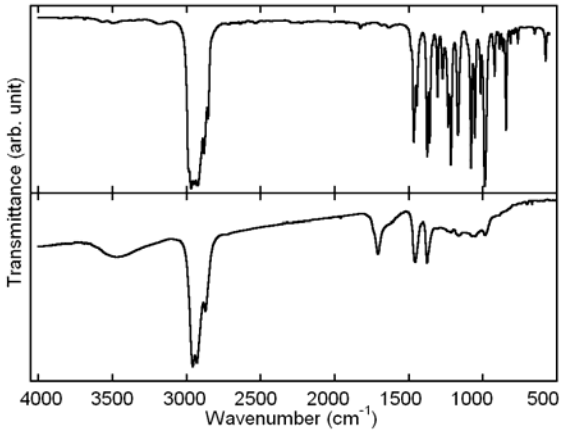

Figure 4: FTIR spectra of 1,8-Cineole monomer (top spectrum) and 1,8-cineole based polymer (bottom spectrum).

3.3 Optical Properties

In addition to the thickness measurements, ellipsometry was utilised to determine the optical properties of the polymer. Refractive index and extinction coefficient of the polymer for various thicknesses were measured, in addition to the transmission of the polymer and glass slide, and they are shown in Figure 5. The refractive index of the 1,8-cineole polymer was slightly greater than that of the glass slide, while the extinction coefficient demonstrated that there was negligible absorption at wavelengths greater than 400 nm. The polymer was shown to be optically transparent, as revealed by the transmission data. At low wavelength, a deviation occurs with respect to thickness for the measured optical parameters. Both the refractive index and extinction coefficient tended to increase with increasing thickness at approximately 200 nm, while the transmission tended to decrease with increasing thickness at approximately 350 nm. This deviation was however insignificant and restricted to a small wavelength region, and thus for the thickness range measured, the optical constants of the 1,8-Cineole polymer film were independent of thickness. It will be possible to tailor the optical properties to suit different optical applications by changing the deposition parameters.

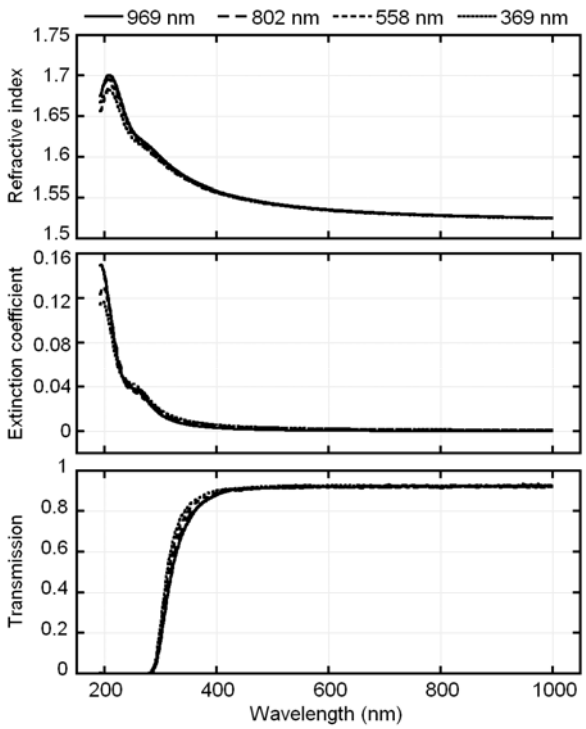

Figure 5: Refractive index (top panel) and extinction coefficient (middle panel) of the 1,8-cineole based polymer film and transmission (bottom panel) of polymer and substrate.

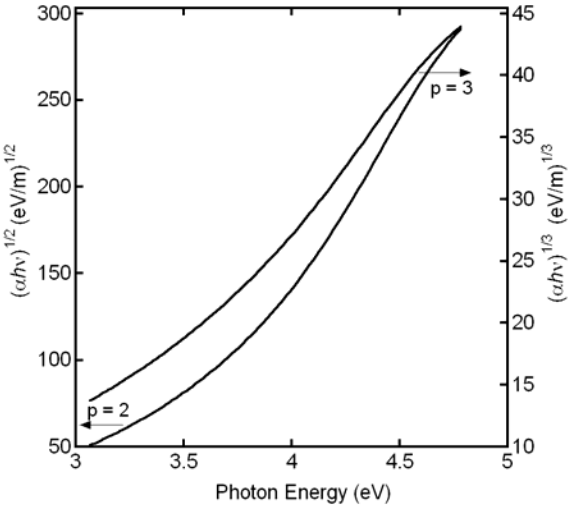

Figure 1: Absorption edge of 1,8-cineole based polymer obtained from ellipsometric data, derived from Equation (2) for p=2 and p=3.

The optical band gap (E_O) was derived using absorption coefficient data obtained from spectroscopic ellipsometry measurements using the procedure outlined previously[14]. Briefly, E_O is calculated using the Tauc relation[17]:

(2),

where hv is the energy of light, p is a constant connected to the density of states, and B is linked to the length of localised state tails. p can values of 2, 3, ½, etc. depending on the nature of the electronic structure. Figure 6 demonstrates the fit for p=2 and p=3 for the cineole based polymer sample. It was found that p=3 provided the best fit, resulting in E_O=2.83 eV.

3.4 AFM Study

AFM images were obtained in semi-contact mode of the 1,8-Cineole based polymer films to provide information on the surface of the polymer. An image of the film with scan size 1 x 1 μm is presented in Figure 7. Scan size of 10 x 10 μm is not shown, however, was employed for determining the average roughness for the film surface. An average roughness of 0.39 nm was obtained for the films using AFM, and this compared favourably with that obtained from ellipsometry (0.37 nm). Both the image and the roughness results indicate that the surface was very smooth and uniform.

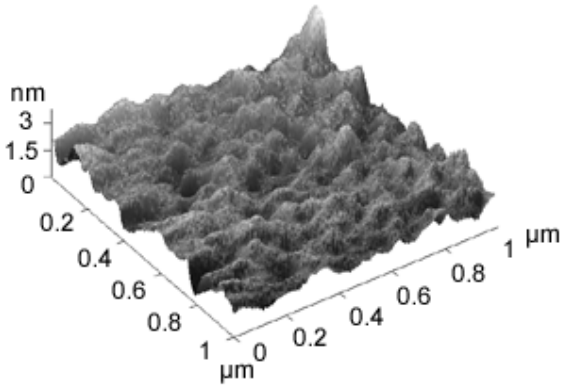

Figure 7: AFM image (1 x 1 μm) of 1,8-Cineole based polymer film

3.5 Water Contact Angle

The equilibrium contact angle was determined using a KSV 101 system. As outlined previously [18], the experimental procedure was confirmed by measuring the WCA of polytetrafluoroethylene, where the data was represented by a linear fit with equation y = -0.01t +119.95 and $R^2 = 0.97$, where t represents time. Figure 8 demonstrates the water contact data for the 1,8-Cineole polymer film, where the error bars in the plot represent 95% confidence levels at each time interval. Extrapolating the line of best fit to time zero resulted in a WCA of 89.8º, where the generally accepted cutoff between a hydrophilic and hydrophobic surface is 90º,though this is an arbitrary value. The range of WCA values obtained are on the proposed borderline between hydrophobic and hydrophilic, therefore based on this criteria alone it was difficult to assign the polymer as either hydrophilic or hydrophobic. However, at the contact angle values recorded, beading of the water droplets was observed, suggesting the surface was more likely mildly hydrophobic.

Within the first few seconds after initial contact with the surface, the rate of change in contact angle differed from the remainder of the measurements. An initial rapid rate of change in contact angle was typically assigned to absorption of water by the sample [19]. However the deviation of the data from the line of best fit at the beginning of the experiment was minimal as shown in the case of the 1,8-Cineole polymer. In addition, the line of best fit was given by the equation y = -0.0197t + 89.771, which indicated that the change in water contact angle in this study was -0.02 $º \cdot s^{-1}$, compared with -0.2 $º \cdot s^{-1}$ for poly(acrylic acid) [19]. These results indicated that it was highly unlikely that interactions such as swelling or reorientation of polar groups were occurring at the liquid-solid interface, and thus the 1,8-Cineole polymer was structurally stable while in contact with water. It has been demonstrated previously [20] that plasma polymerised films with contact angles between 60 to 90° provide favourable dose response of ^{125}I-protein A uptake to human immunoglobulin G (hIgG). Based on the results presented here, the 1,8-cineole polymer has the potential to be employed in biomedical applications. If the antimicrobial activity of the 1,8-cineole monomer could be maintained during the polymerisation process then the resulting polymer could be employed as a non-bio-reactive coating. This would allow fabrication of surface coatings for medical devices without the need for additional processing to include an antimicrobial component, such as a silver ion filler [21].

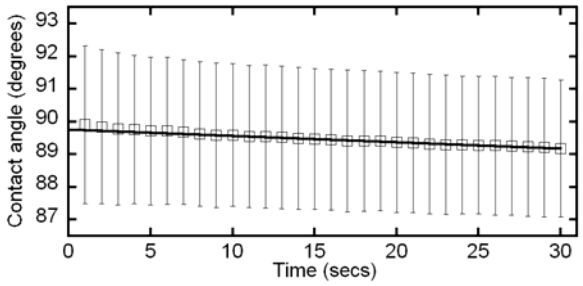

Figure 8: Water contact angle versus time for the 1,8-Cineole based polymer.

4. Conclusion

Polymer thin-films have been fabricated from the saturated monoterpene 1,8-Cineole and the properties of the material have been examined. The deposition rate was found to be approximately 55 nm/min, comparable with other precursors employed in plasma polymerisation. FTIR spectra of both the monomer and resultant polymer have been examined. Some of the functional groups observed in the monomer were retained during the polymerisation process by comparison the two spectra. C-H stretching and bending associated with methyl and methylene groups were present in the polymer, in addition to C=O stretch assigned to ketone and O-H stretch indicating the presence of alcohol. The optical properties of the polymer were investigated using ellipsometry. Transmission spectra of the films confirmed that they were optically transparent. The refractive index of the polymer was only slightly greater than that of glass, while the extinction coefficient demonstrated that there was no absorption at wavelengths greater than 400 nm. All optical parameters measured were found to be independent of thickness within the range measured. An optical band gap of E_O=2.83 eV was measured. AFM investigation of the polymer demonstrated a surface that was very smooth and uniform, with an average roughness of 0.39 nm, confirmed by ellipsometry. Water contact angles for the polymer demonstrated that the surface was weakly hydrophilic and structurally stable. These results predict that the polymer could be employed in a number of applications including optoelectronic and biomedical. Use in applications such as a non-bio-reactive coating however requires additional study into the schemes to maintain and enhance the antimicrobial nature of the monomer during polymerisation.

Acknowledgements

The authors are grateful to the financial support provided under the RIRDC and ARC LIEF and DP schemes. CDE is grateful to the APA, RIRDC and GRS (JCU) scholarships. We are thankful to Dr B. Rengarajan and Mr. K. Frost for assistance in obtaining the FTIR spectra, and Dr S. Askew for assistance in obtaining the AFM images.

References

[1] Z. V. Vardeny, A. J. Heeger, and A. Dodabalapur, Synthetic Metals 2005;148(1):1-3.

[2] M. Berggren and A. Richter-Dahlfors, Advanced Materials 2007;19(20):3201-3213.

[3] A. Hiratsuka and I. Karube, Electroanalysis 2000;12(9):695-702.

[4] M. C. Kim, S. H. Cho, J. G. Han, B. Y. Hong, Y. J. Kim, S. H. Yang, and J. H. Boo, Surface & Coatings Technology 2003;169(595-599.

[5] U. S. Sajeev, C. J. Mathai, S. Saravanan, R. R. Ashokan, S. Venkatachalam, and M. R. Anantharaman, Bulletin of Materials Science 2006;29(2):159-163.

[6] A. J. Beck, F. R. Jones, and R. D. Short, Polymer 1996;37(24):5537-5539.

[7] R. Forch, A. N. Chifen, A. Bousquet, H. L. Khor, M. Jungblut, L. Q. Chu, Z. Zhang, I. Osey-Mensah, E. K. Sinner, and W. Knoll, Chemical Vapor Deposition 2007;13(6-7):280-294.

[8] U. R. Juergens, U. Dethlefsen, G. Steinkamp, A. Gillissen, R. Repges, and H. Vetter, Respiratory Medicine 2003;97(3):250-256.

[9] U. R. Juergens, T. Engelen, K. Racke, M. Stober, A. Gillissen, and H. Vetter, Pulmonary Pharmacology & Therapeutics 2004;17(5):281-287.

[10] A. Serafino, P. S. Vallebona, F. Andreola, M. Zonfrillo, L. Mercuri, M. Federici, G. Rasi, E. Garaci, and P. Pierimarchi, Bmc Immunology 2008;9(

[11] S. Dalleau, E. Cateau, T. Berges, J. M. Berjeaud, and C. Imbert, International Journal of Antimicrobial Agents 2008;31(6):572-576.

[12] D. S. Kumar, K. Nakamura, S. Nishiyama, H. Noguchi, S. Ishii, K. Kashiwagi, and Y. Yoshida, Journal of Applied Polymer Science 2003;90(4):1102-1107.

[13] M. V. Jacob, C. D. Easton, G. S. Woods, and C. C. Berndt, Thin Solid Films 2008;516(12):3884-3887.

[14] C. D. Easton and M. V. Jacob, Thin Solid Films In press;

[15] M. S. Silverstein and I. Visoly-Fisher, Polymer 2002;43(1):11-20.

[16] J. Coates. In: R. A. Meyers editors. Interpretation of Infrared Spectra, A Practical Approach, Chichester, UK: John Wiley & Sons Ltd, 2000. pp. 10815-10837

[17] J. Tauc, R. Grigorovici, and A. Vancu, physica status solidi (b) 1966;15(2):627-637.

[18] C. D. Easton, M. V. Jacob, R. A. Shanks, and B. F. Bowden, Chemical Vapor Deposition In Press;

[19] M. R. Alexander and T. M. Duc, Polymer 1999;40(20):5479-5488.

[20] S. Kurosawa, N. Kamo, N. Minoura, and M. Muratsugu, Materials Science and Engineering: C 1997;4(4):291-296.

[21] R. Kumar, S. Howdle, and H. Munstedt, Journal of Biomedical Materials Research Part B-Applied Biomaterials 2005;75B(2):311-319.

CHAPTER 8 CONCLUSIONS AND FUTURE WORK

The development of organic polymers with optimised properties is a key research area. Advancement in this area has resulted in significant progress in the development of organic semiconductors and conductions for electronic and optical applications, in addition to the move from synthetic to organic materials for use in biomedical applications. Improvement and expansion in many fields is dependent on the fabrication of polymers with desirable properties specific for the intended application. Additionally, there is a global interest to implement environmentally friendly fabrication procedures and precursor materials at a commercial level. The aim of this work was to develop organic polymers for use in emerging technologies from environmentally friendly resources. Fabrication and characterisation of *Lavandula angustifolia* essential oil (LAEO) based polymer thin films and films produced from individual components have been detailed in this thesis. In addition, the methodology required for thin film characterisation has been defined, and when necessary, derived. With the current global interest in producing environmentally friendly products, the LAEO based polymer provides an alternative to existing technology through the development and implementation of natural resources.

8.1 FABRICATION AND CHARACTERISATION OF LAEO BASED POLYMER FILMS

A fabrication facility was established within the Electronic Materials Research Lab (EMRL) at James Cook University (JCU). Characterisation tools including spectroscopic ellipsometry were incorporated into the EMRL, while other facilities were accessed through collaborations with other researches. Plasma polymer thin films from LAEO were fabricated and the material properties examined in order to determine the feasibility of implementing the polymer in particular applications. Fabrication was performed using a low-temperature thermally non-equilibrium plasma. The plasma was generated within a customer made cylindrical polymerisation cell, where the RF energy was delivered to the system via capacitively coupled external electrodes. The parameters and procedures for the fabrication facility including deposition time, pressure and RF power were optimised to improve the properties of the resultant polymers.

8.1.1 Development of a new characterisation procedure for determining the dielectric parameters of a thin film

The methodology required for undertaking characterisation of thin films was defined and contributed to the knowledge of thin film characterisation within the EMRL at JCU. This involved employing and adapting strategies established in the literature. In the case of dielectric measurements of low permittivity thin films, limitations with the established non-destructive techniques resulted in inadequate measurement resolution. The split post dielectric resonator method was known to be an accurate tool for determining the dielectric properties of a material at microwave frequencies. This technique relies on the material under test to induce a frequency shift when placed in the resonator in order to determine the dielectric parameters. However, it was found that if the thickness and permittivity of the sample was too small, it was not possible to obtain a large enough frequency shift and thus adequate measurement resolution. To overcome this, a new measurement technique was developed for the non-destructive complex permittivity measurement of low permittivity thin film materials (Chapter 4).

The dielectric resonators employed operate at $TE_{01\delta}$ mode. This means that the electric field within the resonator only has an azimuthal component, in other words, only has a component in the plane of the substrate. Due to this, it was possible to increase the thickness of the sample by stacking a number of samples on top of each other within the resonator. The increase in sample thickness allowed adequate measurement resolution. The technique was verified and published in a peer reviewed journal [1]. The dielectric constant (ε) and loss tangent ($\tan\delta$) were obtained at 10 GHz (ε=2.57; $\tan\delta$=0.021) and 20 GHz (ε=2.61; $\tan\delta$=0.021) for the LAEO based polymer films fabricated at 25 W.

8.2 PROPERTIES OF LAEO BASED POLYMER FILMS

Properties of the LAEO based polymer fabricated at varying RF powers were examined employing the characterisation facilities established within the EMRL and using equipment made available through collaborations. A summary of the major findings are provided in the following sections.

8.2.1 Surface properties

The surface topology of the polymers was shown to be uniform and pinhole free using SEM (Chapter 2) and AFM (Chapter 3) images. Surface profiles were obtained employing AFM and the affect of RF power on the topology examined, where the peaks decreased in surface area while the number increased in magnitude. Average surface roughness was derived from AFM data and was comparable to Ellipsometry values (Chapter 4). The polymers were shown to be very smooth, with an average roughness of approximately 0.4 nm.

8.2.2 Chemical properties

Chemical analysis of the polymers was performed using FTIR and NMR spectroscopy (Chapter 3). FTIR results were obtained for films fabricated using RF powers between 10 to 75 W, in addition to the spectrum for the LAEO monomer. It was found that the LAEO based polymers were hydrocarbon dense, with strong bands assigned to methyl and methylene groups. In addition, bands associated with oxygen containing functional groups including alcohol and ketones were allocated. It was discovered that an increase in RF power during deposition resulted in a decrease in intensity of the majority of bands, within the exception of the methyl and methylene groups. Therefore, an increase in RF power resulted in a decrease in the oxygen containing functional groups, resulting in a less polar polymer.

The polymer fabricated at 10 W and the LAEO monomer were examined using NMR spectroscopy. Samples fabricated at higher RF powers were not investigated as they resisted solubilisation in chloroform. These spectra confirmed the polymer was hydrocarbon dense with the presence of acetate and methyl ketone functionality. The NMR results also indicated the presence of hydrogens on aromatic rings. Bands assigned to aromatic rings were not observed in either the FTIR spectra or the NMR spectra of the LAEO monomer. Therefore aromatics in the polymer structure were formed during the polymerisation process, most likely via dehydration of the linalool hydroxy group, cyclization of the resultant polyene structures and dehydrogenation reactions of six-membered ring structures.

8.2.3 Optical properties

Optical characterisation of the polymer fabricated at RF powers between 10 to 75 W were examined using UV-Vis spectroscopy (Chapter 4) and spectroscopic ellipsometry (Chapter 2 and 4). UV-Vis spectra of the polymers examined demonstrated that an increase in RF power during deposition did not result in a shift in the peak absorption position and/or broadening of the peak. The main absorption peak occurred outside the visible region of the spectrum and thus provided experimental confirmation of the optical transparency observed in the polymers. The optical transparency was confirmed for all samples from ellipsometry measurements obtained in transmission mode. Ellipsometry was employed to confirm that the polymers were optically isotropic, an expected result for a polymer with a high degree of disorder in the molecular structure.

For the regression analysis of the ellipsometric data, it was found that a combination of a Tauc-Lorentz and a Gaussian oscillator provided the best fit, with lower mean-squared error and minimum correlation between fitting terms. It was found that the refractive index of the LAEO based polymers was only slightly greater than that of glass, and the affect of RF power was minimal, with refractive index values ranging from 1.530 to 1.543 at 500 nm for samples fabricated at 10 and 75 W respectively. It was observed that the refractive index of the polymer was not thickness dependent upto thicknesses of 1000 nm. For all films measured, the extinction coefficient was zero at wavelengths greater than 500 nm. Although the refractive index and extinction coefficient were unaffected by applied RF power, the optical band gap was found to decrease with increasing RF power.

8.2.4 Stability of the polymer under different environmental and physical conditions

Changes in the properties of the polymer when exposed to ambient conditions for an extended period of time were examined, which was referred to as the aging of the polymers (Chapter 5). This was performed using spectroscopic ellipsometry and FTIR spectroscopy. Monitoring of the optical properties demonstrated that the bulk of the

degradation occurs during the first 100 hours after deposition. The chemical characterisation established that the aging occurs via oxidation, as observed by the increase in the OH stretch assigned to alcohol. The change observed was relatively small and thus the polymers were quite stable.

Contact angle measurements were performed with six solvents on the polymers fabricated at various RF power levels to provide information concerning how the polymer interacts with these solvents (Chapter 3 and 5). Water contact angle data demonstrated that the polymer was stable while in contact with water. In addition, the hydrophilcity of the polymer could be tuned with RF power, with the contact angle ranging from 81.93º to 91.95º for samples fabricated between 10 to 75 W respectively. An increase in RF power resulted in an increase in contact angle, indicating a less polar surface, which confirmed the decrease in oxygen content of the polymer. For the remaining solvents, the data indicated that the stability of the polymer increased with increasing applied RF power.

Surface tension components for the LAEO based polymers were calculated from the measured contact angle data. These components demonstrated that the polymers were monopolar in nature. Ranges for the surface tension were established based on results from three different techniques. The surface tension components were employed to determine the interfacial tension values and subsequently the solubilisation for the polymer-solvent systems. It was revealed that the LAEO polymer should resist solubilisation from the solvents explored.

The thermal properties of the polymers were measured using the head stage attachment for the ellipsometer (Chapter 5). It was found that the refractive index undergoes a large change between 200 and 300 ºC, suggesting the polymer undergoes a phase change within this temperature range. An increase in RF power during deposition resulted in an increase in the temperature at which thermal decomposition beings, thus representative of an increase in the thermal stability of the polymer. Film thickness retention after heating to 405 ºC was minimal, ranging from 2.2 to 0.4 %.

FTIR spectra were recorded after successive heat treatments to determine the affect on the chemical structure. Heating up to 150 ºC, and hence before the observed phase change, resulted in no significant affect on the spectrum. In this region the thermal degradation was associated with weight loss. Spectrum of the polymer heated to 245 ºC presented a significant change. Peaks assigned to C-H bonding had all decreased, while peaks assigned to C-O stretches increased in intensity. In addition, a peak allocated to C=C bonding was now visible. Upon heating to high temperatures, it was believed that the polymer loses hydrogen, most likely by the elimination of water, and the subsequent formation of either C-O or C=C bonds, resulting in a less hydrocarbon dense polymer.

Adhesion testing was performed using the crosshatch tape adhesion test complying with standard ASTM D3359 (Chapter 5). The LAEO based polymer was deposited at RF powers between 10 to 75 W on glass, poly(ethylene terephthalate), and polystyrene. The adhesion quality of the polymer was found to improve with increasing RF power, and was associated with an improvement in interfacial bonding.

8.3 FABRICATION OF POLYMERS FROM THE MAJOR COMPONENTS OF LAEO

Throughout this thesis, the monomer employed in the fabrication of the polymers was sourced from the same batch as supplied by G. R. Davis Pty. Ltd. It is known from the literature that LAEO contains many components and that the content of these components can vary between oils obtained from different sources. This information raises doubts concerning the reproducibility of the polymer properties obtained in this thesis when employing LAEO from different sources. In addition, knowledge of which components are contributing to the overall polymer formation is important in terms of understanding the fundamental properties as well as reproducing the polymer from alternative resources. Using gas chromatography – mass spectrometry, the major components of the LAEO monomer employed throughout this thesis were determined. The identified components were then polymerised and the properties of the resultant polymers determined and compared with the established LAEO based polymer in order to provide clarification regarding these issues (Chapter 6). From the six components explored, five had oxygen containing functional groups such as ketones, and one

component was a pure hydrocarbon (cis-β-ocimene). It was found that for the components that contained oxygen functional groups, the resultant chemical and optical properties were almost the same and very similar to that obtained for the LAEO based polymer. Greater variation was observed in the surface topology and water contact angle data, however the results were still similar to the LAEO based polymer. Overall, the cis-β-ocimene based polymer showed the greatest variance in properties compared to the other polymers. The results demonstrated that polymers with similar characteristics could be fabricated from the LAEO monomer irrespective of the composition. A deposition rate study indicated that fabrication of the LAEO based polymer most likely involved a number of components.

1,8-Cineole can make up to 20 % of the content of LAEO depending on the source, however no amount of cineole was detected in the batch of monomer employed in this thesis. Cineole is also a major component of eucalyptus oil and has been employed in medical applications due to its favourable properties. Polymer thin films were fabricated from 1,8-cineole and the properties of the resultant films examined, including the chemical, optical, and surface properties (Chapter 7).

8.4 POTENTIAL APPLICATIONS AND RECOMMENDATIONS FOR FUTURE WORK

Based on the results obtained during the characterisation stage, a number of potential applications have been identified. The permittivity and loss tangent results (Chapter 4) indicate that the material has the potential of being used as a low permittivity dielectric in IC fabrication. Due to the organic nature of the monomer precursor, the LAEO based polymer is an ideal candidate for use as a dielectric layer in organic FET (OFET) circuits. In order to implement the polymer within these applications in conjunction with other (high temperature) procedures, it is advisable to either lower the total thermal budget of the IC fabrication process and/or increase the thermal stability of the polymer. Potential solutions include fabricating the polymer at increased RF power levels, or through co-polymerisation with precursors that are known to provide thermal stability upon polymerisation.

The optical properties (Chapter 4) including tuneable optical band gap suggest the polymer could be employed in optoelectronic applications. Transparency in the optical region in addition to the stability while in contact with water (Chapter 3) demonstrated that the material could be used as an encapsulate for photovoltaics, perhaps as part of a multicomponent system. However, further work on the durability of the polymer would be required.

Oxygen containing functional groups, including hydroxy, are considered important for the covalent binding of biomolecules. Such functional groups were found in the LAEO based polymer (Chapter 3). Together with the stability of the polymer while in contact with water, the LAEO based polymer is a potential candidate for use in biomedical applications. Depending on whether the polymer repels or promotes the attachment of biomolecules to the surface, the polymer can be implemented as either a non-bio-reactive or bio-reactive coating. An example of a biomedical application for these coatings involves bioassays, such as an Enzyme-linked immunosorbent assay (ELISA). This diagnostic tool is used to determine the amount of antibody or antigen contained in a sample. A bio-reactive coating would be employed to bind the antigen or capture antibody to the plate, depending on the ELISA type, while the non-bio-reactive coating is used to reduce the background signal resulting from non-specific binding of biomolecules. An initial antimicrobial activity test with the polymer in E-coli performed with Prof. Elena Ivanova (Swinburne University of Technology, Melbourne) indicated no inhibition of growth of the bacteria on the experimental plates. Therefore the LAEO based polymer favours bio-reactivity.

The 1,8-cineole based polymer also has the potential for use in biomedical applications (Chapter 7). In monomer form, it has already been employed in medical applications for use an as anti-inflammatory and its antifungal activity has been confirmed. If these favourable properties of the monomer can be maintained during polymerisation, then the resultant polymer would be an ideal candidate for use as an antimicrobial non-bio-reactive coating.

Further work in the area of implementing the polymers in these biomedical applications is required. The stability of the polymer in solvents such as ethanol or while exposed to steam (autoclave) are required for sterilisation. The solubility study indicated that the LAEO based polymer should resist solubilisation from ethanol (Chapter 5), however confirmation would be required prior to any biomedical testing. Ethanol extraction has been employed previously to stabilise plasma polymers in aqueous solutions [2]. Thus this technique provides a potential avenue for stabilisation while providing the additional benefit of sterilisation. Once stability in aqueous environments is confirmed and sterilisation undertaken, testing involving protein binding and cell adhesion should be undertaken to confirm the bio-reactivity of the LAEO based polymer, while antimicrobial/biofilm experiments are required for the 1,8-cineole based polymer.

The thermal degradation results (Chapter 5) specify that the LAEO based polymer is well suited as a sacrificial material. Such materials are used to create nanofluidic channels in chip based bio/chemical analysis, and in semiconductor devices to produce ultra low permittivity dielectrics. The tuneable decomposition onset temperature could prove vital when integrating into a multi-component system, while the film retention is comparable or less to that of current technology. Implementation of the LAEO based polymer in the formation of air gap structures in the form of a prototype would be an important step in confirming the feasibility of the polymer in this field.

Although a number of properties of the essential oil based polymers were explored, progression of the essential oil based polymer films into applications would benefit from additional characterisation. Supplementary chemical characterisation employing surface sensitive techniques including X-ray Photoelectron Spectroscopy (XPS) and Time-of-Flight Secondary Ion Mass Spectroscopy (ToF-SIMS) would be of advantage for applications where knowledge of the surface chemistry is important, particularly the biomedical field. Investigation of the electrical carrier mobility and low frequency conductivity would aid in the integration of these polymers into organic electronic applications. In addition, X-ray scattering analysis techniques such as Small Angle X-ray Scattering (SAXS) would assist in answering fundamental questions concerning density and porosity of the polymer films.

8.5 OVERALL CONCLUSIONS

In conclusion, polymer thin films have been fabricated from LAEO at varying deposition parameters and a comprehensive study of the properties of the resulting films undertaken. A summary of the major findings are provided in Table 1. Based on the characterisation data obtained during the course of the thesis, potential applications have been identified and recommendations to achieve successful implementation have been given. The methodology derived has contributed to the knowledge of thin film characterisation within the EMRL at JCU. A technique for measuring the dielectric parameters of low permittivity thin films has been developed. The results obtained have demonstrated the advantages of implementing an essential oil as a precursor in the fabrication of polymers.

Table 1: Major properties of LAEO based polymers fabricated at different RF power levels

Polymer property	RF power employed during polymerisation (W)			
	10	25	50	75
Refractive index (500 nm)	1.530	1.540	1.547	1.543
Extinction coefficient (500 nm)	0	0	0	0
Optical band gap (eV)	2.75	2.55	2.55	2.34
Average roughness (AFM) (nm)	-	0.418	-	0.368
Water contact angle (º)	81.93	83.64	84.46	91.95
Thermal degradation onset temperature (ºC)	~60	~60, 170	~130	~170
Adhesion quality to common substrates (scale 0 – 5)	0 – 1	0 – 2	3 – 5	4 – 5
Range of surface tension values (mJ/m^2)	39.5–45.9	33.9–36.3	34.2–37.6	36.6–38.3

REFERENCES

[1] C. D. Easton, M. V. Jacob, and J. Krupka, "Non-destructive complex permittivity measurement of low permittivity thin film materials," *Measurement Science & Technology*, vol. 18, pp. 2869-2877, 2007.

[2] L. Q. Chu, W. Knoll, and R. Forch, "Stabilization of plasma-polymerized allylamine films by ethanol extraction," *Langmuir*, vol. 22, pp. 5548-5551, 2006.